Analysis of Force Generation and Cell-Cell Recognition during Zipping in Dorsal Closure of *Drosophila melanogaster*

Dissertation

zur

Erlangung der naturwissenschaftlichen Doktorwürde (Dr. sc. nat.)

vorgelegt der

Mathematisch-naturwissenschaftlichen Fakultät

der

Universität Zürich

von

Magdalene Adamczyk

aus

Deutschland

Promotionskomitee

Prof. Dr. Damian Brunner (Vorsitz, Leitung der Dissertation)
Prof. Dr. Konrad Basler
Prof. Dr. Carl-Philipp Heisenberg
Prof. Dr. Esther Stoeckli

Zürich, 2016

Contents

Summary

Epithelial fusion events are crucial for the correct formation and function of many organs. Dorsal closure of *Drosophila melanogaster* serves as a paradigm for such epithelial fusions. During dorsal closure, an epidermal opening filled with an extra-embryonic tissue, the amnioserosa, on the dorsal side of the Drosophila embryo is closed. In this process two opposing epithelial sheets move towards one another until they meet and fuse at the dorsal midline to form a continuous epidermis. A process, termed zipping, is required for the final step of dorsal closure. Zipping starts at the anterior and posterior canthi when initial contacts are formed between matching leading edge cells of opposing epithelial sheets. These contacts are made by actin-based filopodia and lamellipodia, which extend from leading edge cells. Once these protrusions engage, they are believed to pull on each other, thereby bringing the next neighbours closer together and pushing the amnioserosa tissue down into the embryo. In this work I studied two integral parts of the zipping process: force generation and cell-cell recognition.

Actin-based protrusion shortening has been hypothesised to provide the zipping force. However, new evidence suggests that microtubules (MTs) play a role in force generation during zipping. Past work has already shown that MTs are required for zipping progression. Now, a 3D reconstruction of the zipping process has revealed that during lamellar overlap shortening, which is likely the step where zipping force generation occurs, MTs are abundant whereas actin bundles are not detected.

We hypothesise that a conserved mechanism that involves a cortical interaction of MTs and dynein generates the zipping force. Thereby, cortical dynein grabs incoming MTs, walks on them and thus exerts a pulling force, which drags the epithelial sheets together. In this work, I could show that MT dynamicity is essential for zipping and zipping force generation. My attempts to interfere with the dynein function to investigate its role in the zipping process, however, proved challenging. I performed immunolabelling experiments of dynein, which displayed an enrichment of dynein along the leading edge, indicating a function for zipping. Yet, the use of genetic means to study dynein function did not give conclusive results as maternally provided dynein is sufficient for embryonic development. A recently discovered drug that specifically inhibits dynein, did cause an arrest of zipping, but also affected the amnioserosa tissue. Thus, for studying a dynein function during zipping, a tool for selective dynein elimination is needed. Hence, I started the development of a new tool to generate conditional dynein mutants, which will hopefully allow us to get

more insights into a possible dynein function in zipping force generation.

The second part of my work dealt with the recognition process of opposing leading edge cells during zipping. Since the embryo at this stage is patterned into repetitive segments consisting of stripes of cells with defined positional identity, perfect matching of cells with identical positional identity is of fundamental importance to dorsal closure. To find the underlying mechanisms and molecules regulating this process, I performed a forward EMS mutagenesis screen, which unfortunately did not give positive results. In addition, I have analysed mutants of multiple factors, involved in recognition processes during axon guidance, yet no mismatching defects were observed. The lack of proper null mutants or maternal contribution, however, might mask a possible phenotype. Axon guidance molecules remain promising candidates, as they have been shown to play a role in cell-cell recognition during ventral enclosure of *Caenorhabditis elegans*, a process with analogy to dorsal closure.

Zusammenfassung

Epitheliale Fusionsereignisse sind wesentlich für die fehlerfreie Entstehung und Funktion von Organen. Die sogenannte "Dorsal Closure" (DC), ein Prozess bei dem eine dorsale Öffnung in der Epidermis, welche während der Embryogenese von *Drosophila melanogaster* entsteht, geschlossen wird, dient als Musterbeispiel für solche Fusionsereignisse. Diese Öffnung ist mit einem extra-embryonalen Gewebe gefüllt, dem Amnioserosagewebe. Während der DC bewegen sich die seitlich liegenden Epidermislagen aufeinander zu, bis sie auf der dorsalen Mittellinie aufeinander treffen, sich verbinden und eine durchgehende Epidermis bilden. Ein Prozess, welchen man als "Zipping" bezeichnet, ist für den letzten Schritt der DC erforderlich. Dieser Prozess beginnt an den anterioren und posterioren Enden der dorsalen Öffnung, wenn erste Zellkontakte zwischen identischen Epidermiszellen der beiden gegenüberliegenden Epidermislagen entstehen. Solche ersten Kontakte werden von speziellen aktinreichen Zellausstülpungen der vordersten Epidermiszellen, sogenannten Filopodien und Lamellipodien, gebildet. Nachdem Ineinandergreifen solcher Zellausstülpungen, vermutet man, dass eine gegenseitige Zugkraft entsteht, welche dazu führt, dass benachbarte Epidermiszellen näher zusammengebracht werden und dadurch die Amnioserosazellen in das Innere des Embryos drücken. In dieser Arbeit habe ich zwei der für das Zipping erforderlichen Prozesse untersucht: die Entstehung der Zugkraft und die spezifische Zell-Zell-Erkennung gegenüberliegender Epidermiszellen. Es wird vermutet, dass die Verkürzung der Aktinbündel in den Zellausstülpungen, die für den Zipping-Prozess benötigte Zugkraft, generiert. Jedoch gibt es neue Indizien, die daraufhin deuten, dass Mikrotubuli eine Funktion in der Erzeugung einer solchen Zugkraft haben. Es wurde bereits gezeigt, dass Mikrotubuli für das Zipping notwendig sind. Nun konnte anhand einer 3D Rekonstruktion des gesamten Zipping-Prozesses gezeigt werden, dass es während dieses Prozesses zu einer Verkürzung von überlappenden Lamellen kommt, und dies wahrscheinlich der kraftgenerierende Moment ist. Dabei wurden in diesen Überlappungen zahlreiche Mikrotubuli gefunden, wohingegen Aktinbündel nicht entdeckt wurden. Diese Ergebnisse lassen uns vermuten, dass ein bekannter, evolutionär konservierter Mechanismus, in welchem eine Interaktion von Mikrotubuli und dem Motorprotein Dynein am vorderen Zellkortex der frontalen Epidermiszellen die für das Zipping notwendige Zugkraft erzeugt. Hierbei, greifen sich kortikal befestigte Dyneine entgegenkommende Mikrotubuli-Plusenden, laufen in Richtung ihrer Minusenden und generieren dabei eine Zugkraft, die dazu führt, dass die beiden gegenüberliegenden Epidermis-

lagen zusammenkommen. In dieser Arbeit konnte ich zeigen, dass die Mikrotubuli-Dynamizität sowohl für den Zipping-Prozess als auch für die Erzeugung der Zugkraft essentiell ist. Weiterhin habe ich versucht die Funktion des Motorproteins Dynein während des Zippings zu untersuchen, jedoch stellte sich dies als schwierig heraus. In Immunofluoreszenzexperimenten konnte ich zeigen, dass Dynein in den vorderen Epidermiszellen akkumuliert und damit eine Funktion für den Zipping-Prozess suggeriert. Dagegen führte die Analyse einer Funktion Dyneins mit Hilfe genetischer Mittel während dieses Prozesses zu keinen eindeutigen Ergebnissen, da maternal bereitgestelltes Dynein die Embryonalentwicklung über die DC hinaus ermöglicht. Ferner, habe ich den kürzlich entdeckten spezifischen Dynein Inhibitor in Embryonen injiziert. Dadurch wurde der Zipping-Prozess zwar gehemmt, aber auch das Amnioserosagewebe beeinträchtigt. Somit wird eine Methode benötigt, die eine selektive Eliminierung oder Hemmung von Dynein erlaubt. Mit der Entwicklung einer Methode, mit der man konditionale Dynein Mutanten generieren kann, habe ich bereits begonnen und dies wird hoffentlich dazu beitragen, dass wir mehr Erkenntnisse über eine mögliche Rolle von Dynein im Zipping-Prozess gewinnen.

Der zweite Teil meiner Arbeit beschäftigte sich mit der Zell-Zell-Erkennung gegenüberliegender Epidermiszellen der beiden Epidermislagen. Da der *Drosophila* Embryo während der DC Phase eine Struktur aus sich wiederholenden Segmenten, welche aus Zellstreifen mit gleicher positioneller Identität bestehen, aufweist, ist eine fehlerfreie Paarung von Zellen mit gleicher positioneller Identität von elementarer Wichtigkeit für DC. Um die zugrundeliegenden Mechanismen und Moleküle, welche einen solchen Prozess regulieren, zu identifizieren, habe ich einen EMS Mutagenese "Screen" durchgeführt, der jedoch leider keine positiven Resultate hervorgebracht hat. Darüber hinaus habe ich Mutanten analysiert, welche in verschiedenen Erkennungsmechanismen bei der axonalen Wegfindung eine Rolle spielen. Auch hier konnte ich keine eindeutigen Erkenntnisse gewinnen, da das Fehlen von klaren Null-Mutanten oder auch maternal beigetragene Proteinfunktion einen möglichen Phänotypen überlagern. Dennoch bleiben Moleküle, welche in die axonale Wegfindung involviert sind, vielversprechende Kandidaten. Es wurde gezeigt, dass sie für die Zell-Zell-Erkennung während eines morphogenetischen Prozesses im Laufe der Entwicklung von *Caenorhabditis elegans*, der Analogien zur DC in Drosophila aufweist, benötigt werden.

Acknowledgements

First and foremost, I would like to thank Professor Damian Brunner for giving me the opportunity to perform this research in his lab and for his ongoing support during the past five years. I am especially grateful to him for fostering such a friendly and open atmosphere in the lab as well as his enthusiasm and guidance throughout.

Besides my advisor, I would also like to thank my thesis advisory committee members Professors Konrad Basler, Esther Stoeckli and Carl-Philipp Heisenberg for their encouragement and insightful comments.

A big thanks to all the past and present members of the lab for contributing to the productive and enjoyable working environment as well as all the fun times both in and out of the lab. I especially want to thank Werner Boll for his experimental advice and help with the microscopes, Erich Frei for his help with the fly work and stimulating conversations, Mandy Börmel for being both an invaluable lab neighbour and a great friend also outside the lab, Laurynas Pasakarnis, Steve Huisman, Maria Heimlicher, Marisa Oliveira and Nadia Dubé for the many insightful discussions, valuable feedback and most of all their friendship.

Last, but by no means least, I want to thank my family. To my parents for their support and encouragement throughout all my studies, and to my partner John for his love, support and for embarking with me on the next big adventure in my life.

1 Introduction

1.1 Studying epithelial fusions

There are many occasions in embryonic development when two opposing tissues come into contact and fuse together to form one continuous structure. Such epithelial fusion events are fundamental for the proper formation and function of many organs and tissues. In vertebrates, epithelial closure events occur during the development of the heart, neural tube, eyes, face and body wall. Disruption of epithelial fusion processes leads to various birth defects including spina bifida (Copp et al., 1990), cleft palate (Abbott, 2010) and heart defects (Wenink & Zevallos, 1988). Thus, it is of fundamental importance to understand the underlying mechanisms driving such fusion events.

In essence, all epithelial fusion events require initial forces that bring two opposing epithelial sheets together, and a mechanism by which the epidermal fronts can be knitted together to form one continuous epithelium. Although the exact mechanisms how epithelial sheets are brought together might vary, the final adhesion event itself is thought to be highly conserved (Martin & Wood, 2002). Such closure events display also parallels to wound healing processes, thus understanding tissue closure events might also extend the knowledge of tissue repair processes (Martin & Parkhurst, 2004).

Several different model organisms are used to study epithelial fusions. Yet, dorsal closure in the common fruitfly *Drosophila melanogaster* represents the single most thoroughly characterised example of epithelial movement and fusion in invertebrates. It is genetically the most tractable and serves as a paradigm for such morphogenetic events. During dorsal closure, which is one of the last major morphogenetic steps in *Drosophila* embryogenesis, a dorsal opening in the embryo is closed to form a continuous epidermis. Thus, studying dorsal closure will shed light on shared mechanisms and pathways used for the various other morphogenetic events for *Drosophila* itself and other organisms.

1.2 *Drosophila* embryogenesis

The *Drosophila* life cycle, from egg to adult fly, takes an estimated $9 - 10$ days at $25°C$. After embryogenesis, *Drosophila* progresses through both the larval and pupal stages before reaching adulthood. Each one of these developmental stages is distinguished by markedly different body plans.

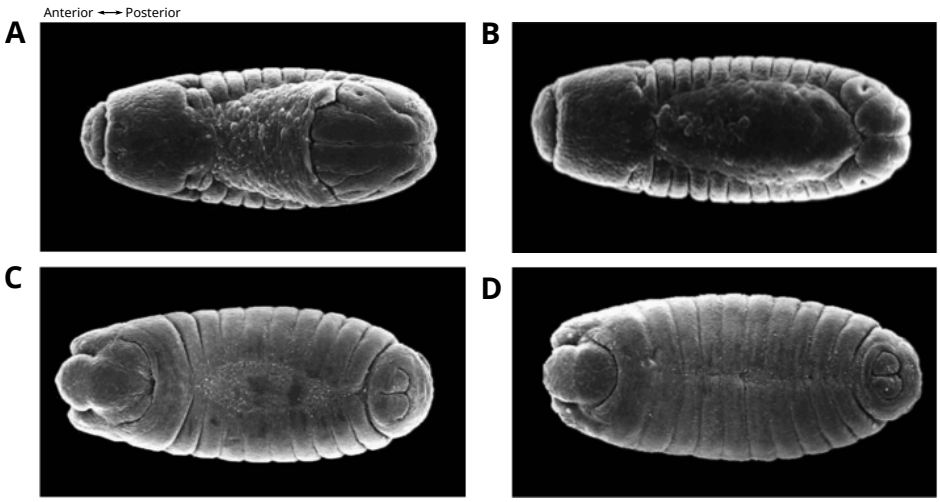

Figure 1: Selected stages of *Drosophila* embryogenesis.
(A-D) Scanning electron microscopy images of the *Drosophila* embryo during embryonic stages 12-15 (www.sdbonline.org). Dorsal view. (A) Stage 12. Germband retraction. Amnioserosa tissue is spreading to cover the dorsal surface. (B) Stage 13. Germband retraction is completed. Head involution starts. Epidermal sheets of both sides start to move dorsally, initiating dorsal closure. (C) Stage 14. Embryo during head involution and dorsal closure. (D) Stage 15. Completion of dorsal closure. Head involution continues.

After fertilisation of the egg, the zygote nucleus undergoes 13 mitotic divisions. During these stages of nuclear divisions, the embryo is called a syncytial blastoderm, meaning that all nuclei share a common cytoplasm, as no cell membranes exist yet other than that of the egg itself. Following nuclear division 13, cellularisation starts. During this process, the cellular blastoderm is formed, in which all cells are arranged in a single layer around the yolk of the egg. Immediately after cellularisation, the ventral furrow along the ventral midline starts to form, thus marking the beginning of gastrulation, a process that transforms the blastoderm into a multi-layered embryo with the three germ layers mesoderm, endoderm and ectoderm. During ventral furrow invagiation, the cells fold inwards on the ventral side of the embryo. which gives rise to the future mesoderm. Along with the pole cells, which later give rise to the germ cells, the prospective endoderm invaginates at the anterior and posterior ends of the ventral furrow and will form the future midgut.

The next major morphogenetic process is the germband extension. The convergence and extension of ectodermal cells on the surface and the mesoderm lead to the formation of the germband. The germband extends around the posterior end of the embryo and folds over onto the dorsal side, wrapping the embryo. At the same time, body segments start to form. Later on, the germband retracts posteriorly. This process is accompanied by the transition of parasegmental to segmental

division of the embryo. During germband retraction, the amnioserosa tissue unfolds from its compressed state and fills the hole of the dorsal surface. In the process of segmentation, deep ventral grooves form, which correspond to the incipient segmental boundaries and will be the sites of future muscle attachments. After germband retraction, dorsal closure starts. In this process the opening on the dorsal surface of the embryo, which is covered by the amnioserosa tissue, is closed. Another morphogenetic process, which occurs almost simultaneously to dorsal closure is head involution. Once head involution and dorsal closure are completed, the period of extensive morphologic rearrangements in the embryo is brought to an end (Campos-Ortega & Hartenstein, 2013; Gilbert, 2000).

1.3 Dorsal closure

Dorsal closure (DC) is a paradigm of epithelial fusion that occurs in mid-embryogenesis of *Drosophila* and leads to the sealing of a dorsal epithelial hole. It represents one of the most thoroughly characterised examples of morphogenetic cell movements. Thus, what is learned about DC is widely applicable, since other processes of epithelial fusion, e.g. wound healing, require many of the same proteins (Harden, 2002). During DC, an epithelial hole, which resulted from germband retraction, is closed. The hole is covered by an extra-embryonic epithelium, the amnioserosa (AS). The AS tissue is composed of a single layer of large flat multilateral cells, which do not contribute to the adult fly and undergo apoptosis when the dorsal opening is closed (Jacinto et al., 2002). Two opposing lateral epidermal sheets, which flank the AS, elongate in the dorsal-ventral (D/V) axis and move dorsal-ward, completely covering the AS and fusing along the midline, thus sealing the dorsal opening (Campos-Ortega & Hartenstein, 2013).

1.3.1 Forces contributing to dorsal closure

Three main cellular processes generate coordinated forces that are thought to be required for DC: 1) Actin-cable formation, 2) Amnioserosa cell constriction and 3) zipping force.

Actomyosin cable: At the onset of DC, activation of the Jun N-terminal kinase cascade (JNK) pathway in the leading edge (LE) epidermis induces a reorganisation of the actin cytoskeleton. Epidermal LE cells start to polarise as filamentous actin (F-actin) and non-muscle myosin II (MyoII) accumulate at their apical edge and

form a thick cable. This accumulation occurs initially at actin nucleation sites (ANCs), which are located in between cells at the level of adherence junctions and grow over time. Thus, each cell of the LE forms a cable at the apico-dorsal side which is connected via adherence junctions to cables in neighbouring cells forming a supracelluar actomyosin cable surrounding the dorsal gap (Kaltschmidt et al., 2002).

It is suggested that the cable acts as a contractile purse string providing a force for DC (Young et al., 1993; Kiehart et al., 2000). However, there is new evidence that the actomyosin cable is not essential for DC as MyoII depletion in the epidermis did not inhibit DC, yet the cable provides a line tension which straightens the epidermis fronts (Pasakarnis et al., 2016).

Amnioserosa cell constriction: Another force contributing to DC is the surface constriction of AS cells, which is MyoII dependent. It was suggested that at the onset of DC the AS cells contract and decrease their apical surface gradually, thereby pulling the surrounding epidermis towards the dorsal midline (Kiehart et al., 2000; Franke et al., 2005). Yet, a new model shows that AS contraction is not occurring gradually but in a pulsed manner and takes place long before DC starts. As the AS cells constitutively pull on the surrounding epidermal tissue, it was further suggested, that the actomyosin cable acts like a ratchet to prevent ventral-ward retraction of the epidermis after force pulses (Solon et al., 2009). However, as previously described, the actomyosin cable is not required for DC, thus dismissing the ratchet model. Nevertheless, pulsed apical AS cell surface contractions are essential for closure, as MyoII depletion in the AS tissue arrests DC at an early stage (Pasakarnis et al., 2016).

Zipping force: The final force for DC is provided by the zipping process resulting in the sealing of the gap. Zipping starts at the anterior and posterior canthi of the dorsal opening, when the two lateral epidermal fronts are close enough to form initial contacts. These contacts are actin-based protrusions and are believed to progress zipping by pulling on each other, which brings the next neighbours closer together and thus pushes the AS cells down inside the embryo. It was hypothesised that actin-mediated protrusion shortening is the force driving mechanism during the zipping process (Jacinto et al., 2000). However, there is evidence of an alternative mechanism for this force generating process, which will be described in detail in Section 1.3.3.5.

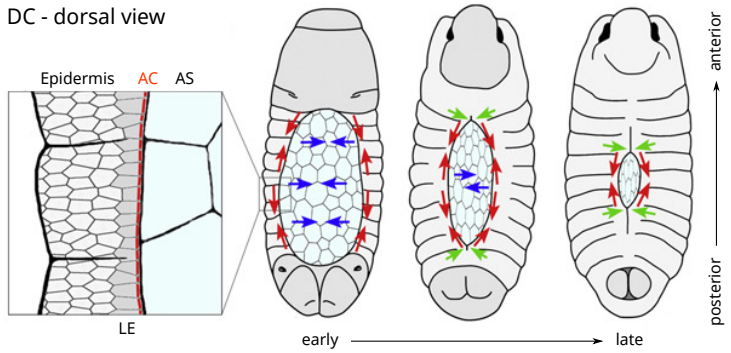

Figure 2: Forces contributing to dorsal closure.
This cartoon shows dorsal closure stage embryos. The coloured arrows depict forces contributing to dorsal closure. The blue arrows indicate contractile forces of individual AS cells. The red arrows depict force provided by the actomyosin cable (AC) and the green arrows indicate zipping forces at the canthi of the opening. The black arrows show the direction of leading edge (LE) movement (from Solon et al., 2009).

1.3.2 Signalling pathways involved in dorsal closure: JNK and Dpp signalling

The Jun N-terminal kinase cascade (JNK) was shown to be a central component of the signalling controlling DC. JNK belongs to the highly conserved mitogen-activated protein kinase (MAPK) family. MAPK cascades are involved in a variety of fundamental processes, such as proliferation, differentiation, motility, and stress response (Harden, 2002).

The *Drosophila* JNK pathway acts as a classic MAPK cascade resulting in the activation of an Ap-1 transcription factor comprised of DJun and DFos (Riesgo-Escovar & Hafen, 1997a). In *Drosophila* DJun and DFos are encoded by *Djun* and *kayak* (*kay*) respectively. DJun/DFos activation leads to upregulated expression of *decapentaplegic* (*dpp*), which encodes a secreted morphogen belonging to the TGF-β family (Riesgo-Escovar & Hafen, 1997b), and *puckered* (*puc*), which encodes a JNK phosphatase and functions as a component of a negative feedback loop leading to the downregulation of JNK activity through dephosphorylation of JNK, which is encoded by the *Drosophila* gene *basket* (*bsk*; Martín-Blanco et al., 1998). Expression of *bsk* is required for the initiation of DC, as epidermal cells do not elongate in the dorsal-ventral axis in *bsk* mutants and die at the end of embryogenesis with a dorsal hole in their cuticle (Riesgo-Escovar et al., 1996; Nüsslein-Volhard et al., 1984). Furthermore, JNK signalling is required for the maturation of ANCs, and thus for the proper formation of the actomyosin cable, as well as the stimulation of filopodia and lamellipodia formation in the leading edge (Kaltschmidt et al., 2002).

Prior to the onset of DC, the JNK pathway is active in both the LE epidermis as well as in the AS tissue. At the onset of DC, JNK signalling is downregulated in the AS, but remains active in the LE epidermis. This difference in JNK activity in the LE cells and the AS cells is important for DC progression. As the consequence of active JNK signalling in the LE epidermis, the expression of *dpp* and *puc* is induced in these cells (Reed et al., 2001). *Dpp* expression in LE cells lasts until completion of DC. Overexpression of Dpp is sufficient to rescue defects of JNK pathway mutants, indicating that JNK signalling is operating through Dpp (Riesgo-Escovar & Hafen, 1997b).

Dpp signalling is essential for epidermal LE cells. In zygotic mutant embryos that lack Dpp receptor activity (*thick veins*, *tkv*), LE cells fail to elongate properly in a coordinated manner and exhibit abnormal morphologies. In addition, microtubule (MT) bundles are not organised in a D/V axis as in wild-type embryos. Lateral epidermal cells start elongating but eventually this movement fails. Together, such defects in Dpp signalling mutants block the zipping process (Fernández et al., 2007).

1.3.3 Zipping process

Zipping represents the final stage of DC. Once the epithelial cells of opposing epidermal sheets are close enough to meet, the zipping process starts. Zipping proceeds at both the anterior and posterior canthi of the dorsal opening, which exhibits an eye-shaped morphology, until the opposing epithelial sheets meet and fuse at the midline. During zipping, LE cells of opposing epithelial sheets with identical positional identity recognise each other and build up adhesion sites (Jacinto et al., 2000; Millard & Martin, 2008). Thereby, the cells exert a pulling force on each other, which pushes the interjacent AS cells down inside the embryo. To establish contacts between epithelial sheets, LE cells form protrusions, which consist of highly dynamic actin-based filopodia and lamellipodia. Inhibition of filopodia formation caused by dominant-negative expression of the small GTPase Cdc42 in alternating epidermal stripes results in misalignment along the dorsal midline showing that protrusions are required for correct matching of epidermal stripes. Thus, filopodia are believed to scan the space above the AS tissue in search for their matching cell from the opposing epithelial sheet (Jacinto et al., 2000). In addition to actin, zipping also depends on MTs. Elimination of MTs in LE cells leads to a zipping arrest (Jankovics & Brunner, 2006).

1.3.3.1 Cell-cell recognition during zipping

At the dorsal closure stage, the epithelium is patterned into repetitive segments consisting of stripes of cells with defined positional identity (St Johnston & Nüssslein-Volhard, 1992; Kornberg & Tabata, 1993; Martinez-Arias & Lawrence, 1984; Rivera-Pomar & Jãckle, 1996). To maintain such patterning it is of importance that alignment of the epithelial sheets occurs with high accuracy. Indeed, the opposing epithelial sheets fuse with high accuracy resulting in a perfectly established pattern across the fusion seam at single cell resolution. To form such a precise pattern, each cell within the leading edge must recognise and fuse specifically with its matching cell in the opposing epithelial sheet. Experiments have shown that filopodia are required for correct cell matching (Jacinto et al., 2000). The loss of filopodia leads to misalignment along the dorsal midline. Thus, filopodial recognition ensures that epithelial fusion occurs accurately. Furthermore, filopodia are able to correct misaligned cells by pulling them into the correct alignment Millard & Martin (2008). Consistently, dominant-negative Cdc42, a small GTPase that regulates actin polymerisation, leads to misalignment at the dorsal midline. Such mutants show longer and more persistent filopodia (Nadia Dubé, unpublished). The misalignment might occur because filopodia are able to establish contacts with cells from a neighbouring segment, which they usually would not be able to reach. This data supports the important role of filopodia during the recognition process and suggests that segment identity is an important basis for positional cell-cell recognition.

Thus, the recognition process occurs at two levels during zipping. First, cells often seem to pair with cells from the opposite side that are within the same segment, but independent of their exact position within the segment (Millard & Martin, 2008). Only after this first interaction and subsequent pulling providing the zipping force (Eltsov et al., 2015), cells will sort out their correct partners within the segment and eventually establish permanent adhesion structures. The initial, imperfect matching of cells within equivalent segments is somewhat surprising, since preceding zipping, the same cells also make transient contacts with the neighbours in their own segment without effect (Jacinto et al., 2000). This suggests that cells not only recognise segments but also can distinguish cells of the own segment from cells of the same segment on the opposite side. This shows that zipping involves more complex cell-cell interactions than previously thought. These may well serve as a paradigm for other cell type-specific interactions.

1.3.3.2 Microtubule organisation during zipping

Most studies focus on the role of the actin cytoskeleton during DC, with little attention paid to MTs involvement in the process. However, a possible role for MTs during DC was first suggested in 2002 by Kaltschmidt et al., who have shown that MT organisation changes towards the end of germband retraction and before the onset of DC. During germband retraction the epidermal cells display a web of MTs distributed irregularly over the cytoplasm. As germband retraction is nearly completed, the epidermal cells begin to elongate in the dorsal-ventral axis and their MTs form apical bundles along this axis. Yet, these observations were made in fixed embryos using immunostaining. An extensive study using real-time fluorescence imaging to describe the spatial distribution and dynamic behaviour of MTs in DC was performed by Jankovics & Brunner (2006). Live-imaging revealed that MTs are distributed throughout epithelial cells before the onset of DC. As DC proceeds, MTs form stable bundles aligned along the dorsal-ventral cell axis and spatially restricted to the apical cell cortex. This specific rearrangement of MTs is first observed in LE cells and only later in the remaining epithelial cells. These bundles, in which individual MTs remain highly dynamic, are made of anti-parallel MTs. Once closure is completed, the MT bundles dissolve and adopt a distribution similar to the one observed before the onset of DC. Moreover, it was shown that MTs constantly invade cellular protrusions of LE cells and are often present in the entire length of the growing and shrinking filopodium (Jankovics & Brunner, 2006).

1.3.3.3 Microtubules are required exclusively for zipping

MT rearrangement often coincides with their involvement in performing specialised tasks (reviewed in Müsch, 2004). As MTs transiently reorganise during DC, they may have a specific role in this process. Jankovics and Brunner addressed the role of MTs in DC by eliminating MTs specifically during this morphogenetic process. Following the injection of the MT depolymerising drug colcemid into DC stage embryos, embryonic development arrests without completing DC. Yet, the drug-injected embryos display normal apical constriction, since convergence of the two epithelial sheets is normal and epithelial sheets move with a similar velocity as control embryos towards the dorsal midline. However, the dorsal opening becomes abnormally narrow compared to the ellipsoidal shape during normal wild-type closure, revealing an almost absent zipping process. To exclude that the observed phenotype results from defects in other tissues, since drug injections are global and eliminate MTs in all em-

bryonic cells, they eliminated MTs specifically in alternating epidermal stripes. For this, the MT-severing protein Spastin, which causes MT disassembly, was ectopically expressed in engrailed stripes during zipping. Zipping was shown to arrest as soon as the Spastin-expressing stripes met at the midline. The zipping arrest is overcome as the continued convergence of epithelial sheets brings the adjacent stripes of wild-type cells close enough to enable interaction and thus zipping progresses normally until the next Spastin-expressing stripes meet. Finally, wild-type stripes allow the embryos to complete DC, but the entire process is significantly delayed. Both experiments suggest that MTs are exclusively required during zipping in DC, however, their functional role is not yet fully understood (Jankovics & Brunner, 2006).

1.3.3.4 Zipping involves cytoskeletal reorganisation

To get a better understanding of the cytoskeletal processes occurring during zipping, Eltsov et al. (2015) have reconstructed the zipping process by large-volume correlative electron tomography. Zipping can be subdivided into three different regions: early, mid and late. During early zipping, initial cell-cell contacts are formed by filopodia of opposing LE cells, which then develop into significant lamellar membrane overlaps. In addition to actin bundles, MTs are also detected in these protrusions, where they frequently reach the protrusion tip. This was already seen using light microscopy by Jankovics & Brunner (2006). As MTs are both close to and precisely aligned with the actin bundles, this suggest that they might also be involved in protrusion formation. The expanded lamellipodia generate a single overlapping surface between opposing LE cells, whereas more complex membrane intertwining occurs between neighbouring LE cells. Such an observation of complex intertwining was previously suggested for LE cells of opposing epithelial sheets (Jacinto et al., 2000). Furthermore, premature adhesion sites form at inter-membrane regions of the lamellar overlaps of opposing LE cells. The number of MTs in these overlap regions rapidly increases, while actin bundles disappear. These MTs are dynamic, and both growing and shrinking MT plus ends can be detected. More growing than shrinking MT plus ends are observed, which is consistent with a dynamic equilibrium, since MT depolymerisation is significantly faster than polymerisation (Kirschner & Mitchison, 1986). During mid-zipping, the lamellar overlap areas shorten and cell-adhesions mature. This lamellar overlap shortening likely produces the zipping force. At the same time, the distribution of growing and shrinking MTs changes. An excess of shrinking MT plus ends is present, and these ends are localised in the

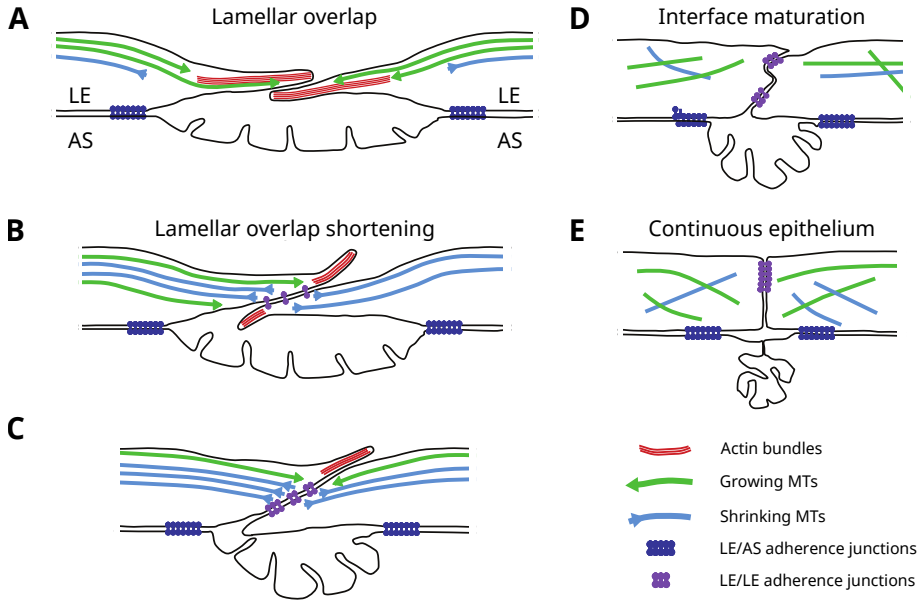

Figure 3: The zipping process.
(A-E) A schematic representation of cell membrane organisation and cytoskeletal remodelling of the leading edge cells during zipping. **(A)** In early zipping, single lamellar overlaps are formed between leading edge (LE) cells, actin bundles (red lines) and microtubules (MTs; green and blue lines) are present. **(B-C)** In mid-zipping lamellar overlaps shorten and cell adhesions mature. Actin bundles disappeared and cells are filled with MTs. More shrinking (blue) than growing (green) MTs are are detected close to putative adhesion sites (purple dots). **(D)** In late zipping, the interface of opposing LE cells adopts the orientation of normal epidermis interfaces. **(E)** After zipping completion, a continuous epithelium is formed (adapted from Eltsov et al., 2015).

cell-cell contact regions. Moreover, the intertwined membranes of neighbouring LE cells resolve. During late zipping, the interface of opposing LE cells adopt the orientation of normal epidermis cell interfaces, until eventually resulting in the typical linear arrangement of epidermal adherence junctions.

1.3.3.5 Microtubule- versus actin-mediated force generation during zipping

Previous work, using traditional electron microscopy, has suggested that during zipping filopodia and lamellipodia of opposing LE cells form a complex and strong intertwined interaction surface (Jacinto et al., 2000). Actin-based protrusion shortening was hypothesised to drag the epithelial fronts together, thus resolving the complex interdigitations and leading to the formation of mature adherence junctions between normal epithelial cells. This process is thought to generate the zipping force. The previously described work of Eltsov et al. (2015), who performed a 3D reconstruction

of the entire zipping process using large scale electron tomography, suggest a new mechanism for zipping force generation. During the shortening of lamellar overlaps in mid-zipping, which is likely the zipping force-generating step, no actin bundles were found in these lobes, instead they are filled with MTs throughout the shortening period. This indicates that the zipping force generation is an MT- rather than an actin-based process. This is further supported by recent experiments that have shown that zipping also occurs in the absence of epidermal MyoII (Pasakarnis et al., 2016). Such a function for MTs is in accordance with previous work of Jankovics & Brunner (2006), who have shown that MTs are required exclusively during zipping, whereas in the absence of MTs, zipping arrests. Furthermore, in the absence of MTs, cells from opposing epithelial sheets recognise each other and form adherence junctions. Therefore, MTs are not essential for cell-cell recognition or junction formation (Eltsov et al., 2015).

1.3.3.6 A role for dynein in zipping force generation

Eltsov et al. (2015) suggested a role for MTs in force generation as, during the shortening of the lamellar overlap, which likely generates the zipping force, these overlaps were crowded with MTs, whereas actin bundles were absent. In addition, they detected more shrinking MTs than growing MTs.

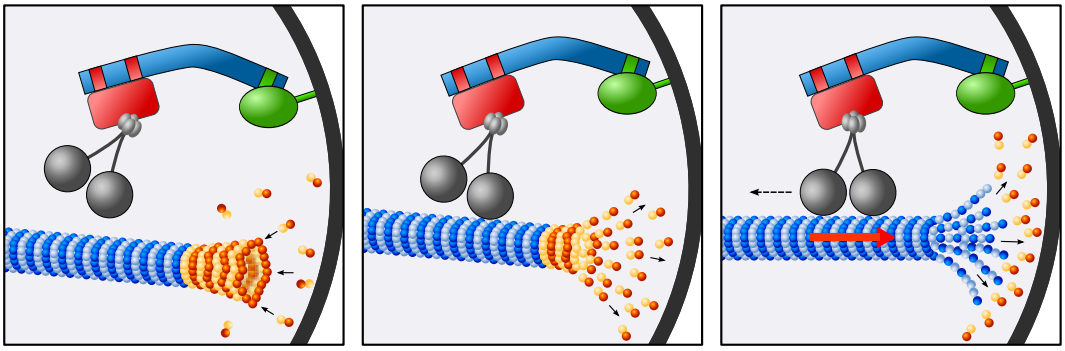

Figure 4: A possible mechanism for microtubule and cortical dynein mediated pulling force generation during zipping.
The minus-end directed motor protein dynein is tethered to the cell cortex presumably by other cortical anchors. Dynein captures incoming microtubule plus ends, and pulls on them by walking towards their minus end, even while they are depolymerising. The resulting pulling might provide the zipping force and drag the epithelial sheets together (adapted from Nguyen-Ngoc et al., 2007).

As the majority of shrinking MT plus ends are localised end-on at the putative adhesion sites, this indicates that MTs are not freely deploymerising but are tethered to the cortex. Such a MT behaviour points to a well-known mechanism: In

Caenorhabditis elegans one cell stage embryos as well as human cells, cortically anchored dynein motors position mitotic spindles by pulling on astral MTs. Thereby, dynein captures incoming MT plus ends and pulls on them by walking towards their minus ends, even while they are depolymerising. The same mechanism might also drive zipping during DC.

1.4 The microtubule motor dynein

To move, divide and spatially organise their teeming interiors, eukaryotic cells use motor proteins to transport cargoes and generate forces along cytoskeletal filaments. Dynein, kinesin and myosin are the three major families that convert chemical energy in form of ATP (adenosine triphosphate) into mechanical forces and movement. Whereas myosins are actin-based motors, dyneins and kinesins move along MTs. Dyneins moves towards the minus ends of MTs, which in most cells are collected into the MT organising center (MTOC) near the nucleus, while kinesins move towards MT plus ends, which in most cells extend towards the cell periphery. Yet there is one exception within the kinesin family. Members of the kinesin-14 family move like dynein towards the minus ends of MTs (Kardon & Vale, 2009).

Dynein was discovered in the 1960s as an ATPase in *Tetrahymena pyriformis* cilia and was named after the unit of force, the dyne, by Gibbons and Rowe (Gibbons, 1963; Gibbons & Rowe, 1965). There are three classes of dyneins. The majority belong to the axonemal dyneins, which drive coordinated beating of cilia and flagella. Only two dyneins, however, transport cargoes along MTs: intraflagellar (IFT) dynein, which transports proteins in the axoneme; and one cytoplasmic dynein, which performs most of all minus-end directed transport within the cytoplasm, such as transport of organelles, mRNA and proteins (Wickstead & Gull, 2007; Höök & Vallee, 2006; Kardon & Vale, 2009). Cytoplasmic dynein (hereafter referred to simply as dynein) was also shown to be involved in various force generating processes, which will be described in Section 1.4.3.

1.4.1 Dynein composition

Dynein is unique compared with kinesin and myosin because dynein molecules form a large multi-subunit complex ($\sim 1.5MDa$). Cytoplasmic dynein comprises two identical heavy chains as well as several intermediate, light-intermediate and light chain subunits (reviewed in King, 2000).

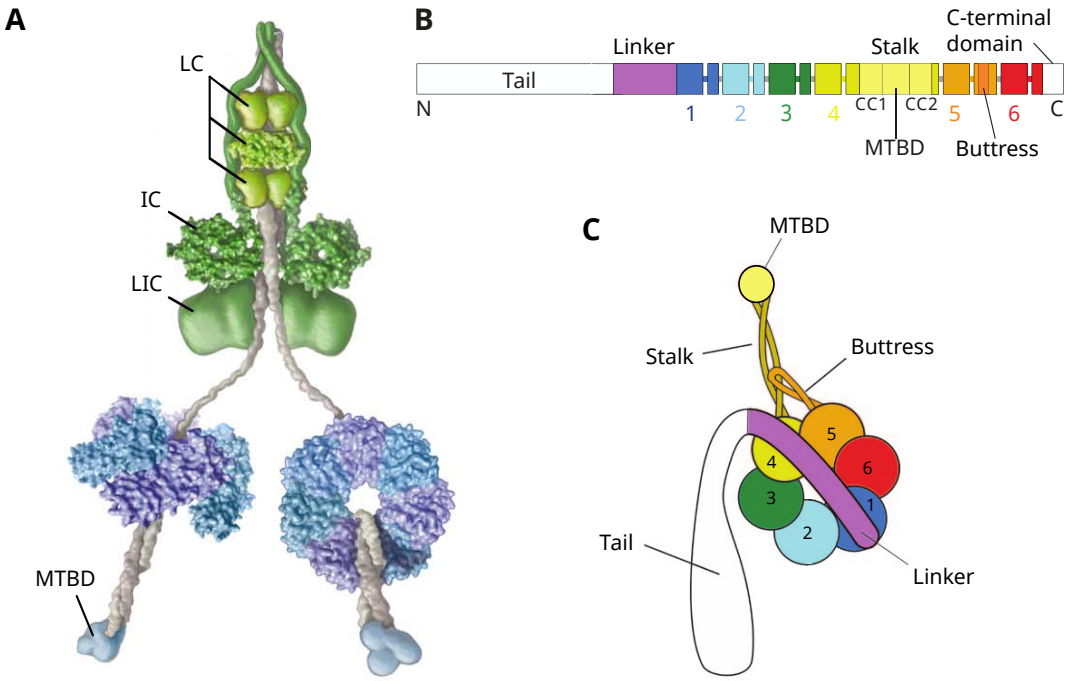

Figure 5: Cytoplasmic dynein.
(A) Representative structure of cytoplasmic dynein. Dynein is a minus-end directed MT motor protein. It binds MTs through a microtubule-binding domain (MTBD) and the end of the coiled-coil stalk (grey). The motor domain is composed of a ring of six AAA+ domains (blue, purple). The N-terminal tail (grey) is involved in dimerisation and binding to dimers of intermediate chains (ICs), light intermediate chains (LICs) and three light chains (LCs). These accessory chains mediate cargo binding. **(B)** Schematic illustration of the primary structure of cytoplasmic dynein heavy chain, showing the N-terminal tail, the linker, the six AAA+ domains and the MTBD. **(C)** Cartoon of the dynein motor domain organisation. The stalk with the MTBD at its tip emerges from AAA4 and is supported by coiled-coil from the small domain of AAA5, called the buttress. The motile linker spans across the AAA+ ring and connects into the N-terminal tail (adapted from Vale, 2003; Carter, 2013; Schmidt et al., 2012).

Each heavy chain is enormous, about $500kDa$, and serves multiple purposes. The overall structure of the heavy chain is divided into four domains: N-terminal tail, linker, head and coiled-coil stalk. The long N-terminal tail domain binds other structural and regulatory components of the dynein complex and contains docking sites for cargoes. The motor region of dynein consists of the linker and the head domain. The head is composed of a ring of six AAA+ (ATPase associated with diverse cellular activities) domains, of which four bind and hydrolyse ATP. The linker consists of bundles of α-helices and lies across the AAA+ head domain, forming a $10nm$ long rod-like structure and is likely to be involved in driving motility (Burgess et al., 2003; Kon et al., 2005). The stalk domain of dynein was identified as the MT-binding domain (MTBD). It emanates from the C-terminal face of AAA4 (the fourth nucleotide-binding AAA+ domain in the ring), extends as one α-helix of an anti-parallel coiled coil (CC1), forms at the tip the small, globular MTBD, and then returns as the partner helix of the coiled coil (CC2) and joins AAA5, which is a non-nucleotide binding AAA+ domain. Compared to kinesin and myosin motors, in which the polymer- and nucleotide-binding sites are integrated within a single globular domain, a long ($\sim 15nm$) and somewhat flexible coiled-coil separates the motor domain and MTBD in dynein motor proteins (Gee et al., 1997; Koonce, 1997; Carter et al., 2008). Furthermore, it was shown that the affinity of the MTBD for binding to MTs is very sensitive to the configuration of the putative coiled-coil residues in the adjacent region of the stalk. To stabilise a high affinity conformation of the MTBD, on one side, a well structured coiled coil in the region of the stalk adjacent to the MTBD is required and on the other side, a correct alignment between the two strands of the coiled coil, CC1 and CC2, is required (Gibbons et al., 2005).

1.4.2 Dynactin: the dynein activator complex

A complex dynein is often associated with, is dynactin (dynein activator complex). It is a multi-subunit protein that directly interacts with dynein and is required for many cellular functions of cytoplasmic dynein in eukaryotes, including organelle transport and mitotic spindle assembly (reviewed in Schroer, 2004). Its largest subunit is p150 Glued, which plays a particularly important role, as it participates in direct interaction with dynein and enhancement of dynein's motor processivity (Karki & Holzbaur, 1995; Vaughan & Vallee, 1995). However, to function properly in *Drosophila*, it was shown that p150 Glued must be associated with the other dynactin subunits, because mutations that prohibit Glued from being incorporated into dynactin result in a non-functional protein (McGrail et al., 1995).

Another dynactin subunit is p50 dynamitin. Overexpression of dynamitin causes dynactin to dissociate from dynein. Therefore, all dynactin-dependent dynein processes will be inhibited. This was successfully shown not only in tissue culture and transgenic mice, but also in the *Drosophila* oocyte and syncytial embryos (LaMonte et al., 2002; Burkhardt et al., 1997; Sharp et al., 2000b; Januschke et al., 2002).

1.4.3 Dynein function in force generation

Cytoplasmic dynein is primarily known as a minus-end directed MT motor for transport of different cargoes along the cytoskeletal tracks. Yet, cortically localised dynein has been shown to capture and tether MTs to the cell periphery, thus exerting tension on the MTs (Laan et al., 2012a; Hendricks et al., 2012). Due to MT dynamic instability, a process in which MTs undergo alternating periods of growth and shortening, MT plus ends can explore the cellular space (Kirschner & Mitchison, 1986). Thus, selective anchoring of MT plus ends at the cell cortex can contribute to processes such as spindle and nuclei positioning or fibroblast migration (Kiyomitsu & Cheeseman, 2012; Kotak et al., 2012; Vogel et al., 2009; Dujardin et al., 2003). Thereby, cortical-tethered dynein applies a pulling force on the MT cytoskeleton by either walking towards the minus end of MTs or binding to depolymerising MT plus ends (Laan et al., 2012a; Hendricks et al., 2012).

A very prominent model of spindle positioning occurs during asymmetric cell division of the *C. elegans* one cell stage embryo. In this model, cortical-attached dynein exerts pulling forces on the plus ends of astral MTs that reach the cortex. During metaphase and early anaphase, positive regulators of dynein are more concentrated at the posterior cortex of the embryo which leads to a greater net pulling force towards the posterior end. Thus, the spindle moves towards the posterior side, so that cytokinesis generates daughter cells of different sizes (Gönczy et al., 1999; Grill et al., 2001, 2003; Park & Rose, 2008).

1.4.4 Cytoplasmic dynein function during early *Drosophila* development

In *Drosophila Dhc64* encodes the cytoplasmic dynein heavy chain polypeptide and shows high similarity in sequence and structure to cytoplasmic dynein isoforms reported for other organisms. Dhc64 is expressed throughout embryogenesis in adult ovaries and testes, as well as at other developmental stages (Hays et al., 1994; Li et al., 1994). Several *Dhc64* mutations have been isolated in an EMS screen and characterised, providing direct evidence that dynein heavy chain is essential for

Drosophila development (Gepner et al., 1996).

Dynein has been shown to be essential for *Drosophila* oocyte patterning. It is required for proper localisation of *bicoid* and *oskar* mRNAs to the anterior cortex and posterior pole, respectively, which define the anterior-posterior axis of the egg and future embryo. Moreover, dynein is involved in anchoring the oocyte nucleus to the cell cortex (Januschke et al., 2002; Duncan & Warrior, 2002). Furthermore, dynein was shown to regulate spindle positioning during early oogenesis (McGrail & Hays, 1997). During *Drosophila* embryogenesis, *Dhc64* mutant analysis revealed that dynen is essential for spindle pole separation during mitotic divisions occurring in the syncitial cytoplasm of the developing embryo (Robinson et al., 1999). Moreover, a model was proposed, in which dynein is anchored to the cortex and pulls on astral MTs, thus helping to separate the spindle poles in early *Drosophila* embryos (Sharp et al., 2000a).

However, dynein function has not yet been studied at later stages of embryogenesis, e.g. during dorsal closure, as homozygous dynein mutants complete embryogenesis, suggesting that maternally provided dynein function is sufficient for embryonic development (Gepner et al., 1996). Most of the described dynein effects during oogenesis and early embryogenesis were analysed in either homozygous dynein mutant clones, or in eggs and embryos of heteroallelic female adult flies, of which the majority of embryos arrests in early embryogenesis before cellularisation (McGrail & Hays, 1997; Robinson et al., 1999).

1.5 Experimental tools used in *Drosophila*

1.5.1 The Gal4/UAS system: two-component system for targeted gene expression

Over the years, researchers have developed a vast array of genetic tools that make *Drosophila* an attractive model organism for research. One such tool is the Gal4/UAS system, which is a binary expression system allowing spatial and temporal expression of genes of interest during *Drosophila* development (Brand & Perrimon, 1993). This system is based on the yeast *Gal4* gene, which encodes a transcription activator protein GAL4, and the GAL4 DNA binding-motif UAS (Upstream Activation Sequence). Binding of GAL4 to UAS activates gene transcription of a gene fused to the UAS enhancer. One can use this system for spatial and temporal control of gene expression. Thereby, *Gal4* is placed under the control of a cell- or tissue-specific enhancer/promoter, which in turn can activate for example, a wild-type or modified

gene, or a fluorescent reporter controlled by the UAS promoter. A large number of *Gal4* lines was created in the last decades allowing expression of target genes in a variety of tissues. Furthermore, numerous extensions to the Gal4/UAS system have been made, making it a powerful and versatile tool for various applications to study mechanisms that control development (reviewed in Duffy, 2002).

1.5.2 Methods for protein depletion

To study a gene function using mutant alleles can be limiting, in particular during later stages of *Drosophila* development. One reason might be that mutants do not reach the developmental stage of interest at all, or if they do, defects might have accumulated earlier in development, thus making it difficult to evaluate whether the observed phenotype is a direct consequence of the mutation at this stage, or if it is because of earlier accumulated defects. Furthermore, maternal contribution can mask a possible phenotype during embryonic development. An alternative to mutant alleles is RNA interference (RNAi), a widely used method resulting in the mRNA depletion of the target gene. Expression of RNAi against a gene of interest can be spatially and temporally controlled using the Gal4/UAS system. However, also RNAi has some limitations, in particular during embryogenesis. If maternally provided proteins are stable, depletion of newly expressed mRNA may not have a significant effect. Yet, in later stages of *Drosophila* development, RNAi has proven to work successfully. Recently, methods have been developed to acutely deplete proteins. Two established methods in *Drosophila* will be described in the next sections.

1.5.2.1 The deGradFP system

The deGradFP system is a method for direct and fast depletion of target GFP-tagged proteins that has recently been established by Caussinus et al. (2012). It relies on the evolutionary highly conserved ubiquitin degradation pathway and thus can be used in any eukaryotic system. Ubiquitin mediated protein degradation is carried out by a cascade of specialised enzymes (E1, E2 and E3), which results in the binding of ubiquitin to lysine residues of targeted proteins. The polyubiquitinated proteins are subsequently degraded by the proteasome (Ciechanover, 1998). The E3 ubiquitin ligases contain different F-box proteins (FBPs) that determine substrate specificity. Caussinus et al. generated a fusion protein, consisting of the F-box domain of a *Drosophila* FBP, Slmb (Jiang & Struhl, 1998), fused to a single-domain

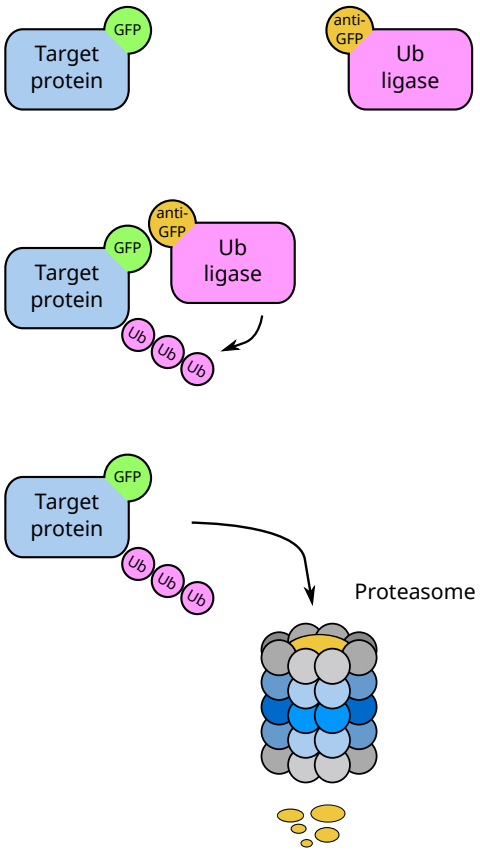

Figure 6: Protein depletion using the deGradFPsystem.
The deGradFP system takes advantage of the conserved ubiquitin degradation pathway. A protein of interest tagged with GFP will be recognised by the anti-GFP nanobody. This recognition will lead to the covalent attachment of multiple ubiquitin molecules to the substrate protein and the subsequent degradation by the proteasome.

antibody fragment VhhGFP4, which is directed against GFP. Thus, expression of NSlmb-vhhGFP4, also termed anti-GFP nanobody, leads to the degradation of GFP-tagged proteins. As the GFP tag allows easy monitoring of protein removal, this method is called deGradFP (degrade Green Fluorescent Protein). Protein depletion can be performed in a time- and tissue-specific manner, as the anti-GFP nanobody expression can be controlled by the Gal4/UAS system (Brand & Perrimon, 1993).

1.5.2.2 TEV induced protein inactivation

The TIPI (TEV protease induced protein inactivation) system was shown to target proteins for degradation in a controlled and reversible way in *Saccharomyces cerevisiae* (Taxis et al., 2009). This system was adapted for *Drosophila* by former members of our laboratory. In the TIPI system, a dormant N-degron is attached to

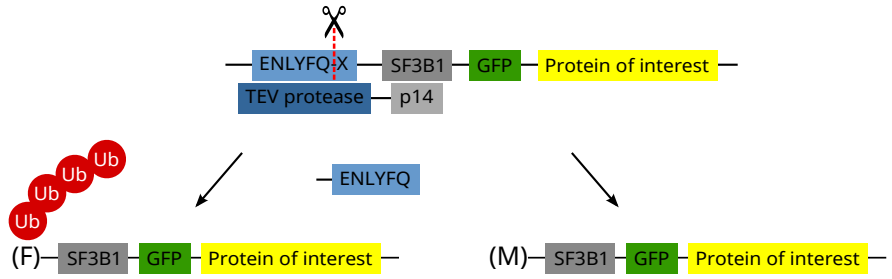

Figure 7: Protein degradation using the TIPI system.
The TIPI-tag containing the dormant N-degron is fused to the 5'-end of a GFP-tagged protein of interest. Upon TEV expression, the protease binds to the target protein. Binding is mediated by the interaction of p14 with SFB1. This interaction directs efficient cleavage of the TIPI-tagged protein by the TEV protease at its recognition site (ENLYFQ-X). TEV cleavage leads to the deprotection of the dormant N-degron. The exposed amnio acid X will determine the fate of the protein; X=M leads to a stable protein, X=F renders an instable protein, which will be poly-ubiquitylated and degraded by the proteasome.

a protein of interest that can regulate the rate of protein degradation. N-degrons constitute natural or artificial amino-terminal tags, which are proteolytically processed, leading to the exposure of an amino acid other than methionine at the N-terminus of a protein. The exposed amino acid serves as a recognition signal for poly-ubiquitylation, which leads to the degradation mediated by the ubiquitin-proteasome system (UPS). The degradation is based on the N-end rule pathway, in which the first amino acid of a mature protein determines the half-time and thus the stability of the protein (Bachmair et al., 1986). This degradation mechanism was shown to be conserved from bacteria to higher eukaryotes (Varshavsky, 1997).

Taxis et al. (2009) developed an N-degron which is protected by an attached peptide that can be removed by proteolysis using the site-specific tobacco etch virus (TEV) protease. The TEV protease recognises a very specific seven amnio acid recogntion site and cleaves between position 6 and 7. As the TEV protease tolerates different amnio acids at position 7, it allows changing the amino acid at this position (Kapust et al., 2001). Upon TEV cleavage, this amino acid will become the new N-terminal amino acid of a protein, thus determining its stability. With this method it is possible to induce degradation by unmasking the N-degron upon TEV-mediated cleavage. The affinity of the TEV protease to its cleavage site was enhanced by the SF3B1 protein domain, which is fused to the TEV recognition site. The TEV protease in turn is fused to the human splicesome subunit p14 (Spadaccini et al., 2006), a direct binding partner of the SF3B1 domain. In addition, tagging the protein of interest with GFP allows one to monitor its degradation. To perform an acute protein knockdown, the Gal4/UAS system (Brand & Perrimon, 1993) can be

used for time- and tissue-specific TEV expression.

1.5.3 The CRISPR/Cas9 system

The clustered regularly interspaced short palindromic repeat (CRISPR)/CRISPR-associated (Cas) system is an extraordinarily powerful tool that has been developed recently for inducing site-specific double-strand breaks (DSBs) in the genomes of a variety of organisms. CRISPR/Cas has been discovered in bacteria and archaea acting as an adaptive defence system against viruses and plasmids (Jansen et al., 2002; Koonin & Makarova, 2013; Jinek et al., 2012). Upon host invasion, small DNA fragments from the invading virus, termed protospacers, are captured and integrated into the microbial genome to form a CRISPR array (Kim & Kim, 2014). Such a CRISPR array consists of short palindromic repeats of approximately $20bps$ which are separated by the protospacers, hence giving the name of the system (Brouns et al., 2008). Following this adaptive phase, the CRISPR array is transcribed into precursor CRISPR RNA (pre-crRNA), which is then processed into small crRNAs that guide Cas endonucleases to cut foreign DNA by base pairing between the $20nt$ spacer sequence in the crRNA and the DNA (Brouns et al., 2008; Jinek et al., 2012).

Three types (I - III) of CRISPR systems have been identified that differ in Cas protein function in crRNA biogenesis, and the recognition and destruction of the foreign DNA. While types I and III require big Cas protein complexes, type II only requires one Cas protein, Cas9, found in *Streptococcus pyogenes* (Makarova et al., 2011). In the type II CRISPR system, a trans-acting crRNA (tracrRNA) is required to form a complex with the crRNA and targets its incorporation into the Cas9 complex (Jinek et al., 2012). For use in genome engineering, the crRNA and tracrRNA were fused into a single synthetic guide RNA (sgRNA or gRNA), making it a two component system for the induction of DSBs at defined sites (Gasiunas et al., 2012; Jinek et al., 2012). However, binding of the Cas9/gRNA complex at a genomic target site requires a trinucleotide protospacer adjacent motif (PAM), which for the commonly used Cas9 is NGG (Sternberg et al., 2014). Cas9-mediated DNA cleavage of both strands occurs within the target sequence three nucleotides upstream of PAM (Gratz et al., 2013b).

Several reserach groups have developed different CRISPR/Cas9 tools to make use of this powerful system for efficient genome engineering in *Drosophila* (reviewed in Bassett & Liu, 2014; Xu et al., 2015).

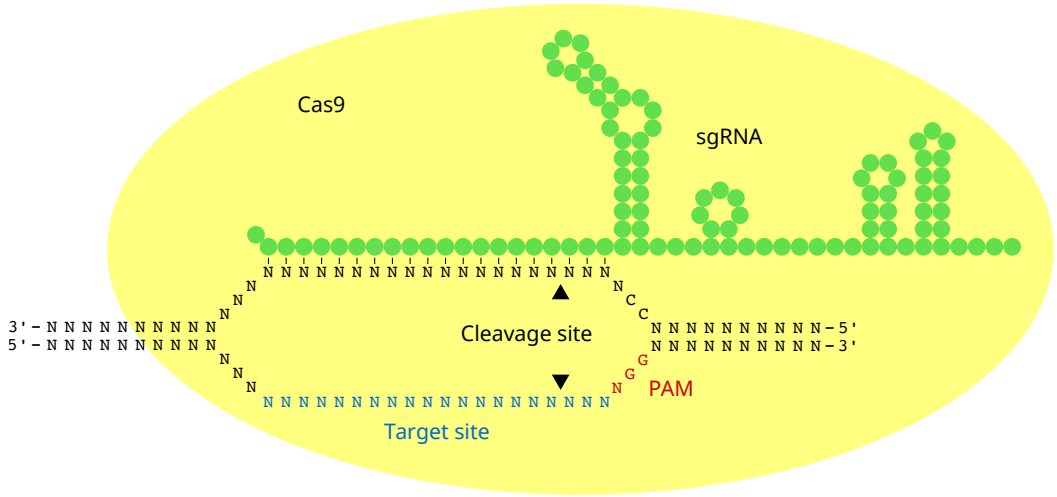

Figure 8: Two-component CRISPR/Cas9 system for genome editing.
The Cas9 protein (yellow oval) is recruited to a target site (blue) in the DNA by a 20nt complimentary sequence in the guide RNA (sgRNA, green). To mediate DNA cleavage Cas9 requires a PAM site (NGG in red) in the DNA. A double-strand break is made three nucleotides from the PAM sequence on both strands of the DNA (cleavage site, black triangles; adapted from Bassett & Liu, 2014).

1.6 Aim

Zipping represents the last step in dorsal closure, which is needed to seal the gap. It starts at the anterior and posterior canthi of the dorsal opening, where two zipping fronts sweep towards each other until they meet at the midline and form a continuous epidermis. During zipping, opposing leading edge cells with identical positional identity recognise each other and build up adhesion sites. By pulling on each other, they bring the next neighbours into closer proximity and thereby push the interjacent amnioserosa cells down inside the embryo.

The aim of my PhD research was to elucidate two mechanisms that are required for the zipping process during dorsal closure: the zipping force, which pulls the epithelial sheets together; and cell-cell recognition, which allows finding the right partner within the opposing leading edge cells. The study of these two mechanisms, described further below, are treated as two independent projects within this thesis and, as such, are detailed in separate results and discussion sections.

1) Zipping force

Recent data (Eltsov et al., 2015) suggests that zipping force is mediated by MTs and not, as previously thought, predominately by actin. A mechanism was suggested, in which the MT motor protein dynein plays a key role. Thereby, dynein is tethered

to the cell cortex, captures the plus ends of incoming MTs and pulls on them by walking towards their minus end and thus providing the zipping force, which drags the epithelial sheets together.

To test this hypothesis, I used various methods to interfere with MT and dynein function during dorsal closure.

2) Cell-cell recognition

The alignment of epithelial sheets occurs with high accuracy resulting in a perfectly established pattern across the fusion seam. To form such a precise pattern, each cell within the leading edge must specifically recognise its matching cell in the opposing epithelial sheet. Although, it is known that filopodia are needed for the recognition process, only little is known about the molecular basis for cell-cell recognition.

To find molecules involved in cell-cell recognition I performed an EMS forward genetic screen and examined candidates, that were shown to play a role in axon guidance.

2 Results: Part 1

2.1 Microtubule dynamics during zipping

2.1.1 Laser cutting experiments on microtubules

Electron tomography data (Eltsov et al., 2015) suggests that zipping is not mediated predominately by actin (Jacinto et al., 2000) as previously thought, but instead microtubules (MTs) may play a significant role in force generation during this process. After initial cell-cell contacts are formed by filopodia of matching leading edge (LE) cells, their lamellipodia expand to generate a single overlap surface. The number of MTs in these overlap regions rapidly increases while actin bundles disappear. The MTs are dynamic, and both growing and shrinking MT plus ends can be detected. As zipping progresses, the overlap regions shorten, which is likely to generate the zipping force. During this part of the process the distribution of growing and shrinking MTs changes. An excess of shrinking MT plus ends is present and these ends are localised in the regions of cell-cell contacts. This suggests that MTs are attached close to cell membranes and their shrinking ends exert a pulling force. A protein, which has been shown to attach MTs to the cell cortex and play a role in generating pulling forces is the minus-end directed motor dynein (Adames & Cooper, 2000; Laan et al., 2012a). We hypothesise that cortical dynein interacts with these MTs at the cell cortex during zipping.

If dynein is pulling on MTs, tension should build up simultaneously within the zipping cells, thus generating the zipping force. To test this, I performed laser cutting experiments on MTs in zipping and non-zipping cells. The aim of these cuts was to observe a loss of such tension, which can be reflected by tissue relaxation. For this experiment, I used embryos expressing two cytoskeletal markers: GFP-tagged β-tubulin (tubulin-GFP), a marker for MTs and thus MT bundles; and an mCherry-tagged actin binding fragment of Moesin (mCherry-Moesin), a marker for actin. As both markers are expressed under the control of the UAS promoter, I used the *pannier* (*pnr*) enhancer element, which was shown to express Gal4 in the dorsal epidermis (Herranz & Morata, 2001). Occasionally, leaky expression in a few amnioserosa (AS) cells can be observed using this driver. The position of the laser was set such that the apically localised MTs in LE cells would be cut perpendicular to their orientation (Figure 9). MTs bundles were cut in single LE cells as well as in several consecutive LE cells. The timing of the cuts was attempted such that the cells would have already formed initial contacts by filopodia of opposing LE cells.

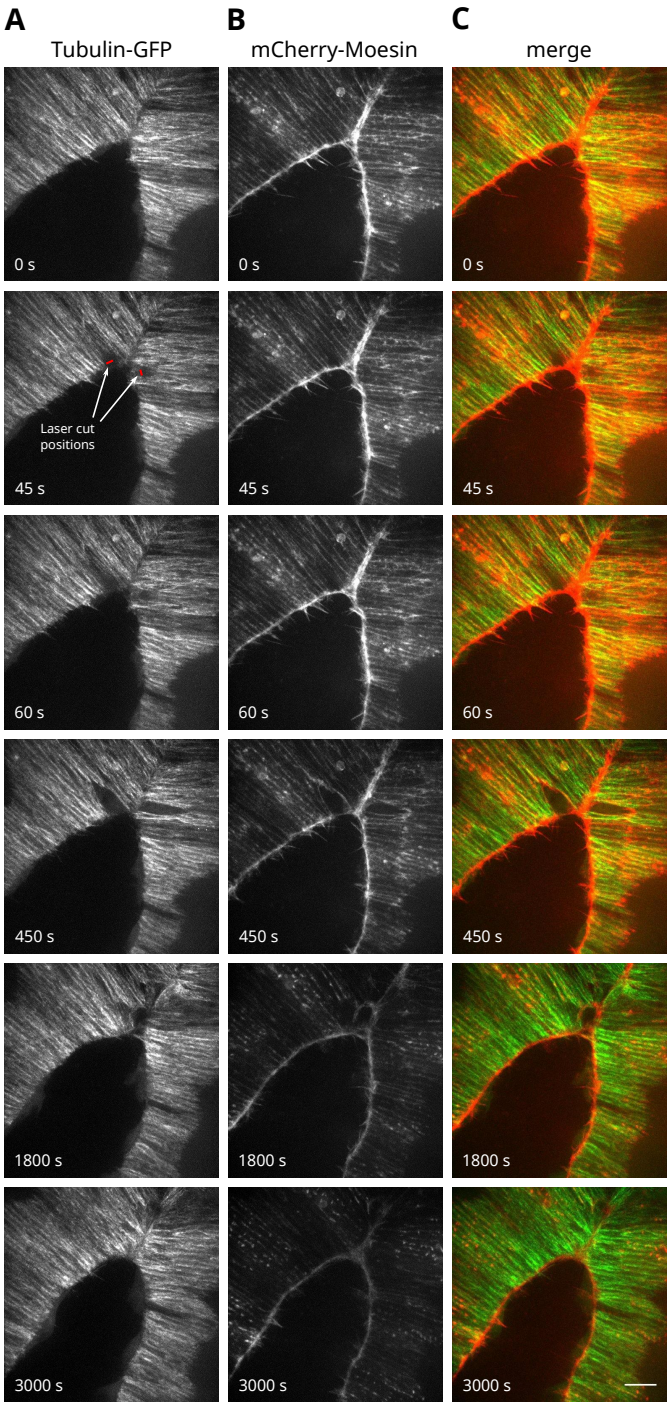

Figure 9: Laser incisions of microtubules in leading edge cells during zipping. Movie sequences of one embryo expressing tubulin-GFP **(A)**, mCherry-Moesin **(B)** and overlay **(C)**. Arrows pointing to laser cut positions in leading edge cells at the posterior zipping canthus. Laser cuts occur at time point $45s$. Later time points show the progression of zipping after laser cuts. Actomyosin ring as a result of wound healing reaction visible at time points $450s$ and $1800s$. Scale bar: $10\mu m$.

Only during mid-zipping stage we expect dynein to pull on MTs, which would lead to an increase of tension in zipping cells.

As a result of such laser incisions, I often observed the loss of both fluorescent signals, tubulin-GFP and mCherry-Moesin, at and around the cut sites, thus preventing the direct observation of possible tissue relaxation. Subsequently, an actomyosin cable formed surrounding the cut sites, which indicated a wound healing response. This suggests that the laser incisions injured the cell rather than cutting only MTs. Such wounds were eventually closed by the actomyosin cable that formed around the cut site, which was shown to act as a contractile purse string (Martin & Lewis, 1992). These injuries likely resulted from cutting the plasma membrane of LE cells. As MTs are localised close to the apical cell cortex, cutting only MTs without injuring the membrane of cells, is very challenging. In other laser cutting attempts using less laser power, only MT bleaching was observed. Thus, these experiments did not give any conclusive results, as it was not possible to cut MTs precisely.

In general, such an experimental setup is not trivial as each experiment requires new adjustments of laser power and a very high level of positional accuracy. Furthermore, the timing of the laser cuts had to be selected carefully as zipping seems to occur in waves, meaning there is a wave of fast zipping, followed by a short break after which another zipping wave starts. A more precise laser cutter might be more suitable for future attempts.

2.1.2 Taxol-induced stabilisation of microtubules

Recent experiments have shown that MTs are essential for zipping during dorsal closure (DC) (Jankovics & Brunner, 2006). The MT depolymerising drug colcemid resulted in arrested embryonic development without completing DC. The convergence of the two epithelial sheets was not affected as they moved towards the dorsal midline with a similar velocity as in control embryos and AS cells displayed normal apical constriction. Zipping, however, was strongly affected by the absence of MTs. The dorsal opening became abnormally narrow as a result of an almost absent zipping process. Furthermore, ectopic expression of the MT-severing protein Spastin in epithelial cells led to MT disassembly and caused a zipping arrest (Jankovics & Brunner, 2006). These experiments show that zipping halts in the absence of MTs.

As our hypothesis suggests that depolymerising microtubules are tethered to the cell cortex by cortical dynein and drive the zipping force, I was interested in finding out how zipping is affected when MT depolymerisation is inhibited. A drug, which was described to mediate inhibition of MT depolymerisation is taxol. Taxol

suppresses the dynamic instability of MTs by stabilising GDP-bound β-tubulin in MTs. Thus, even when GTP hydrolysis occurs at the tip of MTs, no depolymerisation takes place and hence, no MT shrinkage occurs (Schiff et al., 1979; Kumar, 1981; Jordan et al., 1993; Derry et al., 1995).

2.1.2.1 Microtubule dynamics are lost in taxol-treated embryos

First, I tested if taxol inhibits MT depolymerisation during DC. To monitor MT dynamics, I used embryos expressing EB1-GFP, a marker for growing MT plus ends. (Rogers et al., 2002; Akhmanova & Hoogenraad, 2005; Jankovics & Brunner, 2006). I injected a $10mM$ taxol concentration posteriorly into the yolk of DC stage embryos expressing EB1-GFP. As a control, I injected DMSO, the solvent for taxol, into embryos expressing the same marker. Real-time imaging of EB1-GFP in DMSO control embryos showed bidirectional movement of EB1 dots in the epidermis as a consequence of the previously described antiparallel orientation of MTs along the apical side of epithelial cells (Jankovics & Brunner, 2006). On the other hand, in taxol-treated embryos we did not observe EB1 movement, showing that MT dynamic instability is absent. The movement of EB1 dots in taxol-treated embryos and control embryos is illustrated by the kymographs in Figure 10A.

To confirm that MTs are stabilised in taxol-injected embryos, I performed a FRAP experiment with tubulin-GFP expressing embryos. MTs were partially photobleached, covering several epidermal cells perpendicular to the MT bundles. In wild-type embryos we observed fast recovery, however the movie was not long enough to see if full recovery would occur. In contrast, GFP recovery in taxol-treated embryos seemed to be low and very slow (Figure 10, B and C). These results show different GFP recovery kinetics for taxol- and non-taxol-treated embryos. However, to determine the tubulin-GFP turnover in taxol-treated and control embryos more FRAP experiments with the same conditions have to be performed.

Taken together, these results clearly show that taxol-mediated inhibition of MT depolymerisation stabilises MTs during DC.

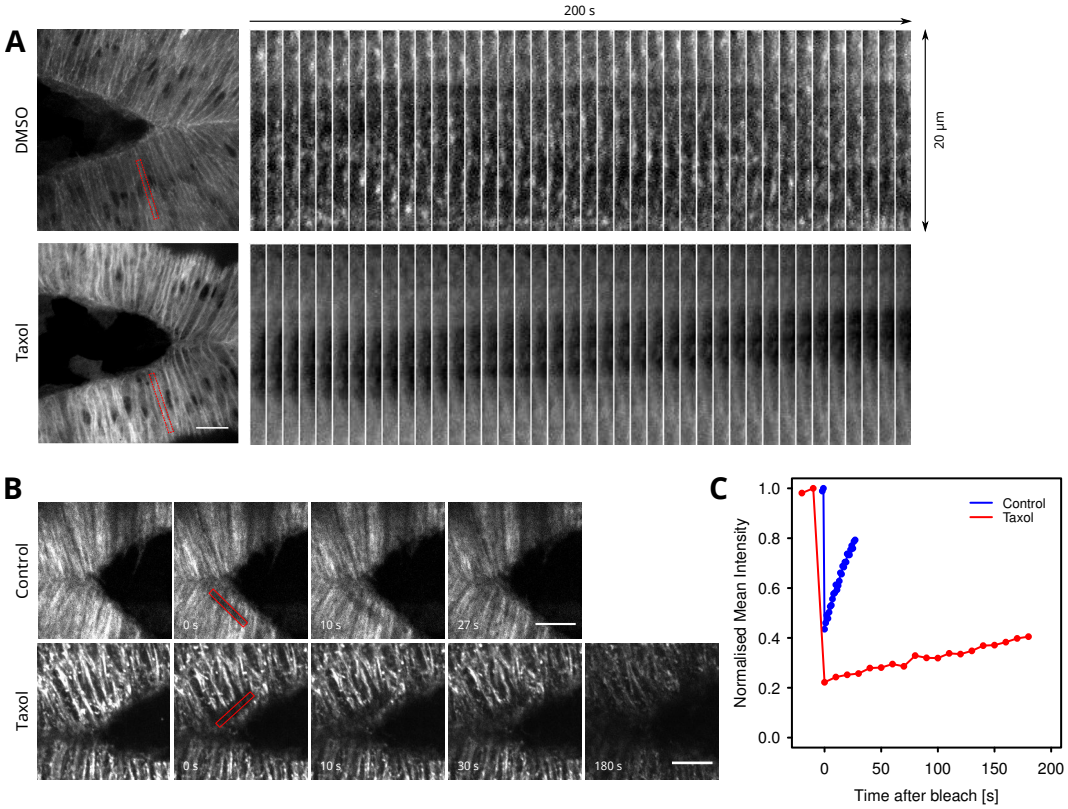

Figure 10: Microtubules in taxol-treated embryos are not dynamic.
(A) EB1-GFP expressing embryos after DMSO and taxol treatment. Kymograph of boxed region showing EB1 movement over 200*s* in DMSO and taxol-treated embryos. Scale bar: 10μm. **(B)** Movie sequences of tubulin-GFP expressing wild-type and taxol-treated embryos in a FRAP experiment. Red boxes show bleach region. Scale bars: 7μm. **(C)** Graph displaying tubulin-GFP recovery kinetics of wild-type and taxol-treated embryos.

2.1.2.2 Taxol-induced inhibition of microtubule depolymerisation leads to a zipping arrest

To further analyse the effect of taxol-mediated inhibition of MT depolymerisation on the zipping process, I injected taxol into embryos at different stages of zipping during DC and imaged them within five to ten minutes after injection. The embryos expressed mCherry-Moesin and tubulin-GFP to visualise actin and MTs respectively. As before, expression was restricted to the epithelium by using *pnrGal4*, which was driving expression of the UAS-controlled cytoskeletal markers, mCherry-Moesin and tubulin-GFP (*pnrGal4* UAS-mCherry-Moesin / *pnrGal4* UAS-tubulin-GFP). As a control, I injected DMSO into embryos expressing the same cytoskeletal markers (Figure 11, A and B).

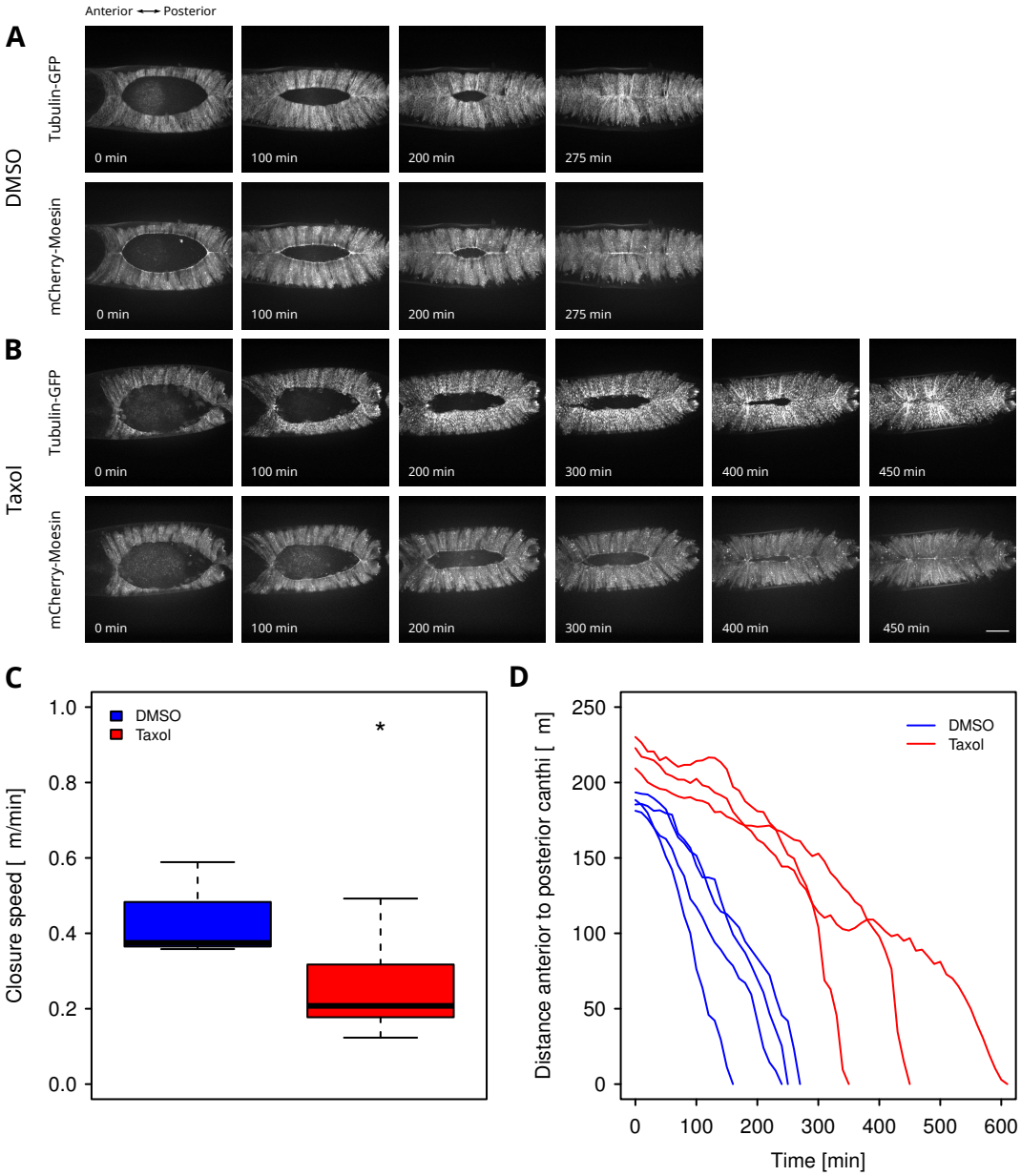

Figure 11: Microtubule-stabilising drug taxol impairs zipping progression. **(A and B)** Movie sequences of tubulin-GFP (upper rows) and mCherry-Moesin (lower rows) expressing embryos. Scale bar: $50\mu m$. **(A)** DMSO-injected embryos. Imaged $5 - 10min$ after injection. **(B)** $10mM$ taxol-injected embryos. Imaged $5 - 10min$ after injection. Closure is strongly delayed in taxol-treated embryos compared to DMSO-treated embryos. **(C)** Box plots displaying the distribution of mean closure speeds of DMSO-treated ($n = 4$) and taxol-treated ($n = 8$) embryos. The whiskers represent the minimum and maximum values. * $p < 0.05$. **(D)** Graph showing zipping kinetics of the epithelial sheets in DMSO and taxol-treated embryos. Progression of zipping was measured every $10min$ starting at various distances between anterior and posterior canthi, but spanning at least $100\mu m$. Each line represents zipping kinetics of one individual embryo.

Live-imaging showed that taxol-induced stabilisation of MTs impaired the zipping process. Compared to the ellipsodial shape we observe during normal zipping (Figure 11A), the dorsal opening became abnormally narrow over time (Figure 11B). This suggests that zipping stops while convergence of the opposing epithelial sheets towards the dorsal midline is not affected by taxol injection. The phenotype is similar to what was observed when injecting the MT depolymerising drug colcemid (Jankovics & Brunner, 2006). However, in the taxol experiments closure eventually completed in 83% of the embryos, although mostly with a strong delay of 3-4 hours approximately. This resulted in a severe puckering phenotype (Figure 12A). Furthermore, as a consequence of taxol-mediated inhibition of MT depolymerisation, I observed long and partially bent MT bundles, which were moving around in the cells, a phenomenon I did not observe in control embryos (Figure 12B). I quantified the mean closure speeds of taxol-treated and DMSO-treated control embryos. The mean closure speeds were significantly slower in taxol-treated embryos compared to DMSO-treated control embryos (Figure 11C). Furthermore, I analysed and plotted the distance between the anterior and posterior canthi over time until the dorsal gap was closed (Figure 11D). This shows that zipping is almost absent at the beginning in taxol-treated embryos, and, as time progresses and epithelial sheets migrate towards each other, closure accelerates and leads to severe puckering. The severe puckering phenotype can be explained as a result of the AS cells undergoing apoptosis, which is an integral part of DC (Reed et al., 2004; Toyama et al., 2008). Thereby, AS cell delamination will further reduce the gap size in a circular manner and bring the epidermis fronts into sufficient proximity to build up contacts accordingly. In addition, we could observe that the actin cable often ruptured close to the anterior canthus (Figure 12A), probably as a result of head involution, a morphogenetic process occurring nearly simultaneously to DC (Campos-Ortega & Hartenstein, 2013; Gilbert, 2000).

In summary, these results indicate that taxol specifically affects the zipping process, as convergence of the epithelial sheets, and therefore the apical constriction of the AS cells seems to progress normally. Moreover, it shows that dynamic MTs are required during the zipping process.

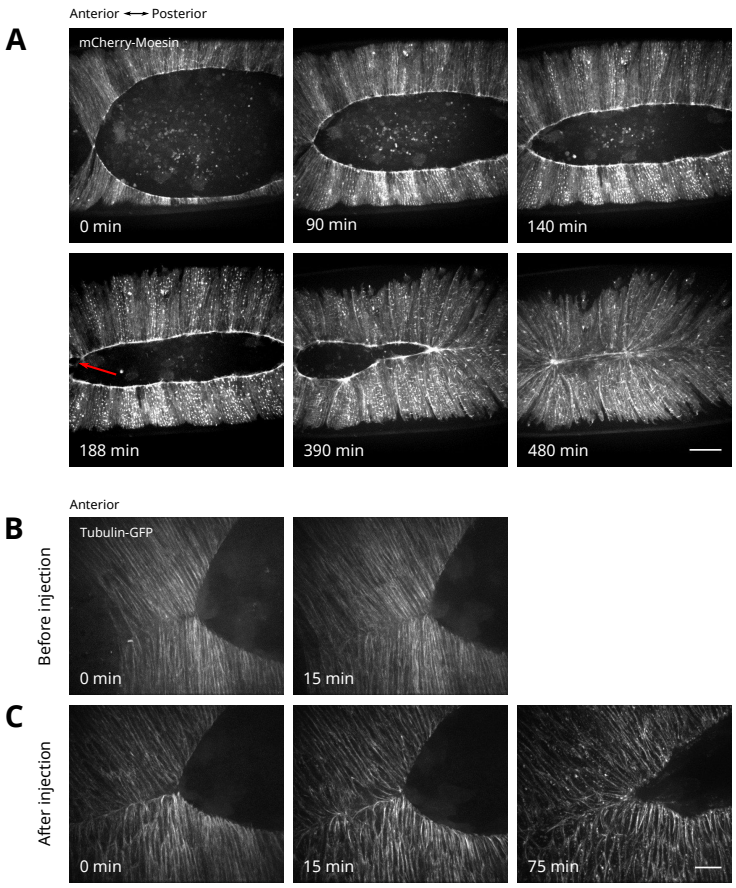

Figure 12: Actin and microtubule cytoskeleton of taxol-injected DC stage embryos.
(A) Movie sequences of a mCherry-Moesin expressing embryo after taxol injection. Scale bar: $30\mu m$. Red arrow indicates rupture of actomyosin cable in leading edge at the anterior side of the embryo. Zipping is mostly absent in taxol-treated embryos. Convergence of epithelial sheets is not affected. Taxol-treated embryos display puckering phenotype (representative images). **(B and C)** Movie sequences of one tubulin-GFP expressing embryo visualising the MT cytoskeleton at 100x magnification before taxol injection **(B)**, and after taxol injection **(C)**. Scale bar: $10\mu m$.

2.2 Dynein function during zipping

Our hypothesis suggests that the minus-end directed microtubule motor dynein generates a zipping force by pulling on microtubules at the cortex of LE cells during DC. To test this hypothesis, dynein function during DC has to be investigated. For this purpose, I studied various available mutants of components of the dynein protein complex as well as of components of dynactin, another protein complex, which has been shown to be required for many dynein functions (Schroer, 2004). Furthermore, I examined the effect of a recently discovered dynein-specific inhibitor, CiliobrevinD, on zipping. The findings will be described in the following sections.

2.2.1 Analysis of the cytoplasmic dynein heavy chain (Dhc64)

The dynein motor proteins are multi-subunit proteins that, compared to other cytoskeletal motors like kinesins and myosins, are much larger in size and more complex. Dyneins consist of two heavy chains, several intermediate chains, light intermediate chains and light chains. The dynein heavy chain gene encodes the protein for producing the actual motor activity as well as the MT binding domain (MTBD; King, 2000). There are seven different dynein heavy chains in the *Drosophila* genome of which six are only expressed in the testes. Only Dhc64 is expressed throughout embryogenesis in all tissues, in adult ovaries as well as at other developmental stages (Li et al., 1994; Hays et al., 1994).

2.2.1.1 Immunostaining shows enrichment of Dhc64 along the leading edge

As there is no live marker to look at Dhc64 expression during DC, I performed an immunofluorescence labelling using antibodies recognising Dhc64. At the same time I used an anti-GFP antibody against armadillo-GFP, the *Drosophila* homolog of β-catenin. Armadillo localises to the cell junctions and therefore provides a good marker for visualising cell borders. Interestingly, the antibody staining revealed dynein enrichment along the first row of epidermal cells (Figure 13A). This is further depicted in Figure 13B where the intensity of Dhc64 is shown to increase from the rear epithelial cells to the LE, before decreasing sharply in the AS tissue.

Mikhail Eltsov, who performed the same experiment in parallel, also observed dynein enrichment at the dorsal end of LE cells (Eltsov et al., 2015). These results support the hypothesis that dynein is involved in generating the pulling force during zipping.

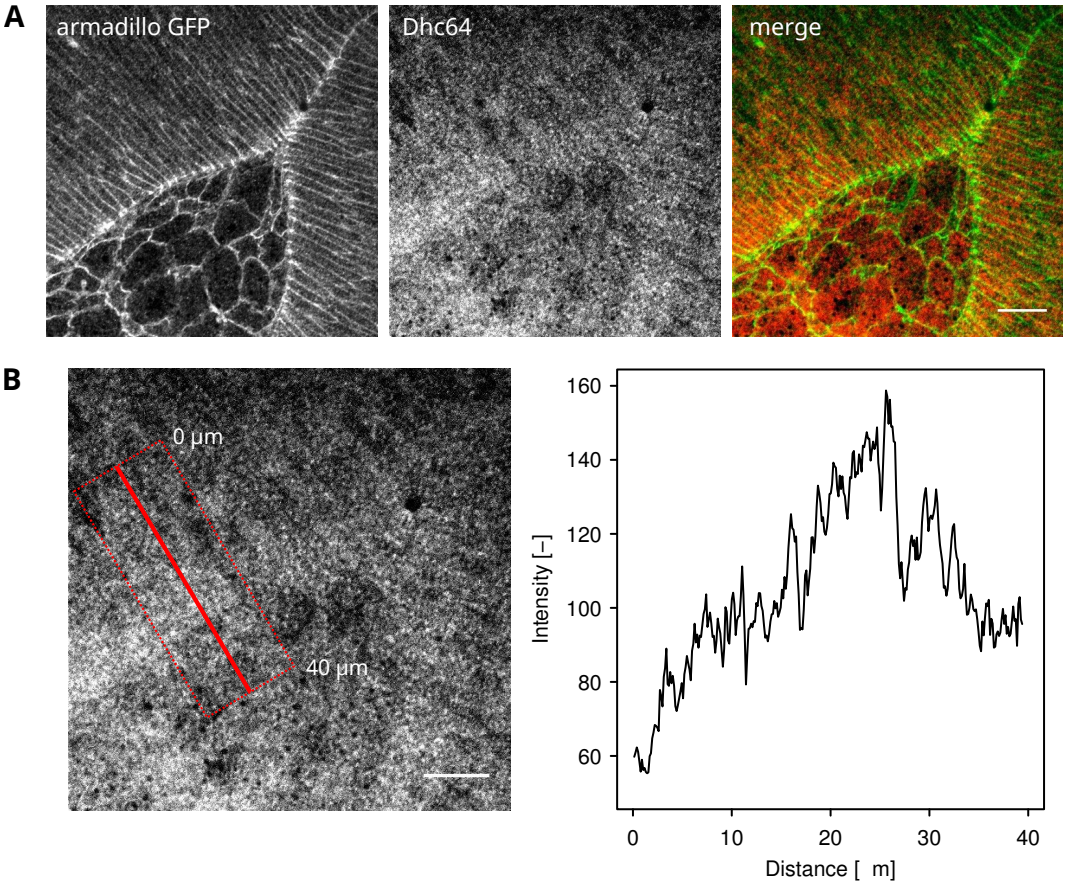

Figure 13: Dynein heavy chain is enriched along the leading edge cells during dorsal closure.
(A) Immunofluorescence labelling of cell boarders (armadillo GFP) and dynein heavy chain (Dhc64). Images show the same single plane. In the merged imaged it can be seen that dynein accumulates in the leading edge cells. **(B)** The graph displays Dhc64 intensity in the boxed region, which is shown to increase from the rear epithelial cells to the leading edge, before decreasing sharply in the AS cells. Scale bars: $10\mu m$.

2.2.1.2 Influence of *Dhc64* mutant alleles on dorsal closure

To study dynein function during zipping, I analysed different mutant alleles of *Dhc64*, the gene encoding the cytoplasmic dynein heavy chain 64 (Dhc64), which is the main Dhc being expressed throughout embryogenesis (Hays et al., 1994; Li et al., 1994). Several *Dhc64* mutant alleles have previously been isolated in an EMS mutagenesis screen by Gepner et al. (1996). It was shown that most of the lethality occurred during larval stages in both homozygous and trans-heterozygous mutant embryos, indicating that zygotic function of dynein is only needed for larval and pupal development. Furthermore, Gepner et al. concluded from lethal phase studies that maternal contribution is sufficient to support most embryogenesis. To support the

conclusion that maternally provided cytoplasmic dynein heavy chain is sufficient for embryonic development, the distribution of three different embryonic markers has been examined in dynein mutants, revealing that morphogenesis during at least the first 16 hours of embryonic development is not affected in dynein mutants (Gepner et al., 1996). However, these experiments were performed using antibody stainings and not the currently available cutting-edge technologies that allow studying development processes like DC live.

I have analysed flies carrying different mutant *Dhc64* alleles (Table 1), which lie on chromosome 3. The mutant alleles were crossed to the fluorescent third chromosome balancer TM3 pAct-GFP to be able to distinguish homozygous from heterozygous mutants during DC. Live-imaging of homozygous *Dhc 4-19*, *Dhc 6-10* and *Dhc 6-8* always resulted in expression of the third chromosome balancer TM3 pAct-GFP for each allele during DC. These observations might indicate that the chromosomes carrying the *Dhc64* alleles have second site lethals that accumulated after having been balanced probably for approximately 20 years. Hence, I examined the trans-heterozygous mutants *Dhc 4-19/Dhc 6-10* and *Dhc 6-8/Dhc 6-10*. Yet again, all analysed DC stage embryos expressed pAct-GFP marker of the balancer. As reported by Gepner et al. (1996), homozygous and trans-heterozygous mutants should be able to complete embryogenesis without major defects. Therefore, the observed effects could be due to the accumulation of a secondary lethal. Although, this seems very unlikely that flies carrying these *Dhc64* alleles would have accumulated exactly the same mutation, as they were kept completely isolated. Alternatively, maternally contributed pAct-GFP marker of the balancer masks homozygosity of the *Dhc64* alleles. Indeed, TM3 pActGFP exhibits strong maternal contribution until at least stage 15 of embryonic development (Reichhart & Ferrandon, 1998). I observed a similar effect of another fluorescent third chromosome balancer TM3 sqh-mCherry.

To avoid further problems with maternal contribution from the balancer markers pAct-GFP and sqh-mCherry, I exchanged them for another third chromosome balancer. This balancer carries a GFP marker controlled by a UAS promoter, which is driven by kruppel-Gal4 (TM3 krGFP Sb; Casso et al., 1999). The mutant alleles *Dhc 4-19* and *Dhc 4-6* were examined with this new balancer. In addition, they carried on the second chromosome the green fluorescent actin marker sGMCA. This marker consists of the *squash* (*sqh*) promoter, which drives expression of a fragement of Moesin tagged with GFP (Kiehart et al., 2000). This marker allowed me to follow the different developmental stages using live-imaging. Embryos homozygous for the *Dhc 4-6* allele developed beyond DC. This suggested that Dhc 4-6 might

Table 1: Analysis of *Dhc64* mutant alleles during dorsal closure.

Mutant	DC phenotype	Used balancer
Dhc 4-19/Dhc 4-19	Lethal before DC, cannot be rescued with *pDhc+*	TM3 krGFP
Dhc 6-10/Dhc 6-10	All show pActGFP expression, balancer has maternal contribution	TM3 pActGFP
Dhc 6-10/Dhc 4-19	All show pActGFP expression, balancer has maternal contribution	TM3 pActGFP
Dhc 6-8/Dhc 6-8	All show pActGFP expression, balancer has maternal contribution	TM3 pActGFP
Dhc 4-6/Dhc 4-6	Proceeds through DC, closes slower than wild-type	TM3 krGFP
Dhc 4-6/Dhc 4-19	Proceeds through DC, closes slower than wild-type	TM3 krGFP

retain partial function as it may not be a complete loss of function, or that maternally provided Dhc64 is sufficient to support embryonic development. However, DC speed analysis showed a decrease in overall closure speed (Figure 14), indicating that zygotic Dhc64 function contributes to DC.

Embryos carrying the *Dhc 4-19* allele were picked around 1 hour after egg-laying and were subsequently imaged. No embryos homozygous for the *Dhc 4-19* allele were observed. The imaged embryos either exhibited GFP expression coming from the balancer or they were unfertilised. This data suggests that secondary lethals accumulated on the chromosome carrying the *Dhc 4-19* allele. We tested this assumption by trying to rescue a homozygous *Dhc 4-19* fly with an additional wild-type copy of *Dhc64 (pDhc+)*, located on the X chromosome, which we obtained from the laboratory of Tom Hays (Gepner et al., 1996). Yet, we could not rescue flies homozygous for *Dhc 4-19*, even after several outcrosses to remove possible secondary lethals. However, it was possible to rescue flies carrying the *dhc 4-19* allele over a *Dhc64* deletion. This strongly suggests the presence of a secondary recessive lethal on the chromosome carrying the *Dhc 4-19* allele. Further, I analysed the trans-heterozygous mutant *Dhc 4-19/Dhc 4-6*. Embryos with this allele combination developed beyond DC, and their mean closure speeds were similar to homozygous *Dhc 4-6* embryos (Figure 14). This suggests that either the *Dhc 4-6* is a stronger

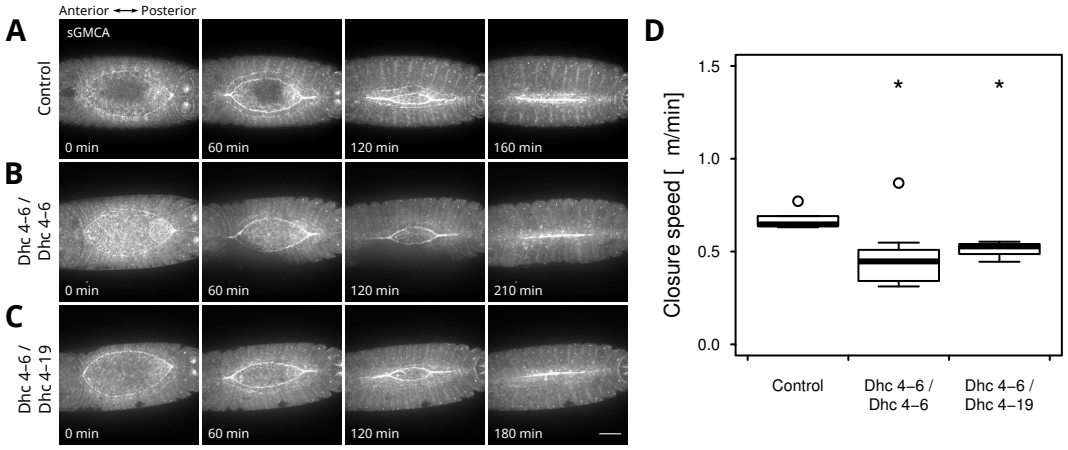

Figure 14: Dynein heavy chain mutants complete dorsal closure with a delay. **(A-C)** Movie sequences of embryos expressing sGMCA. **(A)** Wild-type control embryo, **(B)** homozygous *Dhc 4-6* embryo and **(B)** trans-heterozygous *Dhc 4-6/Dhc 4-19*. Scale bar: $50\mu m$. **(D)** Box plots showing the distribution of closure speeds of control embryos ($n = 5$), *Dhc 4-6/Dhc 4-6* ($n = 8$) and *Dhc 4-6/Dhc 4-19* ($n = 3$). The whiskers represent minimum and maximum values, the circles represent outliers. * $p < 0.05$.

allele than *Dhc 4-19* or additional factors might be present on the chromosome carrying the *Dhc 4-6* allele.

Overall, we can conclude that homozygous as well as trans-heterozygous *Dhc64* mutants are able to proceed through DC without major defects, which is in agreement with the observations made by Gepner et al. (1996). However, we have not tested all existing *Dhc64* mutant alleles, but *Dhc 4-19* as well as *Dhc 4-6* have been described to be strong mutant alleles. Yet, we only observed a decrease in closure speed in such mutant embryos. Thus, one of the major obstacles remaining to study dynein function at the DC stage is the maternal contribution, which seems to be sufficient to support embryonic development. Different approaches to target this problem will be described in Sections 2.4 - 2.6.

2.2.1.3 RNAi against *Dhc64* causes a slight zipping delay but no zipping arrest

As maternal contribution of Dhc64 supports development of the *Dhc64* mutant alleles beyond embryogenesis (Gepner et al., 1996; Section 2.2.1.2), we were not able to analyse *Dhc64* mutants during DC. Hence, I decided to try RNA interference (RNAi) as an alternative method to examine the role of Dhc64 during zipping.

Since the *Dhc64* RNAi construct was expressed under the control of the UAS promoter (UAS-RNAi-*Dhc64*), the RNAi construct was silent unless induced. To

express the RNAi construct, I used the enGal4 driver, which drives UAS-RNAi expression in 4-cell stripes in the epidermis. In addition, *enGal4* is recombined with mCherry-Moesin, an actin marker, also controlled by the UAS promoter (UAS-mCherry-Moesin). To visualise cell stripes in which there was no RNAi expression, the embryos also carried the green fluorescent actin marker sGMCA, which is expressed in the AS tissue and the surrounding epidermis (Figure 15, A and B). Embryos, in which *Dhc64* knockdown was mediated by RNAi, did not exhibit any defects during zipping, both wild-type and RNAi-expressing cell stripes appeared to zip normally. However, when analysing the overall closure speed of embryos in which RNAi expression was driven by *enGal4*, closure was slower than in control embryos without RNAi expression (Figure 15C).

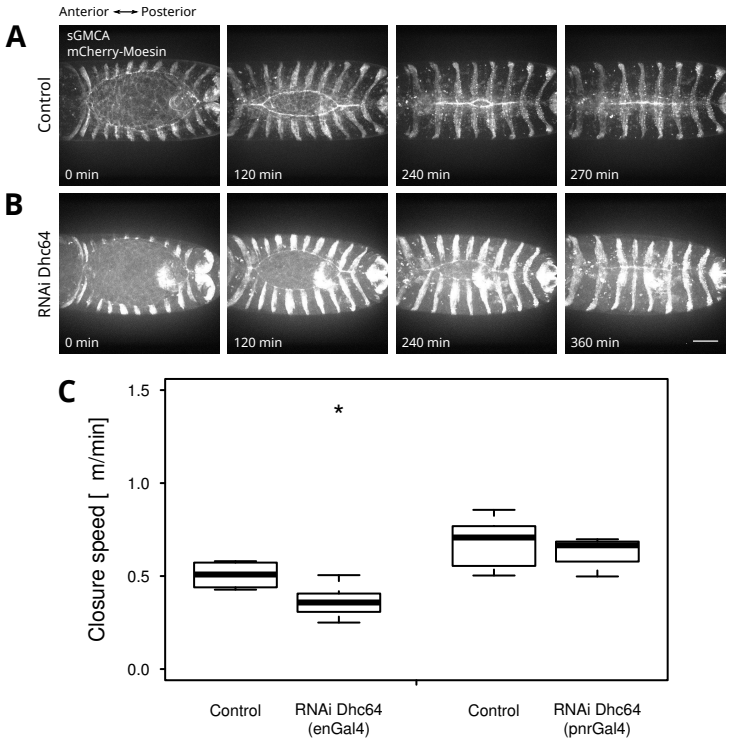

Figure 15: RNAi against *Dhc64* leads to a zipping delay.
(A and B) Movie sequences of embryos expressing sGMCA and *enGal4*, UAS-mCherry-Moesin. **(A)** Wild-type control embryos, **(B)** RNAi Dhc64 construct expresses in engrailed stripes. Scale bar: $50\mu m$. **(C)** Box plots displaying the distribution of mean closure speeds of embryos, in which the UAS-RNAi-*Dhc64* construct is expressed in cell stripes (*enGal4*; $n = 7$) and the whole epidermis (*pnrGal4*; $n = 4$) and their corresponding control embryos (*enGal4*, $n = 14$; *pnrGal4*, $n = 12$). The whiskers represent minimum and maximum values. * $p < 0.05$.

Moreover, I used the *pnrGal4* driver element for Dhc64 RNAi expression in the dorsal epidermis. Although RNAi against *Dhc64* was expressed in the dorsal

epidermis and not only in cell stripes, embryos did not have any zipping problems. Analysis of the overall closure speed did not show differences in speed compared to control embryos (Figure 15C).

Concluding from these results, RNAi against *Dhc64* does not lead to any zipping defects, suggesting that there is insufficient decrease in Dhc64 protein levels or that Dhc64 is not required for DC. Yet, we could observe that the overall closure speed is decreased if RNAi expression is driven by *enGal4*. This could be explained by the fact that *pnrGal4* expression starts only from embryonic stage 10/11 while *enGal4* expression already starts around stage 6 (Tabata et al., 1992; Vincent et al., 2008). Consequently, cells have more time to deplete *Dhc64* mRNA and to loose the protein that was already produced by turnover Furthermore, the yolk cell provides maternally deposited proteins and if the existing proteins are stable, depletion of newly expressed mRNAs does not have a significant effect. Thus, to analyse Dhc64 function during zipping, we have to overcome the maternal contribution problem or find other ways of interfering with protein function.

2.2.2 Analysis of the dynein light intermediate chain

The cytoplasmic dynein light intermediate chain (Dlic) is a component of the dynein motor protein complex. In contrast to the dynein heavy chain, it is encoded by a single gene in flies. Thus, it might be a better candidate to study dynein function during zipping than the heavy chain of which eight genes are found in the *Drosophila* genome. Two different Dlic mutants are available which are both caused by P-element insertions. One P-element insertion is located within the first intron (G0065), the other one is found in the splice-donor site of the seventh intron (G0190). Both insertions are recessive larval lethal and fail to complement each other for viability, showing they are allelic. Furthermore, it has been suggested that these mutations result in loss-of-function mutant phenotypes (Mische et al., 2008).

2.2.2.1 Dlic does not seem to be required for zipping

To study Dlic function during DC, I analysed male embryos of both available X-chromosomal Dlic mutants, G0065 and G0190. Since *Dlic* lies on the X chromosome, male embryos carry only one gene copy. To visualise DC, both mutants expressed an epidermal actin marker and were imaged live. No defects were observed during DC (Figure 16, A – C), however, the overall closure speed in both mutant embryos was slower (Figure 16D) than in wild-type embryos. Nonetheless, we still could not

exclude an involvement of Dlic function during zipping, as there was still maternally provided Dlic, which could mask a possible zipping phenotype. To avoid maternal contribution, we performed an acute protein-knockdown using the the deGradFP system, which was established by the Affolter laboratory (Caussinus et al., 2012). This method takes advantage of a GFP-nanobody fused to a protein domain that recruits the ubiquitin-mediated protein degradation pathway to a GFP-tagged protein of interest. Selective expression of the nanobody fusion protein allows spatially and temporally controlled acute target depletion as described in Section 1.5.2.1.

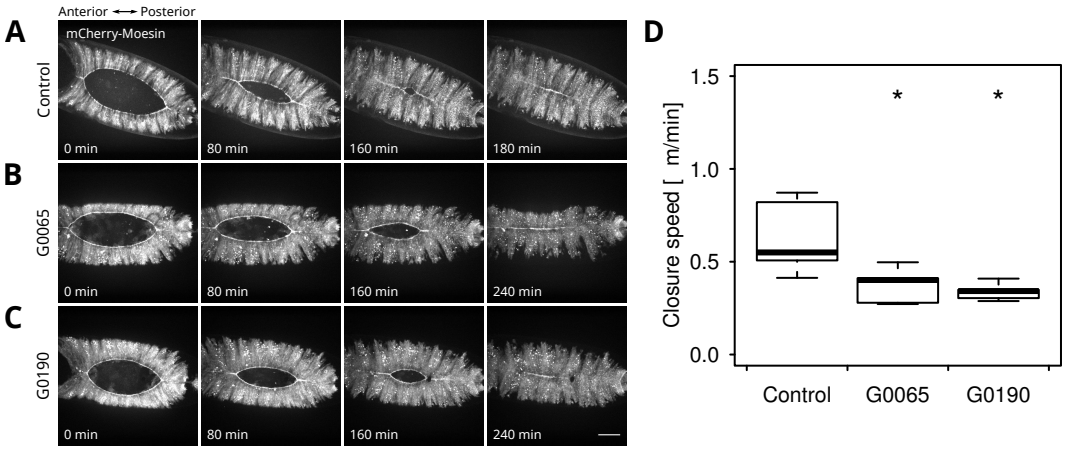

Figure 16: Dorsal closure is delayed in hemizygous *Dlic* mutants.
(A-C) Movie sequences showing mCherry-Moesin expressing embryos during dorsal closure. **(A)** Wild-type control embryo. **(B)** Hemizygous G0065 mutant embryo. **(C)** Hemizygous G0190 mutant embryo. Scale bar: $50\mu m$. **(D)** Box plots showing the distribution of mean closure speeds of control embryos ($n = 6$), hemizyogus G0065 mutants ($n = 6$) and hemizygous G0190 mutants ($n = 5$). The whiskers display minimum and maximum values. * $p < 0.05$.

We crossed both *Dlic* mutants with flies carrying an ubiquitously expressed GFP-Dlic (ubi-GFP-Dlic) construct, made in the laboratory of Jordan Raff. Flies homozygous for each Dlic mutation were rescued with the GFP-Dlic construct. GFP-Dlic embryos expressed cytoplasmic Dlic in the epidermis as well as the AS cells (Figure 17A), allowing us to monitor the effects of Dlic depletion by deGradFP during DC. To drive expression of the anti-GFP nanobody, which is expressed under the control of the UAS promoter, I used several different Gal4 driver lines (Table 2). I imaged embryos that arose from homozygous *Dlic* mutant females carrying the GFP-Dlic rescue construct and from males expressing the Gal4 driver as well as the anti-GFP nanobody. Only male progeny will carry the *Dlic* mutant allele without an additional wild-type copy except the Dlic rescue construct. As the embryos did not have a marker enabling us to distinguish between male and female embryos, we

Table 2: List of Gal4 lines for anti-GFP nanobody expression, number of imaged embryos and adult phenotypes after Dlic depletion.

Mutant	Gal4 driver for anti-GFP nanobody	No. of imaged embryos	Adult phenotype
G0065	*pnrGal4* (expression in epidermis)	6	Short bristles
	enGal4 (expression in epidermal cell stripes)	9	Adult-lethal
	actinGal4 (ubiquitous expression)	22	Adult-lethal
G0190	*pnrGal4* (expression in epidermis)	23	Thorax cleft, short bristles
	enGal4 (expression in epidermal cell stripes)	10	Defects in wings
	69BGal4 (ectoderm expression)	13	Adult-lethal
	daGal4 (ubiquitous expression)	12	Adult-lethal

expected to see an obvious phenotype in about 50% of the embryos if Dlic plays a role in zipping. However, zipping progressed normally in embryos in which anti-GFP nanobody expression was driven by the two epidermal driver lines *pnrGal4* (dorsal epidermis) and *enGal4* (cell stripes) (Figure 17, B and C). As we observed GFP-dots appearing in the cells corresponding to cells expressing the anti-GFP nanobody, a phenomenon previously shown to be a reliable readout for efficient deGradFP-mediated myosin II depletion (Pasakarnis et al., 2016), we assume that Dlic protein depletion occurred at least partially. I measured the mean closure speeds of Dlic depleted and GFP-Dlic control embryos. The closure speed was significantly reduced in embryos, in which Dlic knockdown occurred in the dorsal epidermis using *pnrGal4* (Figure 19). In addition, all male adult flies exhibited a mild thorax cleft and bristle defects. The phenotype was more prominent in G0190 *Dlic* mutant than in G0065 *Dlic* mutants. (Figure 18, B and C). In *enGal4* driven Dlic-depleted embryos, no male progeny hatched from G0065 mutants, and male offspring of G0190 mutants showed defects in wing morphology (Figure 18D).

Another Gal4 driver line I used to deplete the GFP-Dlic protein of the rescued G0190 mutant was the ectoderm-specific *69BGal4*. *69BGal4* expression starts at the embryonic stage 9 which is before the epidermis-specific *pnrGal4* is expressed (stage 10/11) (Brand & Perrimon, 1993; Vincent et al., 2008). Thus, embryos expressing the *69BGal4* driver will have more time for anti-GFP nanobody expression. However, DC was found to progress normally. We observed GFP-dots mainly forming in the AS tissue or the tissue underneath, whereas only few were observed in the surrounding epidermis, suggesting only weak depletion within the epidermis (Figure 17D). To cause a stronger effect the anti-GFP nanobody was expressed ubiq-

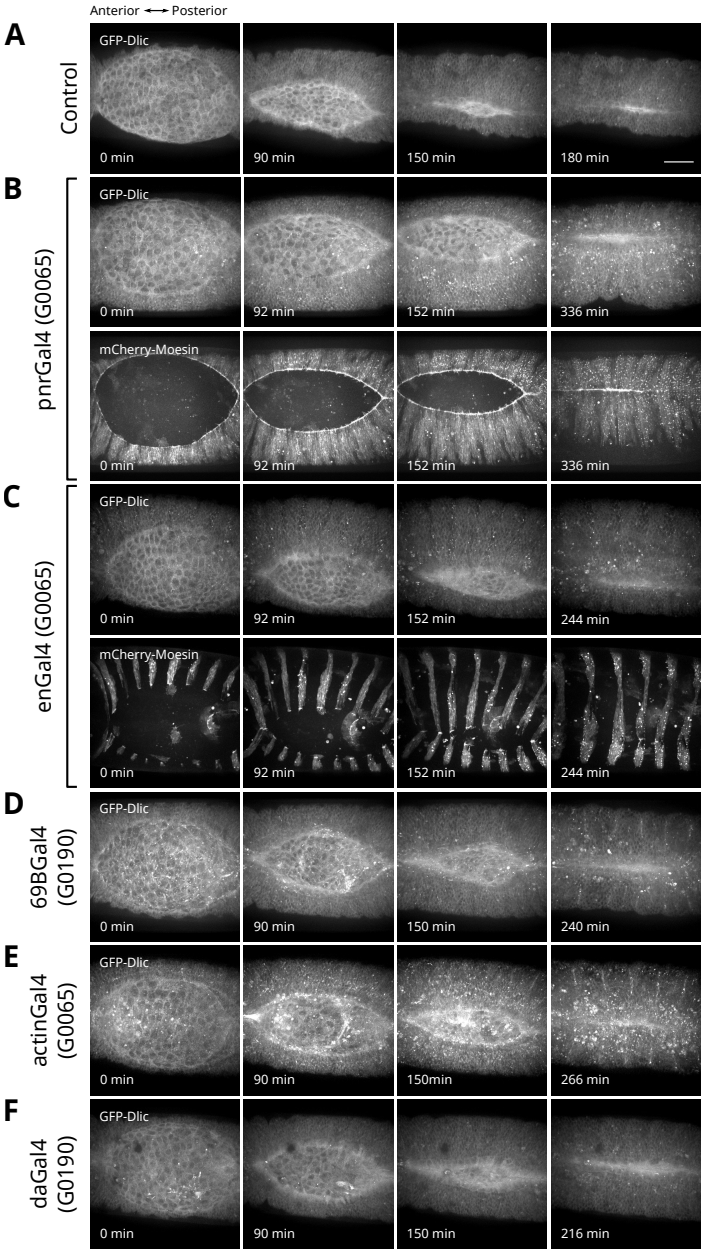

Figure 17: Dorsal closure phenotypes of of Dlic-depleted embryos.
Movie sequences showing control and Dlic-depleted embryos. Different Gal4 driver lines were used for anti-GFP nanobdoy expression to mediate Dlic knockdown. **(A)** Wild-type embryo expressing GFP-Dlic. **(B)** Embryo expressing GFP-Dlic (upper row) and mCherry-Moesin (lower row). Anti-GFP nanobody expression is driven by *pnrGal4* in a G0065 mutant. GFP dots in the epidermis are observed in the GFP-Dlic expressing embryo. **(C)** Embryo expressing GFP-Dlic (upper row) and mCherry-Moesin in engrailed stripes (lower row). Anti-GFP nanobody expression is driven by *enGal4* in a G0065 mutant. **(D)** Anti-GFP nanobody expression is driven by the ectoderm-specific *69BGal4* line in G0190 mutant. GFP dots are observed in the AS tissue, less in the surrounding epidermis. **(E)** Anti-GFP nanobody expression using ubiquitously expressed *actinGal4* driver in a G0065 mutant. Many GFP dots are seen in the AS and the surrounding epidermis. Endoderm closure occurring underneath the AS is observed in the second frame ($90min$). **(F)** Anti-GFP nanobody expression driven by the ubiquitously expressed *daGal4* in a G0190 mutant. Almost no GFP dots are observed in the epidermis, few dots are locally observed in the AS tissue. Scale bar: $50\mu m$.

uitously using the *actinGal4* and *daughterless-Gal4* (*daGal4*) drivers (Table 2). In embryos with anti-GFP nanobody expression driven by *actinGal4*, many GFP-dots appeared along the LE of the two epithelial sheets at the site where the actin cable is formed. Moreover, GFP-dots formed along the LE of the endoderm underneath the AS tissue, where another closure event occurs (Figure 17E). Using the *daGal4* driver, almost no GFP-dots were visible in the epidermal tissue, and only few bigger blobs were seen in the AS cells, indicating that only little Dlic depletion took place. In both situations, we did not observe any defects during zipping (Figure 17F).

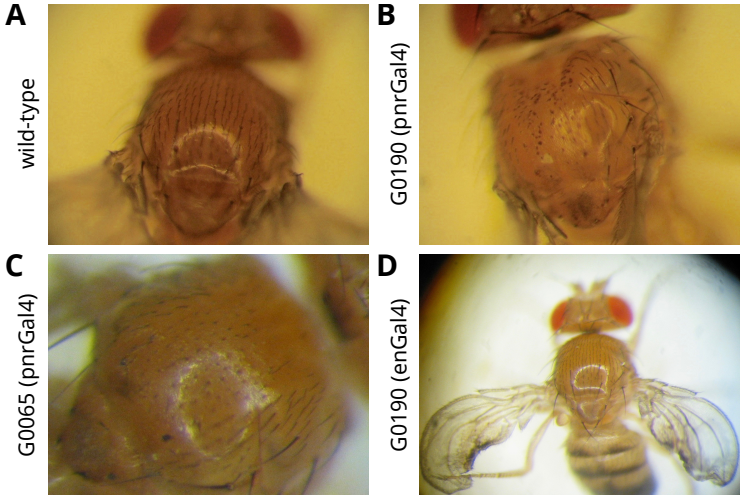

Figure 18: Adult phenotypes of Dlic-depleted embryos.
(A) Thorax of wild-type fly. Thorax of fly in which Dlic depletion was mediated by *pnrGal4* driven anti-GFP nanobody expression in **(B)** G0190 mutants and **(C)** in G0065 mutants. **(D)** Defects in wings of flies in which Dlic depletion was mediated by *enGal4* driven anti-GFP nanobody expression in a G0190 mutant.

The mean closure speeds of embryos, in which anti-GFP nanobody expression was driven by *69BGal4*, *daGal4* and *actinGal4*, were similar to control embryos (Figure 19), however, no male offspring hatched. As the embryos did not carry a marker allowing us to differentiate between male and female embryos, we do not know if male embryos, which carried only the mutant *Dlic* allele, developed until DC stage or died at an earlier stage of embryonic development. Nevertheless, it shows that Dlic function is essential for *Drosophila* development.

To exclude the possibility that only female embryos were imaged, which did not carry the desired phenotype, I have also analysed Dlic-depleted embryos which could be identified as males. To distinguish between male and female embryos, embryos from homozygous G0190 *Dlic* female mutants carrying the GFP-Dlic rescue construct as well as the UAS-controlled nanobody fusion protein and males carrying

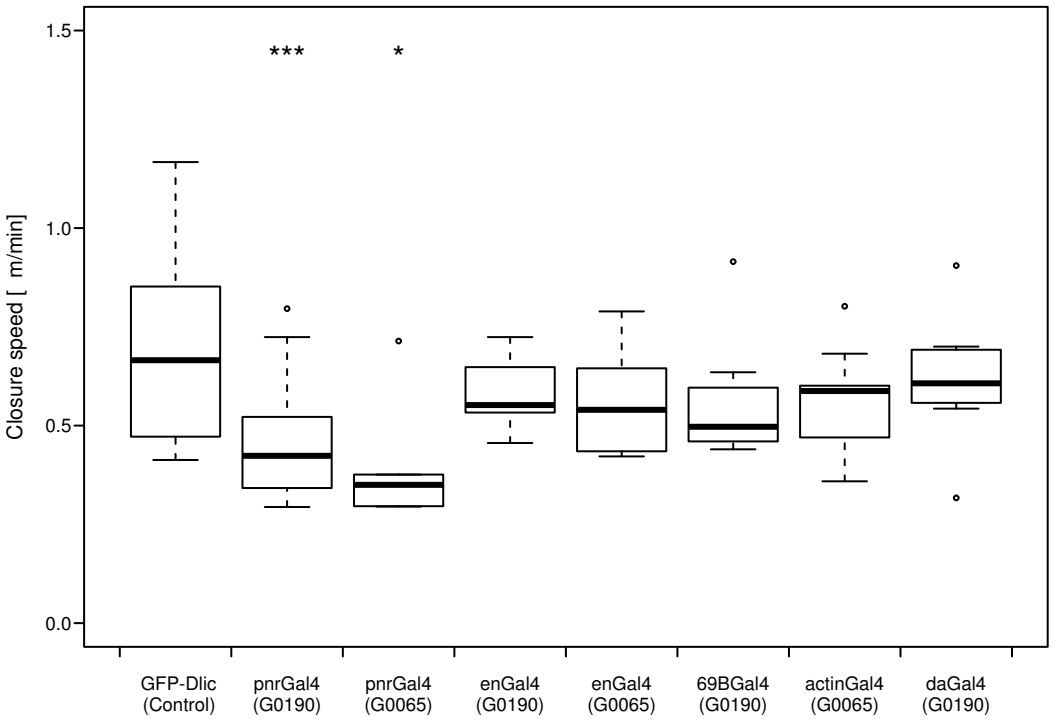

Figure 19: Closure speeds in Dlic-depleted embryos.
Box plots displaying the distribution of mean closure speeds of control and Dlic-depleted embryos using different Gal4 driver lines for Dlic knockdown. (GFP-Dlic: $n = 13$; *pnrGal4*: $n = 22$ (G0190), $n = 5$ (G0065); *enGal4*: $n = 10$ (G0190), $n = 9$ (G0065); *69BGal4*: $n = 9$; *actinGal4*: $n = 18$; *daGal4*: $n = 8$) The whiskers display minimum and maximum values, the circles represent outliers. * $p < 0.05$, *** $p < 0.001$.

the X-chromosomal fluorescent balancer FM7krGFP as and the *pnrGal4* enhancer element. Embryos, which did not express the krGFP marker of the balancer, were identified as males. Dlic depletion in such embryos did not seem to affect the zipping process (Figure 20). The mean closure speeds were slower than in GFP-Dlic control embryos, but similar to *pnrGal4* driven nanobody expression for Dlic depletion. These results strongly indicate, that either Dlic function is not required for DC, or Dlic-depletion is not efficient enough.

Taken together, these results indicate that Dlic does not seem to play a role in zipping during dorsal as we did not observe any zipping defects. Yet, other reasons for the absence of a zipping phenotype might be that Dlic depletion was not complete, or that the *Dlic* mutations, which are both P-element insertions, are not full null mutants. Thus, remaining Dlic activity might mask a possible zipping phenotype.

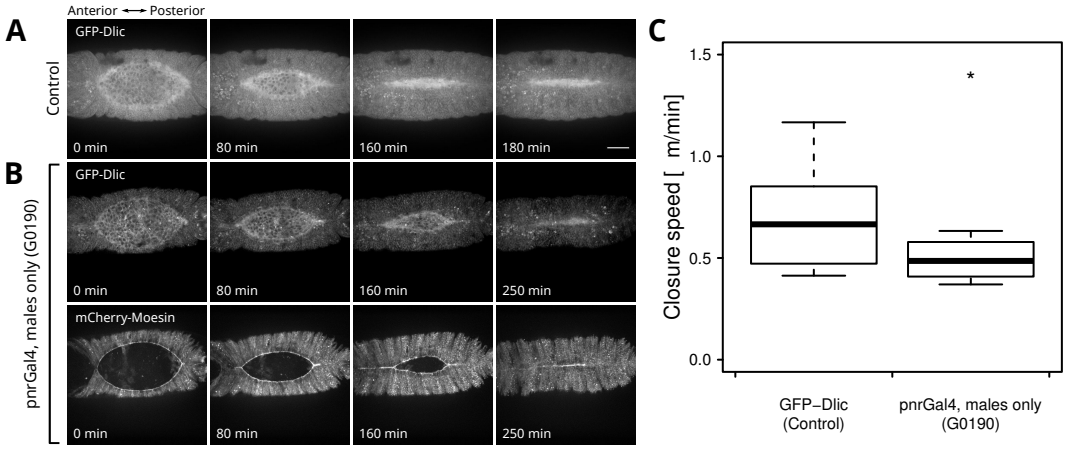

Figure 20: Epidermal Dlic depletion does not cause a zipping phenotype. Movie sequences showing control **(A)** and Dlic-depleted male embryos **(B)**. Dlic depletion was mediated by epidermis-specific (*pnrGal4*) anti-GFP nanobody expression. Embryos complete closure with a delay, but do not show other zipping defects. Scale bar: $50\mu m$. **(C)** The average closure speed of Dlic-depleted embryos ($n = 4$); is slower compared to GFP-Dlic control embryos ($n = 13$). The whiskers display minimum and maximum values. * $p < 0.05$.

2.2.3 Analysis of dynactin during zipping

The dynactin protein complex was shown to be required for many dynein functions and is involved in regulating dynein acitivy (Schroer, 2004). Studying dynactin components might therefore give some insights into dynein function. Here, I will describe experiments I have performed by changing the expression of components of the dynactin complex and my analysis of their influence on DC.

2.2.3.1 p150 Glued is dispensable for the zipping process

Dynactin consists of several subunits. One essential subunit is p150 Glued, which is known to directly bind dynein (Kardon & Vale, 2009). The product of the *Drosophila* gene *Glued*, is the functional homologue of the vertebrate p150 Glued (Waterman-Storer & Holzbaur, 1996). I have examined the effect on the zipping process of two fly lines, each expressing one of two dominant-negative variants of Glued: dnGl84 and dnGl96B. Both lines are a truncated version of the *Glued* cDNA, encoding only the N-terminal 922 amino acids of Glued (Allen et al., 1999). As dnGl84 and dnGl96B are both under the control of a UAS promoter, I used the *engrailed-Gal4* (*enGal4*) to drive dnGl84 and dnGl96B expression in stripes of epidermal cells. To analyse zipping, the embryos carried an additional marker for actin, mCherry-Moesin, controlled by a UAS promoter and thus expression occurs also in stripes

of cells (Figure 21). Embryos expressing dnGl84 and dnGl96B showed no obvious zipping defects. Zipping speed analysis of individual engrailed expressing cell stripes revealed that embryos with dnGl84 and dnGl96B expressing cell stripes have comparable zipping speeds to embryos with wild-type cell stripes (Figure 22, A and B).

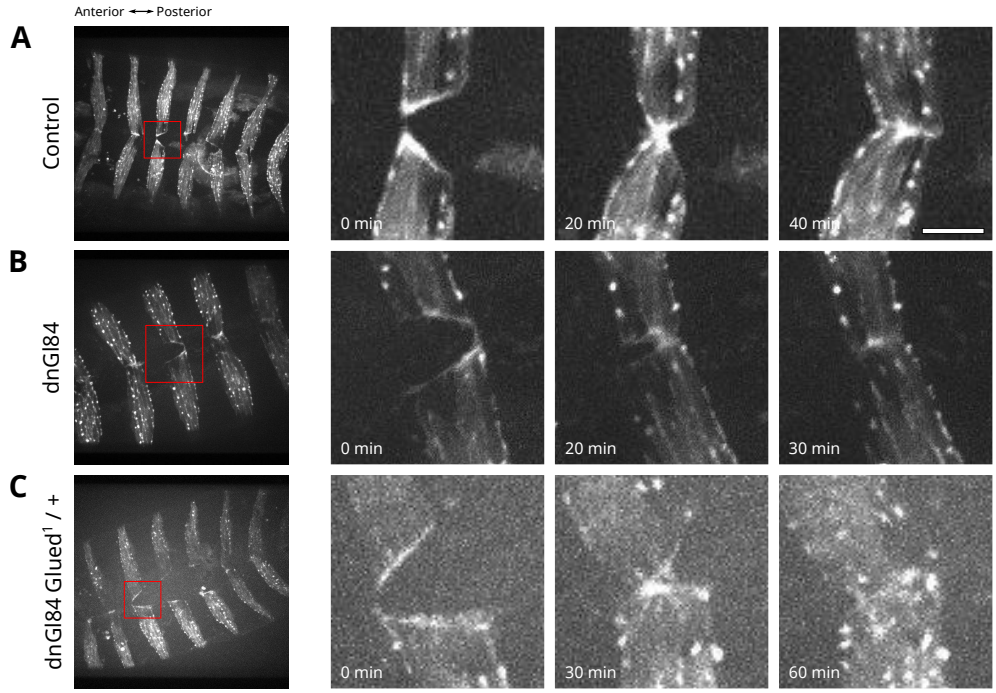

Figure 21: Zipping of engrailed cell stripes in embryos expressing dominant-negative variants of p150 Glued.
Selected movie frames of embryos expressing mCherry-Moesin in engrailed stripes. Showing zipping of 5th stripe (boxed region) from initial contact between opposing cell stripes until full contact. **(A)** Zipping of cell stripe in wild-type control embryo. **(B)** Embryo is expressing dnGl84 in cell stripe. **(C)** Embryo expressing dnGl84 in cell stripe in a heterozygous *Glued*^{1} mutant background. Scale bar: 10μm.

However, it was shown that overexpression of dominant-negative Glued is dosage dependent (McGrail et al., 1995). Hence, to increase a putative phenotype I combined dnGl84 with a heterozygous dominant *Glued*^{1} (*Glued*^{1}/+) mutation (Plough & Ives, 1935), which results in a truncated protein product, that competes with the wild-type protein (Swaroop et al., 1985). The zipping speed analysis of individual engrailed stripes of such embryos showed a decrease in speed compared to wild-type embryos (Figure 22). To test if this effect was not already caused by *Glued*^{1} heterozygosity alone, I examined zipping speeds of engrailed stripes in heterozygous *Glued*^{1} mutants. Heterozygous *Glued*^{1} embryos revealed no obvious differences in zipping speeds of cell stripes compared to wild-type embryos (Figure 22).

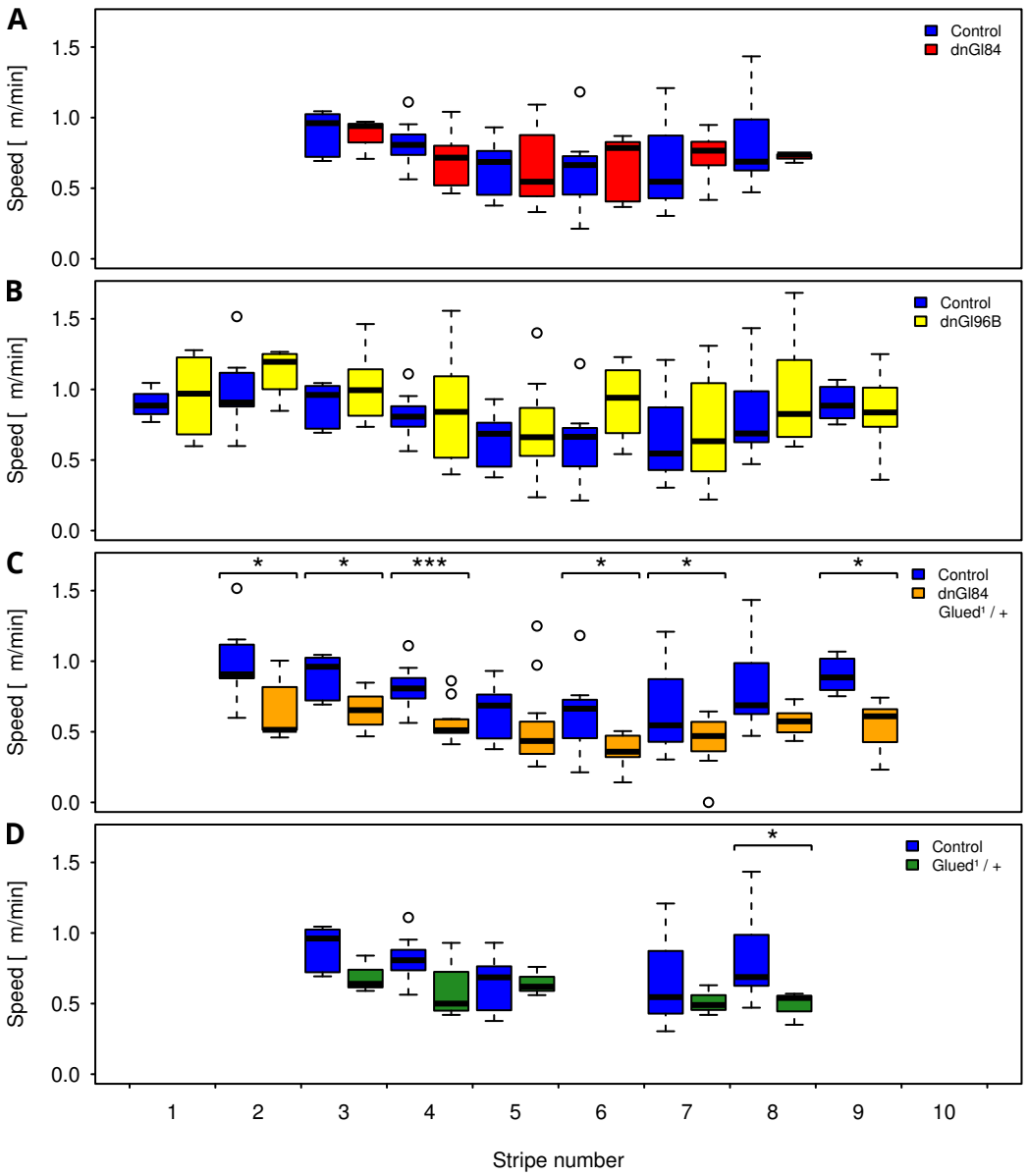

Figure 22: Quantification of zipping speeds of engrailed cell stripes in embryos expressing dominant-negative variants of Glued.
Box plots showing the distribution of mean zipping speeds of individual engrailed stripes. The time to close the maximum distance between opposing epithelial cell stripes after they made initial contact was measured. A minimum of three cell stripes for each box plot were analysed. Box plots depicting mean zipping speeds of engrailed stripes expressing **(A)** dnGl84, **(B)** dnGl96B, **(C)** engrailed stripes in Glued^1/+ embryos, **(D)** engrailed stripes expressing dnGl84 in Glued^1/+ embryos compared to wild-type engrailed stripes. The whiskers show the minimum and maximum values, the circles represent outliers. * $p < 0.05$, *** $p < 0.001$.

Homozygous *Glued*^{1} mutants as well as null mutants at the *Glued* locus were shown to die at the first instar stage of development (Harte & Kankel, 1982, 1983; Waterman-Storer & Holzbaur, 1996). It was suggested, that the ability of embryos to survive to this stage results probably from maternal contribution of *Glued* transcripts to the zygote (Garen et al., 1984; Swaroop et al., 1986; Waterman-Storer & Holzbaur, 1996). Therefore, straightforward analysis of Glued function during DC was not possible.

To summarise, these data shows that overexpression of dnGl84 and dnGl96B alone does not affect zipping, whereas expression of dnGl84 in a heterozygous dominant *Glued*^{1} mutant shows a zipping delay of individual engrailed stripes, but no full arrest. This suggests that Glued may contribute to DC. However, additional copies of dominant-negative Glued might be needed to enhance a phenotype during DC.

2.2.3.2 Overexpression of p50 dynamitin does not affect zipping

It has been reported that overexpression of dynamitin leads to the disruption of dynein motor activity in *Drosophila* oocytes and cells in general (Duncan & Warrior, 2002). Dynamitin does not inhibit dynein directly, instead, it causes the disassembly of dynactin, which is required for dynein-based motility (Melkonian et al., 2007). To test dynein function in DC during the zipping process, I overexpressed the dynactin subunit p50 dynamitin. As dynamitin is under the control of the UAS promoter (UAS-Dmn), I used the epidermis-specific *pnrGal4* driver to overexpress dynamitin and the UAS-mCherry-Moesin marker during DC. Overexpression of dynamitin in DC did not impair zipping. Interestingly, embryos overexpressing dynamitin revealed slightly faster, closure speeds than wild-type embryos, but the difference was statistically not significant (Figure 23). As *pnrGal4* expression starts only during embryonic stage 10/11 (Vincent et al., 2008), dynamitin expression levels might have been too low to interfere with dynein function. Hence, I overexpressed dynamitin in heterozygous *Dhc 4-19* mutant embryos. These embryos have a sensitised background for dynein since they are likely to have less dynein than wild-type embryos. Thus, *pnr*-driven overexpression of dynamitin might lead to a stronger effect. Yet again, zipping appeared not to be affected, however the overall closure speed of such embryos was significantly decreased compared to control embryos (Figure 23). The decreased closure speed was likely a consequence of the combination of dynamitin overexpression and *Dhc 4-19* heterozygosity, as heterozygous *Dhc 4-19* embryos alone have comparable closure speeds to wild-type embryos (Figure 23E).

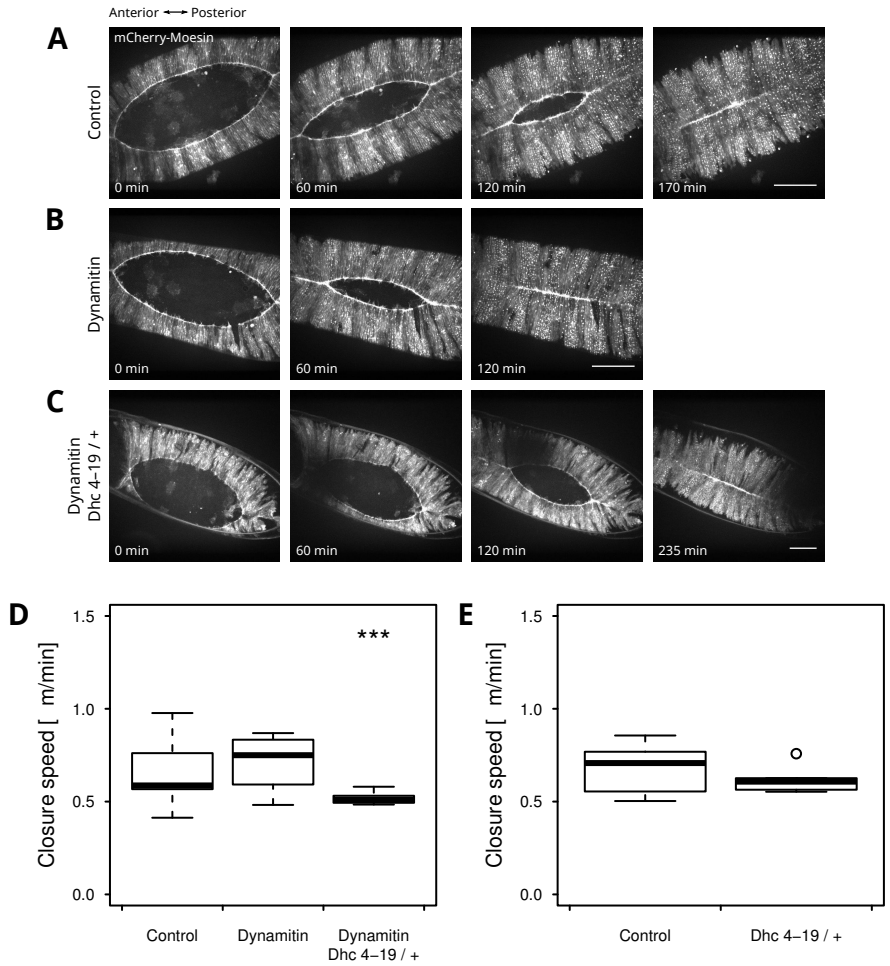

Figure 23: Dynamitin overexpression during dorsal closure.
(A-C) Movie sequences of embryos expressing mCherry-Moesin. **(A)** Wild-type control embryos. **(B)** Dynamitin overexpression driven by the epidermis-specific *pnrGal4*. **(C)** Dynamitin overxpression driven by *pnrGal4* in a *Dhc 4-19/+* mutant background. Scale bars: $50\mu m$. **(D)** Box plots showing the distribution of mean closure speeds in wild-type embryos ($n = 17$), dynmatin overexpressing embryos ($n = 4$) and dynamitn overexpressing embryos in a *Dhc 4-19/+* background ($n = 7$). **(E)** Box plots showing the distribution of mean closure speeds in wild-type embryos ($n = 12$) and *Dhc 4-19/+* embryos ($n = 6$). The whiskers represent minimum and maximum values, the circles represent outliers. *** $p < 0.001$.

Taken together, these results do not appear to support a function for dynein during zipping in DC. However, it is known that dynactin is not needed for all dynein functions. Alternatively, it is possible that the Glued and dynamitin expression levels were not high enough to cause a phenotype during DC. Additional experiments with increased sensitisation of the genetic backgrounds (e.g. combinations of *Glued* and *Dhc64* alleles) combine with dnGl84, dnGl96B and p50 Dynamitin overexpression may help to elucidate this issue.

2.3 The dynein-specific inhibitor CiliobrevinD impairs zipping

So far we have confirmed that MTs are required for zipping, yet we only have indications that dynein might be involved in this force generating process. Unfortunately, dynein mutant analysis was not possible during DC, as embryos carrying the strongest mutant allele develop normally. Development only arrests during early larval stages, indicating that maternal contribution is enough to proceed through embryonic development (Section 2.2.1.2) (Gepner et al., 1996; Port et al., 2015). Recently, Ciliobrevins, a group of small-molecules that inhibit AAA+ ATPases, have been discovered to specifically inhibit cytoplasmic dynein. The precise mechanism by which Ciliobrevins act is not fully understood, but biochemical studies suggest they target the heavy chain motor domain and block ATP hydrolysis in a nucleotide-competitive manner (Firestone et al., 2012).

So far, the use of CiliobrevinD to block dynein function was only demonstrated in *in vitro* experiments. To test CiliobrevinD efficiency to inhibit dynein function in *in vivo* systems, I injected it into syncytial embryos. During this embryonic stage several rounds of mitotic divisions occur for which dynein function is needed (Robinson et al., 1999). CiliobrevinD-treated embryos carrying Jupiter-GFP, a MT marker, exhibited mitotic defects. The predominant phenotypes included multiple spindle arrays and many free centrosomes (Figure 24C). Similar defects occurred in *Dhc64* mutants shown by Robinson et al. (1999). As a control I injected DMSO into the embryos, which is used as a solvent for CiliobrevinD. Such embryos occasionally displayed free centrosomes and multiple spindle arrays (Figure 24B), however, the phenotype was moderate as compared to CiliobrevinD-treated embryos.

These results indicate that CiliobrevinD disrupts dynein function *in vivo*, yet there might be also an effect of DMSO that has to be taken into account.

To study the effect of CiliobrevinD on dynein function during zipping I injected a concentration of $10mM$ CiliobrevinD into DC stage embryos. After injection, the embryos were subsequently imaged. I examined embryos carrying mCherry-

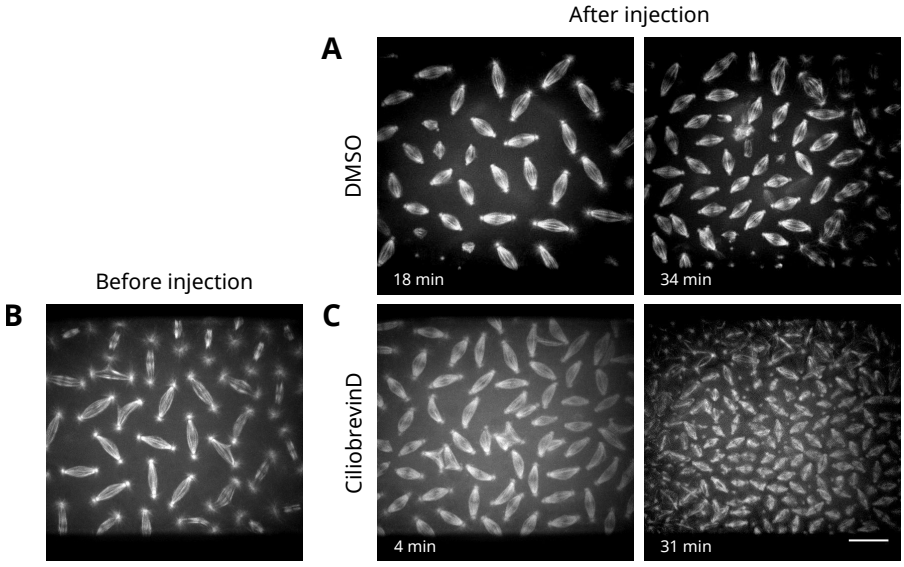

Figure 24: The dynein specific inhibitor CiliobrevinD causes defects during mitotic divisions in syncytial embryos.
Selected movie frames of embryos expressing the MT marker Jupiter-GFP, displaying mitotic spindles in the syncytial embryo. **(A)** DMSO-injected embryo. **(B)** Embryo before CiliobrevinD injection, **(C)** same embryo as in (B) after CiliobrevinD injection. Imaging started within $5 - 10min$ of DMSO or CiliobrevinD injection. Shortly after CiliobrevinD injection, embryos display mitotic defects like multiple spindle arrays. At a later time point more mitotic defects accumulate; mono-polar spindles and many free centrosomes are observed. DMSO control embryos exhibit less severe mitotic defects compared to CiliobrevinD-treated embryos. Scale bar: $20\mu m$.

Moesin, a marker for actin expressed only in the epidermis, as well as embryos carrying armadillo-GFP, which allows visualisation of cell borders as it localises to cell junctions. I observed several different phenotypes (Figure 25, A – D), which were assigned to four categories: zipping normal; zipping slowed down ($< 0.4\mu m/min$); zipping stops; and embryonic tissue expands, ruptures (Figure 25E). About 31% of CiliobrevinD-injected embryos zipped normal and in about 29% zipping was delayed compared to control embryos. Yet, 33% failed to complete zipping and 6% did not even start to zip. Instead, the embryonic tissue expanded often the AS tissue eventually ruptured. In contrast, 83% of DMSO-treated control embryos zipped normally, in 14% zipping was slower and only 3% exhibited a zipping arrest. This shows CiliobrevinD injection inhibits zipping, but also confirms that DMSO injection affects embryogenesis to an extent that cannot be neglected. To exclude an effect on zipping caused through the injection process, I injected water as an additional control. All embryos exhibited normal zipping progression, and closure speed was slightly higher than in DMSO-injected embryos (Figure 26).

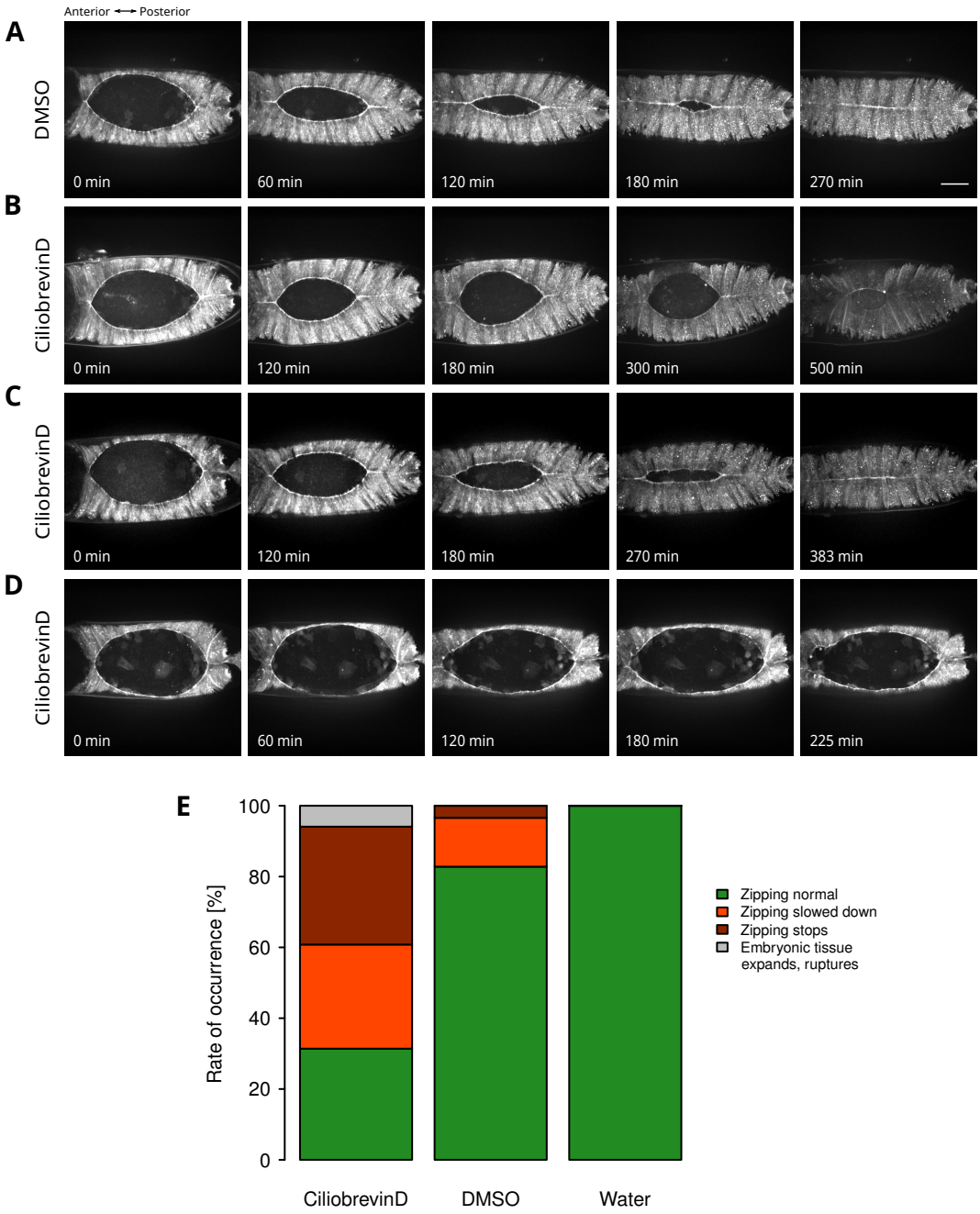

Figure 25: CilibrevinD-injected embryos show various phenotypes during dorsal closure.
(A-D) Movie sequences of embryos expressing mCherry-Moesin in the epidermis of dorsal closure stage embryos. **(A)** DMSO-injected embryo. **(B-D)** $10mM$ CiliobrevinD-injected embryos. Phenotypes occurred in CiliobrevinD-treated embryos were grouped into four different categories: zipping normal, zipping stops, zipping slowed down ($< 0.4\mu m/min$) and embryonic tissue expands, ruptures. Movie sequences show representative phenotypes of the categories after CiliobrevinD injection. **(B)** Zipping arrests. **(C)** Zipping is slowed down. **(D)** Embryonic tissue expands and ruptures. Scale bar: $20\mu m$. **(E)** The graph shows the rate of occurrence of each category in CiliobrevinD-injected ($n = 51$), DMSO-injected ($n = 29$) and water-injected embryos ($n = 13$).

For further quantitative analysis, I measured the distance between the anterior and posterior canthi over time until zipping is completed or arrested of CiliobrevinD and DMSO-treated embryos. (Figure 27A). It is clearly visible that in a larger proportion of CiliobrevinD-treated embryos zipping stops or is slowed down, whereas most of DMSO-treated embryos complete DC and display faster zipping kinetics. The analysis supports the findings represented in Figure 25E. Furthermore, I quantified the overall zipping speeds, showing that zipping is significantly slower in CiliobrevinD-treated embryos compared to DMSO-treated control embryos (Figure 27B).

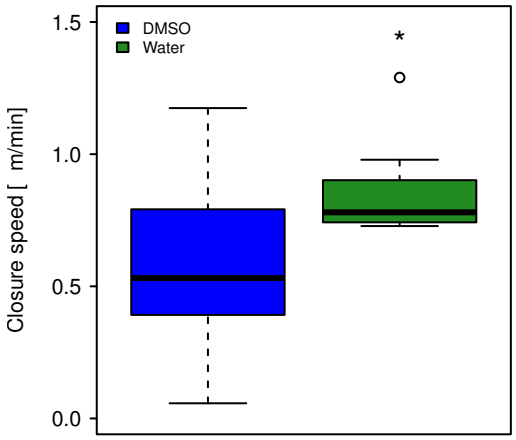

Figure 26: Dorsal closure is slower in DMSO-injected embryos compared to water-injected embryos.
The box plots show the distribution of mean closure speeds of DMSO-treated ($n = 30$) and water-treated ($n = 12$) embryos. The whiskers represent the minimum and maximum values, the circle represents an outlier. * $p < 0.05$.

Nevertheless, it does not seem that CiliobrevinD specifically affects zipping. Both taxol (Section 2.1.2) and colcemid injections (Jankovics & Brunner, 2006) are likely to specifically affect the zipping process, as zipping halts and convergence of the epithelial sheets progresses normally, resulting in an abnormally narrow gap. We did not, however, observe such an abnormally narrow dorsal hole in CiliobrevinD-treated embryos, when zipping arrested or was slowed down. This suggests that CiliobrevinD might affect, in addition to zipping, the convergence of epithelial sheets and thus, apical constriction of the AS cells. Analysing the pulsing of AS cells in CiliobrevinD-injected embryos did not show a clear phenotype. I could observe both normal AS pulsing and a partial or full pulsing arrest in embryos in which zipping stopped or in which the embryonic tissue expanded and ruptured (Figure 27C).

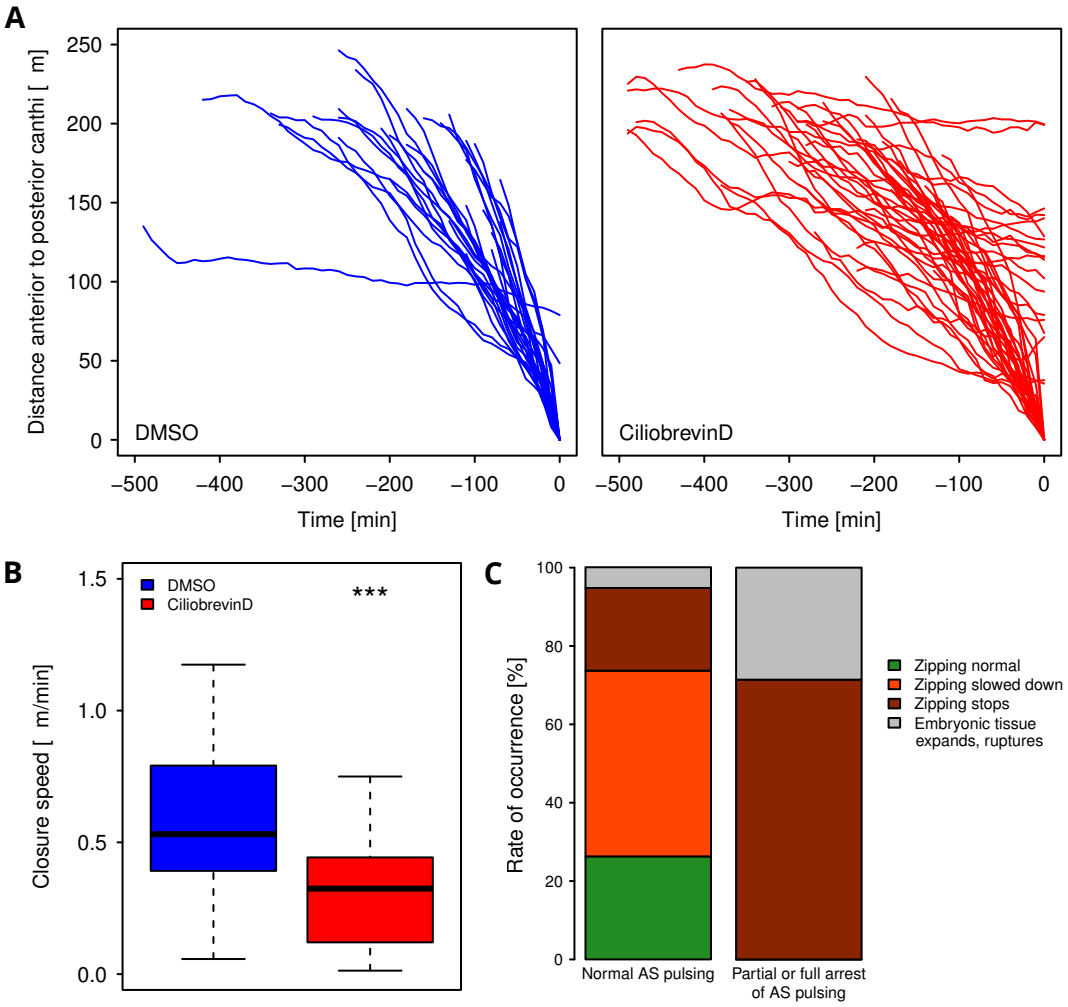

Figure 27: Zipping is impaired in CiliobrevinD-injected embryos.
(A) The graphs show zipping kinetics of DMSO-treated ($n = 30$) and CiliobrevinD-treated ($n = 50$) embryos. Progression of zipping was measured every $10min$ starting at various distances between anterior and posterior canthi, but spanning at least $100\mu m$. Each line represents the zipping kinetics of one individual embryo. **(B)** The box plots display the distribution of mean closure speeds of DMSO-injected and CiliobrevinD-injected embryos from **(A)**. The whiskers represent the minimum and maximum values. CiliobrevinD-treated embryos are significantly slower than DMSO-treated embryos, *** $p < 0.005$. **(C)** The graph shows the occurrence of normal AS pulsing ($n = 19$) and partial or full arrest of AS pulsing ($n = 7$) in each of the categories of DC phenotypes (zipping normal; zipping slowed down; zipping stops; embryonic tissue expands, ruptures) in CiliobrevinD-treated embryos.

Embryos in which zipping progressed normally or was slowed down after CiliobrevinD treatment exhibited normal AS cell pulsing, indicating that the decrease in zipping speed is not a consequence of impaired AS pulsing. In DMSO-treated embryos, AS pulsing appeared normal.

In summary, these data show that the dynein-specific inhibitor CiliobrevinD, impairs the zipping process, indicating that dynein function might be needed for zipping. However, it does not appear to exclusively affect zipping, as also apical constriction of AS cell pulsing seems to be impaired in some cases. This is not surprising, since drug injections often show a global effect. Thus, to analyse dynein function during zipping, tissue-specific dynein depletion is essential.

2.4 Engineering transgenic *Dhc64* constructs to perform an acute protein knockdown

Our analysis of dynein heavy chain mutants as well as previous results of *Dhc64* mutant analysis shown by Gepner et al. (1996) and Port et al. (2015) revealed that homozygous null mutants develop beyond embryonic development. As lethality only occurs during mid larval stages, this suggests that maternally provided Dhc64 function supports development beyond embryogenesis (Gepner et al., 1996). As a result, we were not able to study dynein function during DC with zygotic mutants. However, several different methods have been established to induce time- and tissue-specific protein degradation allowing the removal of maternally contributed proteins. Thus, in parallel I tried three different approaches to perform an acute protein knockdown for which I generated different transgenes (Table 3) which I will describe in the following sections. Additionally, I used a different approach, which would allow the use of the same protein degradation methods presented in the following, which is described in Section 2.6.1.

2.4.1 Generating a *Dhc64* transgene for use with the deGradFP system

As aforementioned, the deGradFP system is a method by which GFP-tagged proteins of interest can be targeted for time- and tissue-specific degradation. It is based on the evolutionary highly conserved ubiquitin degradation pathway and thus can be used in any eukaryotic system. Protein depletion is mediated by the anti-GFP nanobody, a fusion protein that binds GFP and directs it to the proteasome for degradation. Thus, the GFP-tagged protein has to be the only source of a functional protein to permit analysis of gene function without any concerns for interference from any residual protein (Caussinus et al., 2012). As this method has been shown to be universally applicable, I decided to use it for selective Dhc64 degradation. I generated a transgene encoding an N-terminally GFP-tagged Dhc64. Since splicing of the *Dhc64* gene results in eight different transcripts, I used the genomic *Dhc64* sequence ($\sim 18kb$) from the *pDhc+* transgene provided by the Hays laboratory, that was successfully used for *Dhc64* mutant rescue (Gepner et al., 1996). To integrate the construct containing the GFP-tagged *Dhc64* gene I made use of the ϕC31 integrase system, which facilitates site-specific recombination (Bischof et al., 2007). For this purpose I injected 300 embryos with a DNA concentration of $500ng/\mu l$. From the injected embryos only 7% hatched as larvae and out of these 20% became fertile adults. The adult flies were then crossed to yellow white (yw) flies to screen

Table 3: List of generated constructs for Dhc64 depletion and corresponding injection results.

Construct	Objective	Construct size	Injected conc.	Injected no. of embryos	Embryonic survival rate	Fertile flies[1]
pMA-attB-EGFP-*Dhc64*	Acute protein knockdown using the deGradFP system	28.4*kb*	$500ng/\mu l$ $250ng/\mu l$	300 480	7% 14%	20% 20%
pMA-attB-TEV Degron-*Dhc64*	Acute protein knockdown using the TIPI system	28.7*kb*	$500ng/\mu l$	620	7%	26%
pMA-attB-Cry2-RFP-*Dhc64*	Protein inactivation upon blue light illumination	29.9*kb*	$250ng/\mu l$ $200ng/\mu l$	300 200	5% 5%	27% 20%
pMA-attB-*Dhc64*	Control injection of additional *Dhc64* wild-type copy	27.6*kb*	$500ng/\mu l$	166	20%	26%

[1] No transgenic flies obtained

for recombinants in the F1 generation. However, I did not obtain any transgenic flies. Typically, embryonic survival rates are expected to be $30 - 40\%$ using the ϕC31 integrate system for stable integration into the *Drosophila* genome (personal communication: Werner Boll). Since the survival rate here was low (7%), this indicates that the applied DNA concentration might be toxic for the embryo. Hence, I injected 480 embryos with a DNA concentration of $250ng/\mu l$. This time the embryonic survival rate was about 14%, yet still low compared to normal embryonic survival rates. Again, no transgenic flies were obtained.

To test if the transgene was working, I transfected it into *Drosophila* S2 cells. As the cells displayed GFP expression, we assume that the transgene is functional (Figure 28A).

These results suggest that either the concentration of the injected transgene is too high or, more likely, that N-terminally GFP-tagged Dhc64 causes a dominant-negative effect and thus early lethality of injected embryo.

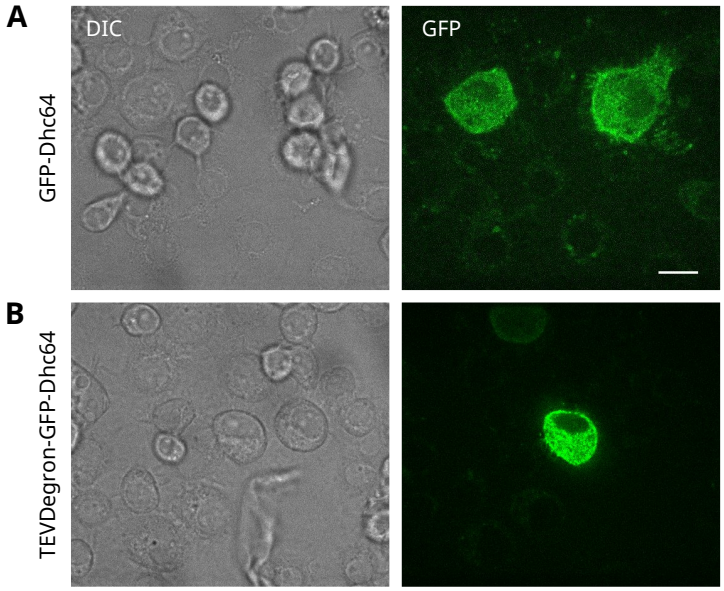

Figure 28: Transient expression of transgenes in S2 cells.
Expression of the transgenes containing **(A)** GFP-tagged *Dhc64* (pMA-attB-EGFP-*Dhc64*) and containing **(B)** the *Dhc64* tagged with the N-degron and GFP (pMA-attB-TEVDegron-*Dhc64*) in S2 cells. Shown are the DIC images and the corresponding fluorescent images. Scale bar: $10\mu m$.

2.4.2 Generating a *Dhc64* transgene for use with the TIPI system

Another approach that has been shown to lead to acute protein degradation is TEV protease induced protein inactivation (TIPI, Taxis et al., 2009), which was adapted to be used in *Drosophila* by Nadia Dubé, a former postdoc in our laboratory. This method is based on the N-end rule where the first amino acid of a mature protein determines its stability. A gene of interest is tagged with a fluorescent protein, followed by an N-terminal degradation signal, called N-degron, which is masked by a stabilising sequence including the TEV cleavage site. Different N-degrons have a different affinity for the targeting by the ubiquitin-proteasome-system (UPS), which determines the protein half-life. The TEV protein recognises the TEV cleavage site and the cleavage triggers the de-protection of the dormant N-degron. If the unmasked N-degron has phenylalanine as its first amino acid, it will be labelled with ubiquitin residues and recognised by the UPS which targets it for degradation. But if the first amino acid is a methionine, the protein will not be degraded. To achieve spatial and temporal control of degradation, the Gal4/UAS system is used to express the TEV protease.

For the TIPI approach, I generated a large DNA construct ($28.7kb$) containing the sequence encoding the TEV cleavage site as well as the N-degron with a

phenylalanine, followed by a GFP tag and the genomic *Dhc64* sequence. Upon TEV expression, TEV cleavage should unmask the phenylalanine and Dhc64 should become unstable and rapidly targeted for degradation. Degradation would be monitored, as the Dhc64 is tagged with GFP. To integrate this transgene into the fly genome, I used ϕC31 integrase system. Of 620 injected embryos with a DNA concentration of $500ng/\mu l$ only 7% developed to larvae and out of those only 26% became fertile adult flies. Yet again, no transgenic flies were obtained. Transfected S2 cells, however, showed GFP expression, suggesting that the construct is working (Figure 28B). These results further indicate that N-terminal tagging of *Dhc64* has a dominant-negative effect in the *Drosophila* embryo.

2.4.3 Generating a *Dhc64* transgene for blue light-mediated protein inactivation

As a third approach for targeted protein inactivation I made use of Cry2, a plant cryptochrome, that forms photobodies upon blue light illumination (Kennedy et al., 2010). Previous work in our laboratory revealed that squash (sqh), the *Drosophila* homolog of the myosin II regulatory light chain, forms aggregates upon blue light illumination if it is tagged with Cry2. The formation of these aggregates very likely results in protein inactivation. The advantage of this method is that formation of aggregates happens within seconds and it is also reversible. However, so far this method was shown to work only in *Drosophila* S2 cells. To apply this system to *Drosophila* embryos, I generated a construct in which genomic *Dhc64* was tagged N-terminally with Cry2 and RFP. Since RFP is excited with a higher wavelength ($561nm$) compared to blue light illumination ($488nm$), RFP-tagging allows the monitoring of aggregate formation upon blue light illumination. As for the other constructs, I used the ϕC31 integrase system to achieve stable integration of the construct into the fly genome. I injected 300 embryos with a DNA concentration of $250ng/\mu l$ and a further 200 embryos with $200ng/\mu l$. The embryonic survival rate for both DNA concentrations was 5%. Only 6 flies in total reached adulthood and were fertile, yet none of their progeny gave rise to a transgenic fly.

Altogether, these findings indicate that N-terminal tagging of the genomic *Dhc64* gene causes a dominant-negative variant of Dhc64 leading to early embryonic lethality as dynein is needed already very early during embryonic development (Hays et al., 1994; Li et al., 1994). To exclude that an additional copy to the wild-type *Dhc64* is not the reason for not obtaining a transgenic fly, I injected a transgene containing only a wild-type *Dhc64*.

Of 166 injected embryos, 20% hatched as larvae and of this 26% were fertile adult flies. Nonetheless, no transgenic fly originated from these injections. On the one hand, this leads to the assumption that an additional copy of Dhc64 is toxic for the fly embryo. On the other hand, as the transgene is quite big ($27.6kb$), a larger number of embryos might have to be injected to create a transgenic fly. The latter seems to be more likely, as it was already shown that it is possible to have an extra copy of Dhc64 (Gepner et al., 1996). Yet, Gepner et al. used P-element mediated integration, which results in varying expression levels compared to the ϕC31 integrase system I applied. However, they were able to generate transgenic flies with up to 6 copies of *pDhc+*.

2.5 Generating a dominant-negative variant of Dhc64

The results presented in the previous section have shown that N-terminal modification of the *Dhc64* gene very likely causes a dominant-negative effect during embryogenesis. Therefore, we decided to make use of this, and to design constructs in which the expression of the modified Dhc64 is controlled under the UAS promoter. Hence, the UAS/Gal4 system can be used for spatial and temporal control of Dhc64 expression. With this approach I aim to overexpress a dominant-negative variant of Dhc64 to interfere with the wild-type copy of Dhc64 specifically during DC in order to study possible zipping defects.

Table 4: List of generated constructs for Dhc64 overexpression and the corresponding injection results

Construct	Objective	Construct size	Injected conc.	Injected no. of embryos	Embryonic survival rate	Fertile flies[1]
pMA-UAS-EGFP-Dhc64	To generate a dominant-negative variant of Dhc64	$27kb$	$250ng/\mu l$ $100ng/\mu l$	210 705	12% 12%	31% 56%
pMA-UAS-Dhc64 (mutated MTBD)	To generate a dominant-negative variant of Dhc64	$26.2kb$	*Not yet injected*			

[1] No transgenic flies obtained

Therefore, I generated two overexpression constructs (Table 4). The first construct encodes N-terminally GFP-tagged Dhc64. Expression of *Dhc64* is regulated by 10 copies of the UAS promoter (10xUAS::GFP::*Dhc64*) ensuring a strong expression of GFP-tagged Dhc64 once activated by Gal4. To integrate this transgene into the fly genome, the vector backbone possesses an attB site for ϕC31 integrase mediated site-specific recombination. I injected 210 embryos with a DNA concentration $250ng/\mu l$. Only 12% of the embryos hatched and of these only 31% developed into fertile adult flies. Yet, no transgenic fly was found when analysing the F1 generation. As the trasngene has a size of $26.3kb$, it might be difficult to integrate such a big construct into the fly genome. Hence, I injected more embryos (705). Although I reduced the injected DNA concentration to $100ng/\mu l$, again only 12% of injected embryos hatched and 41% of these became fertile adult flies. Yet again, none of the F1 progeny carried the transgene. These results may indicate that UAS controlled expression of GFP-tagged Dhc64 is not fully tight. Thus, there might be enough translated product from the gene to cause a dominant-negative effect leading to embryonic or larval lethality, as transcription of the transgene starts even if it is not

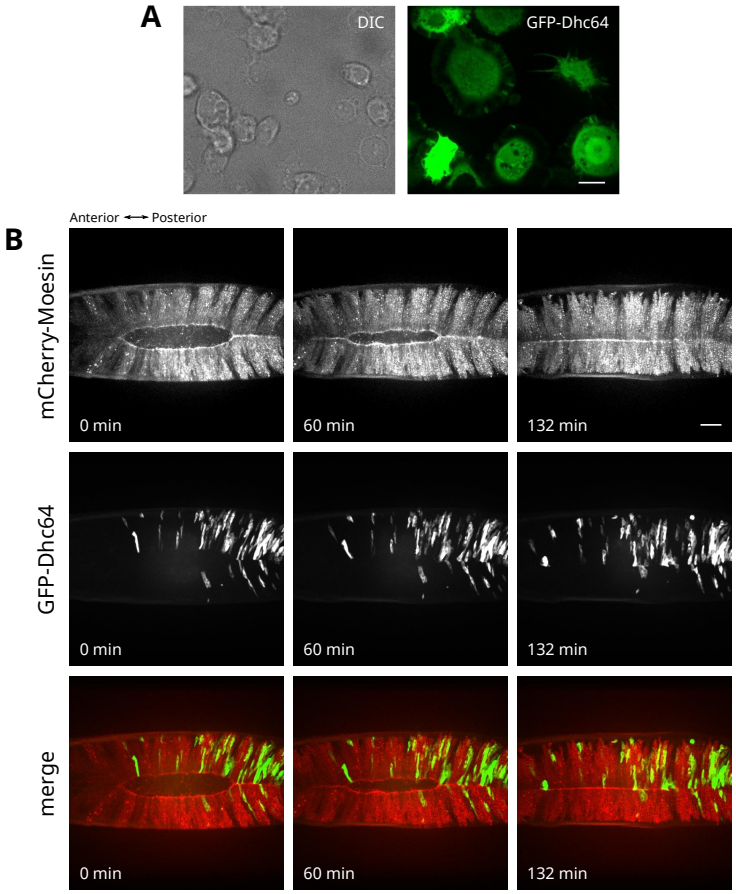

Figure 29: Transient expression of the UAS::GFP::*Dhc64* transgene.
(A) Expression of UAS::GFP::*Dhc64* driven by a transgene containing a *tubulinGal4* driver in S2 cells. Shown is the DIC image and the corresponding fluorescent image. Scale bar: $10\mu m$. **(B)** Transient expression of UAS::GFP::*Dhc64* in embryos. The UAS::GFP::Dhc64 construct was injected into preblastoderm staged embryos carrying *pnrGal4, UAS-mCherry-Moesin*. Embryos were imaged 10-12 hours after injection, when they have reached DC stage. Shown are selected movie frames of an embryo expressing mCherry-Moesin (upper row), GFP-Dhc64 (middle row) and overlay (lower row). Scale bar: $50\mu m$.

yet integrated into the genome.

I have tested the 10xUAS::GFP::*Dhc64* transgene in *Drosophila* S2 cells. Using the *tubulinGal4* driver I observed strong GFP expression in the cells (Figure 29A). Furthermore, I looked at transient expression of the construct during DC. For this, I injected early embryos carrying UAS-mCherry-Moesin, an actin marker, driven by the epidermis-specific *pnrGal4*. I imaged them about 10-12 hours after injection, when DC stage was reached. The embryos showed a mosaic expression of GFP-tagged Dhc64 in the epidermis (Figure 29B). Yet, zipping progressed normally. It is possible that the few cells that expressed the transgene may not be sufficient to show a zipping phenotype.

The second overexpression construct I have generated comprises the genomic *Dhc64* gene with a mutated microtubule binding domain (MTBD) controlled by the UAS promoter (10xUAS). Structural analysis of the dynein heavy chain has shown that two α-helices form an antiparallel coiled-coil stalk (CC1 and CC2). The stalk is kinked by the presence of two highly conserved proline residues. The rest of the MTBD comprises a novel fold of α-helices, which are located at the top of the stalk and make physical contact with the MT (Gee et al., 1997; Gee & Vallee, 1998). I substituted these two proline residues as well as two other conserved prolines which lie within the MT contact region with alanine. As prolines are often found in very tight turns in protein structures or can introduce kinks in α-helices, the introduced mutations will hopefully cause structural perturbations with the result that dynein fails to bind to MTs.

As cloning of the *Dhc64* transgene with the mutated MTBD domain caused technical difficulties due to the large size of the construct and suboptimal restriction sites, time did not permit to inject the final construct. Yet, I expect similar results to the 10xUAS::GFP::*Dhc64* construct, if UAS expression is indeed leaky.

2.6 Targeted manipulation at the *Dhc64* locus using the CRISPR/-Cas9 technology

In the previous sections (2.4 and 2.5) I described approaches on how to study dynein function during DC. As maternal contribution seems to be the main problem, I generated constructs that would allow the use of acute protein depletion methods that can overcome the problem of maternal contribution. However, I was not able to obtain transgenic flies, indicating that the transgenes cause a dominant-negative effect resulting in early lethality of the embryo. Injection of a UAS controlled transgene resulted in the same outcome. I therefore decided next to use the recently developed CRISPR/Cas9 DNA engineering system. This technique allows to generate precise, targeted changes to the genome of different organisms in an efficient and reliable manner (Jinek et al., 2012).

2.6.1 Introducing an attP site into the *Dhc64* locus

Using the CRISPR/Cas9 system, I intended to introduce an attP ϕC31 phage recombination site into the endogenous *Dhc64* gene, which, if successfully integrated, would result in the deletion of the 5' UTR and the first exon coding for Dhc64. In doing so, the previously described approaches for acute protein degradation could be used for Dhc64 protein depletion, as different N-terminal modified variants of exon 1 could easily be reintroduced at the endogenous *Dhc64* locus using the ϕC31 integrase system. Additionally, the resulting deletion of the 5' UTR as well as the first exon of *Dhc64* would cause a *Dhc64* null mutant. For my approach I followed a similar strategy as Gratz et al. (2013a), who have demonstrated a successful replacement of the *yellow* gene with an attP site using CRISPR/Cas9. However, instead of co-injecting a vector encoding for the endonuclease Cas9, I used *nos-cas9* flies. In these flies Cas9 is specifically expressed in the germline by the germline-specific promoter *nannos* (*nos*), which is believed to increase targeting efficiency (Gratz et al., 2013b). To replace *Dhc64* with an attP site, potential CRISPR target sites in the flanking regions of *Dhc64* were identified using the CRISPR Optimal Target Finder (Gratz et al., 2014). For precise transcriptional initiation of the gRNAs by the pU6 promoter, only target sites starting with a guanine were considered. After verification of the CRISPR target sites in *nos-cas9* flies, two plasmids, each containing one gRNA controlled by the pU6 promoter, were generated. As a homology donor for homology directed repair, I used a single-stranded oligonucleotide (ssODN) containing a minimal attP site flanked by $60nt$ long homology arms corresponding to the

Table 5: CRISPR/Cas9 constructs to generate *Dhc64* mutants.

Construct	Objective	Construct size	Injected conc.	Injected no. of embryos	Embryonic survival rate	Fertile flies	Transgenic flies
ssODN gRNA1 gRNA2	Introduce ant attP site into the *Dhc64* gene	$0.2kb$ $3.5kb$ $3.5kb$	$100ng/\mu l$ $250ng/\mu l$ $250ng/\mu l$	1727	2%	38%	None
dsHD gRNA1 gRNA2	Introduce FRT sites flanking exon 10 and 11 of *Dhc64*	$8kb$ $6.4kb$ $6.4kb$	$170ng/\mu l$ $35ng/\mu l$ $35ng/\mu l$	1389	52%	46%	9%
			$500ng/\mu l$ $100ng/\mu l$ $100ng/\mu l$	1461	24%	40%	10%

5' and 3' sequence at the cut sites in the *Dhc64* locus.

The two gRNA plasmids ($250ng/\mu l$ each) were co-injected with the ssODN ($100ng/\mu l$) into 1727 preblastoderm embryos (Table 5). The embryonic survival rate was extremely low (2%). Of these, only 12 flies (38%) developed to adulthood, which then were crossed individually with flies carrying the third chromosome balancer MKRS/TM6B Tb. To screen for flies with successful CRISPR events, individual flies of the F1 generation balanced over TM6B Tb were crossed to a *Dhc64* mutant (*Dhc 6-10/TM6B Tb*). If an attP site was successfully integrated into the Dhc64 locus, all progeny should carry the third chromosome balancer TM6B Tb, as a *Dhc64* loss of function over *Dhc 6-10* would be lethal. Yet, screening revealed also flies without TM6B Tb, demonstrating that no successful CRISPR event had occurred. This finding suggests that CRISPR/Cas9 mediated introduction of the attP was not efficient. Alternatively, Cas9 might have induced a double-strand break, leading to early homozygous lethality, as *Dhc64* mutants were shown to be early larval lethal (Gepner et al., 1996; Port et al., 2015). Yet, the extremely high lethality of injected embryos might also be caused, among others, by the applied concentration of gRNAs. It was shown by a former colleague that a lower gRNA injection concentration results in a higher embryonic survival rate (Fürst, 2015) .

2.6.2 CRISPR/Cas9-mediated FRT insertion at the *Dhc64* locus to generate conditional dynein mutants

Unfortunately, none of the approaches described so far to integrate modified *Dhc64* transgenes or to introduce an attP recombination site into the endogenous *Dhc64* gene to study dynein function during zipping have been successful. As a new attempt

to modify the endogenous *Dhc64* gene I used the CRISPR/Cas9 system to introduce FRT (FLPase recognition target) sites into introns flanking two small exons encoding the dynein MTBD (exon 10 and 11, Figure 30). Thus, the FLP/FRT site-specific recombination system would allow the excision of the two exons located in between the FRT sites. *Dhc64* should not be affected until FLP recombinase is expressed. Therefore, we hope that an early expression of FLP would lead to an abundant amount of transcribed Dhc64 missing exon 10 and 11 to cause a potential zipping phenotype, as these two exons code for the physical contact site of dynein to MTs. Moreover, a successful integration of the FRT sites at the dynein locus would be a great tool to study dynein function during other developmental processes, as FLP expression can be induced in a time- and tissue-specific manner.

Using the CRISPR Optimal Target Finder, I selected two CRISPR target sites without predicted off-target effects. One is located in the intron upstream of exon 10, the second one is lying within the next exon downstream of exon 11. The CRISPR target site sequences were verified in *nos-cas9* flies by sequencing. Two plasmids were generated, each comprising one gRNA, regulated by the pU6 promoter. In contrast to the ssODN used in the previous CRISPR/Cas9 experiment for homology directed repair, the homology donor used for this approach was a double-stranded donor template (dsHD). This donor template with a size of $7982bp$ carried the modified *Dhc64* sequence situated in the two introns flanking exon 10 and 11 consisting of two FRT sites (FRT1 and FRT2), a sequence encoding the DsRed marker with adjacent loxP sites situated in between FRT1 and exon 10 and two homology arms (HR1 and HR2) each with a size of $1kb$ (Figure 30B). The DsRed marker is under the control of an eye-specific enhancer element (3XP3), which will allow screening for DsRed positive eyes in the F1 progeny. The adjacent loxP sites will permit removal of the DsRed marker.

Furthermore, I had to modify the 3' end of exon 9 lying upstream of the first FRT as well as the 5' end exon 10, since FLP mediated excision of the two MTBD encoding exons would result in an unwanted frameshift. Two bases were added two the 3' end of exon 9 in order to encode an otherwise missing alanine that is part of the coiled-coil domain of the MTBD site. These two bases in turn had to be deleted from the exon 10. The dsHD as well as the two plasmids containing the gRNAs were co-injected into *nos-cas9* expressing preblastderm embryos. I performed two rounds of injections with different total DNA concentrations: the recommended concentration of $700ng/\mu l$ by Gratz et al. (2014) and a lower total DNA concentration of $240ng/\mu l$ to have possible increased survival rates (Table 5). Embryonic survival rates were

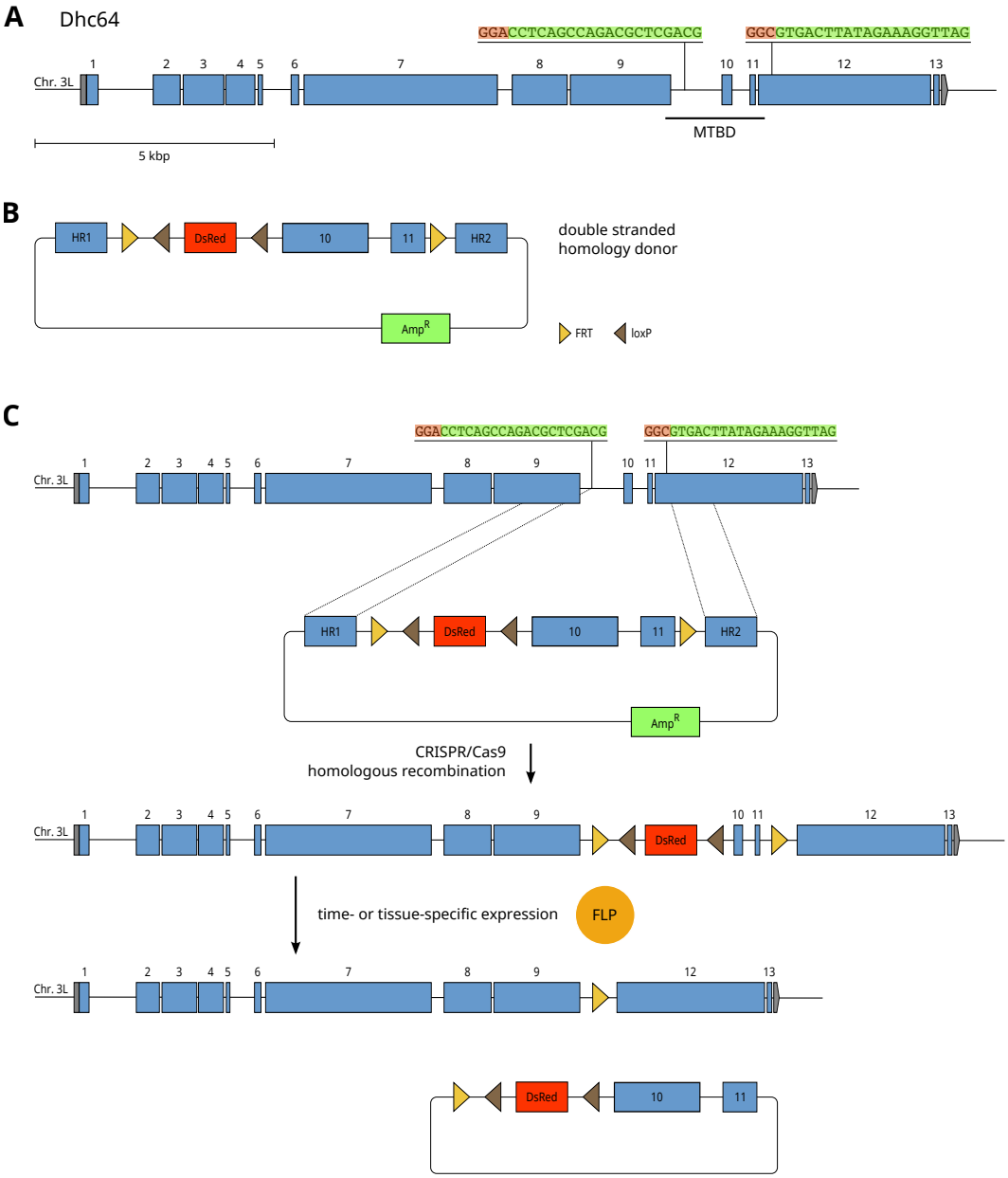

Figure 30: Schematic representation of the experimental setup to generate a conditional *Dhc64* mutant mediated by CRISPR/Cas9.
(A) Schematic view of the *Dhc64* gene and the position and sequence of both gRNAs. Coding sequences are represented in blue and UTRs in grey blocks. MTBD is encoded by several exons, spanning from the end of exon 9 to the first nucleotides of exon 12. **(B)** Schematic of the dsHD template. It includes modified *Dhc64* sequence consisting of two FRT sites situated in the two introns flanking exon 10 and 11, a DsRed marker with adjacent loxP sites and two homology arms (HR1 and HR2), each being $1kb$ long. **(C)** Experimental steps to generate a *Dhc64* mutant: Upon successful exchange of the original *Dhc64* sequence with the modified one of the dsHD template, time- or tissue-specific expression of FLPase can be used to create a *Dhc64* mutant lacking most of its MTBD.

52% for embryos with the lower injected DNA concentration and 24% for those with the higher concentration. Injected embryos that developed to adulthood were crossed with *yw* flies and the F1 progeny was screened for DsRed positive flies. Of 46% fertile adult flies, that were injected with $240ng/\mu l$ total DNA concentration, 9% were DsRed positive. 40% of embryos injected with $700ng/\mu l$ DNA concentration developed into fertile adults, which in turn gave rise to 10% DsRed positive flies.

These results show that the dsHD was successfully integrated into the fly genome. The next steps are to further analyse the obtained transgenic flies and to confirm the sequence of the integrated donor and its integration site. A successful integration of the FRT sites flanking two exons encoding the MTBD domain will offer a unique tool to study dynein function during different times of development using the FLP/FRT system.

3 Discussion: Part 1

In this work I aimed to elucidate the role of dynein in force generation during zipping, which is needed for the last step in dorsal closure (DC) to seal the gap. Previous work has suggested that protrusions of opposing leading edge (LE) cells form a complex and strongly intertwined interaction surface (Jacinto et al., 2000). Actin-based protrusion shortening is thought to generate the zipping force mediating the sealing of the gap and reshaping the surface into normal epithelial cell-cell contacts. However, recent experiments have shown that zipping also occurs without epidermal myosin II, an actin motor (Pasakarnis et al., 2016). Furthermore, there is strong evidence that MTs have a function in force generation during zipping (Eltsov et al., 2015). A 3D reconstruction of the zipping process has shown that after initial cell-cell contacts are formed by filopodia of matching LE cells, their lamellipodia expand to generate a single overlap surface. The number of MTs in these overlap regions rapidly increases while actin bundles disappear. As zipping progresses, the overlap regions shorten, which is likely to generate the zipping force. During this part of the process the distribution of growing and shrinking MTs changes. A much higher number of shrinking MT plus ends is present, and these ends are localised in the regions of cell-cell contacts. This suggests that MTs are attached close to the cell membranes and their shrinking ends exert a pulling force (Eltsov et al., 2015).

We hypothesised that a key player for generating this pulling force by MTs is the motor protein dynein. This is due to the similarity in MT behaviour at the cell membrane during processes like mitotic spindle positioning in human cells or *C. elegans* zygotes (Kotak et al., 2012; Gönczy et al., 1999). In these systems, dynein is tethered to the cell cortex, where it grabs incoming MT plus ends. Due to its minus-end directed motility, cortical dynein generates a pulling force on the MT leading to the depolymerisation of the MT. Since this mechanism appears to be evolutionary conserved, such a mechanism might work in our system with the fundamental difference that the same force is not used to move subcellular components, but to shape cells and tissues. This would suggest a completely novel function for dynein in tissue morphogenesis.

To examine a role of dynein in force generation during zipping, I used various methods to interfere with dynein function during zipping, which I will discuss in the next sections. In addition, I have shown that dynamic MTs are required for zipping.

3.1 Dynamic microtubules are required for zipping

In this study I have shown that dynamic MTs are essential for the zipping process. Taxol, a drug that inhibits MT depolymerisation, was injected into DC stage embryos, which resulted in the stabilisation of MTs and thus, the absence of MT dynamic instability. The absence of MT dynamic instability became particularly obvious when we analysed the movement of EB1, a protein that localises to and controls the plus ends of growing MTs (Vaughan, 2005). When MTs were not affected by taxol injection, we observed bidirectional EB1 movement in the epidermis as a consequence of the previously reported anti-parallel orientation of MTs along the apical side of epithelial cells (Jankovics & Brunner, 2006).

In addition, I have shown that not only the absence of MTs causes a zipping arrest, as shown by Jankovics & Brunner (2006), but stabilised MTs are enough to inhibit the zipping process. Taxol injection specifically impaired the zipping process, as convergence of epithelial sheets and therefore the apical constriction of amnioserosa cells appeared to progress normally. Inhibition of zipping resulted in an elongated, abnormally narrow dorsal opening, yet in most taxol-treated embryos, DC eventually completed, albeit with a strong delay. As a consequence of such abnormal closure, a severe puckering phenotype occurred. The puckering phenotype can be explained as the result of the amnisoserosa cells undergoing apoptosis, which was described to be an integral part of DC (Reed et al., 2004; Toyama et al., 2008). Although zipping is absent, amnioserosa cell delamination will further reduce the gap size in a circular manner, which will bring the epidermal fronts into sufficient proximity to form cell contacts and close the gap. Alternatively, a mechanism similar to a wound healing response during which contractile forces seal a wound might close the dorsal hole when zipping is absent. Thereby, opposing LE cells make contact through actin-based cell protrusions, allowing tugging of opposing cells on one another and sealing the gap (Wood et al., 2002).

Moreover, we frequently observed a rupture of the actin cable close to the anterior canthus. Such ruptures were probably the result of head involution, a morphogenetic process that occurs concomitant with the end stages of DC (VanHook & Letsou, 2008). During this morphogenetic event, a region of the tissue farthest on the anterior side folds into the interior of the embryo while the adjacent lateral epidermis moves anteriorly to cover it. Thereby, the anterior end of the dorsal opening is subject to mechanical stresses due to head involution (Peralta et al., 2007). Such stress might therefore be the cause of the ruptures within the actin cable, which

were observed close to the anterior canthus in embryos that did not zip due to taxol treatment.

Furthermore, MT bundles became long and started bending as a result of taxol-mediated inhibition of MT depolymerisation. In addition, entire MT bundles moved around in the cells. Such MT behaviour might indicate motor activity, as individual bundles cannot move that fast by diffusion only. Since the bundles are located along the apical cell cortex, the moving MT bundles might have disconnected from the cortex or, if not, they remain connected and a motor might be anchored at the cortex allowing such a movement.

These results demonstrate, that dynamic MTs are essential for zipping during DC. In our hypothesis, dynamic MTs interact with cortical dynein and thereby exert a pulling force. However, in *in vitro* experiments it was suggested, that MT shrinkage is necessary for MTs and cortical dynein mediated pulling force generation (Laan et al., 2012a). In taxol-treated embryos, MTs are stabilised and therefore shrinkage is absent. Thus, MTs cannot be pulled further towards the cortex, which prevents dynein from moving towards the MT minus end, and as a result the zipping force cannot be generated. In addition, severe bending of the MT might not allow dynein to walk towards its minus end. Such bending of individual MTs might be very likely, as we observed bent MT bundles in taxol-treated embryos. Thus, stabilised MTs might start buckling before even reaching the cortex of the zipping cell. This buckling behaviour can also be observed in large cells with long MTs (Laan et al., 2012b). Altogether, these results indicate that MT dynamicity is required for zipping force generation.

3.2 Maternally contributed Dhc64 does not allow studying dynein function during dorsal closure

To study dynein function during DC, the most straightforward approach was to analyse existing dynein mutants during this process. Dynein is a large multiprotein complex consisting of two identical heavy chains and a complement of intermediate, light intermediate and light chain subunits (reviewed in King, 2000). The dynein heavy chain (*Dhc64*) encodes the motor activity as well as the microtubule-binding domain (MTBD), thus making it an ideal candidate to test our hypothesis.

First evidence pointing towards a function for dynein during DC is the enrichment of the *Drosophila* Dhc64 in LE cells during DC, which was shown in antibody staining experiments in this work and by Eltsov et al. (2015). This enrichment disappears after zipping is completed, which indicates an involvement of dynein

during zipping. Unfortunately, light microscopy does not allow individual zipping cells to be resolved in such detail, which would enable the examination of possible enrichment of dynein at the cortex of these cells. Yet, analysed homozygous and trans-heterozygous *Dhc64* mutants revealed, apart from a reduced closure speed, normal zipping progression. These results are not that surprising, as it has been previously suggested that maternally contributed Dhc64 is sufficient for embryonic development, whereas zygotic function is required for larval and pupal development (Gepner et al., 1996). We cannot be sure, however, that the analysed alleles are complete loss of function alleles. Hence, we cannot exclude that zygotic Dhc64 function might be needed at late stages during embryogenesis. The CRISPR/Cas9 system has recently been used to induce somatic *Dhc64* mutations resulting in a Dhc64 loss of function (Port et al., 2015). Lethality of such loss of function mutations occurred only at larval stages, supporting the previous findings that maternally contributed Dhc64 protein is sufficient for embryonic development. We observed a similar behaviour as in the analysed *Dhc64* mutants when expressing a UAS-controlled RNAi construct against *Dhc64* in epidermal cell stripes. In such embryos zipping progressed normally, but the mean closure speeds of these embryos were decreased. These findings pointed once more towards maternally contributed Dhc64, which allows development beyond DC. The use of earlier expressed drivers such as actinGal4 might cause stronger reduction in Dhc64 protein levels, however, also secondary defects might accumulate. Furthermore, such drivers may not solve the problem of maternal contribution.

Alternatively, one could use Gal4 drivers, which are active in the germline of the mother. Using a maternal-Gal4 driver for RNAi expression could deplete *Dhc64* mRNA levels in the oocyte, and thus overcome the problem of maternal contribution. However, it was shown that Dhc64 is required already during oocyte formation for proper localisation of *bicoid* and *oskar* mRNAs, which define the anterior-posterior axis of the oocyte (Januschke et al., 2002; Duncan & Warrior, 2002). Hence, the use of maternal-Gal4 to mediate *Dhc64* mRNA knockdown would likely produce embryos with many accumulated defects before the onset of DC.

Thus, maternal contribution of Dhc64 is a main obstacle in the study of dynein function during DC using mutant alleles. A detailed discussion how to overcome this problem will be presented in Section 3.6.

3.3 Dynein light intermediate chain seems to be dispensable for zipping

Since dynein is a large multiprotein complex, other components than the dynein heavy chain can give insights into dynein function during zipping. I analysed the dynein light intermediate chain (Dlic), which is particularly suitable, as it is encoded by a single gene found on the X-chromosome in the *Drosophila* genome. Two recessive larval lethal mutants G0065 and G0190 resulting from P-element insertions haven been described (Mische et al., 2008). Hemizygous G0065 and G0190 males only revealed reduced closure speeds, but no major DC defects were observed. This is not surprising, as lethality was described to only occur at the larval stage (Mische et al., 2008).

Flies carrying a ubiquitously expressed GFP-Dlic construct rescued both mutants. Therefore, we were able to use the deGradFP system (Caussinus et al., 2012) to perform an acute Dlic protein knockdown. I used several different Gal4 lines to express the anti-GFP nanobody for protein knockdown. Such embryos displayed GFP-dots in the Gal4 expressing tissues, which is a phenomenon that has been shown to be a reliable readout for efficient deGradFP-mediated myosin II depletion (Pasakarnis et al., 2016). None of the embryos, however, exhibited a zipping defect. The only observed effect was a decrease in closure speeds of embryos, in which anti-GFP nanobody expression was driven by the epidermis-specific *pnrGal4*. Yet, similar zipping speeds were also observed in hemizygous Dlic mutants. This indicates that Dlic knockdown might not have been efficient enough and thus, there might be remaining Dlic activity. To test the efficiency of deGradFP-mediated Dlic depletion in embryos one could perform Western blot experiments and analyse if Dlic protein levels are reduced after deGradFP-mediated Dlic knockdown.

However, at later stages of development, thorax related defects were identified in flies, in which nanobody expression was driven by *pnrGal4*. Whereas G0065 mutants only exhibited bristle defects, the G0190 mutants showed a mild thorax cleft in addition. Abnormal wing morphology was observed in flies in which Dlic depletion was mediated by *enGal4* driven nanobody expression in G0190 mutants, whereas G0065 mutants did not give rise to adult males. It was suggested by Gepner et al. (1996) that dynein function is required for mitosis in the thorax and in wings. Our results show that Dlic function might also be involved in cell division in the thorax and in wings. As embryos with nanobody expression, driven by *69BGal4*, *daGal4* and *actinGal4* did not give rise to male adult flies this confirmed that Dlic

function is required for development as previously described by Mische et al. (2008). Furthermore, these results demonstrate that deGradFP-mediated Dlic depletion is successful.

The absence of a DC phenotype in Dlic-depleted embryos indicates that Dlic function is not required for this process. However, it should be mentioned, that only male embryos were expected to show a phenotype. Male embryos were analysed in which Dlic knockdown was mediated by *pnrGal4* driven nanobody expression in the G0190 mutant. These embryos did not show any defects despite a decreased DC speed. Embryos with nanobody expression driven by the remaining Gal4 lines did not carry a marker allowing us to distinguish male and female embryos. Yet, due to the number of samples, it is highly unlikely that only female embryos were imaged. However, it could be, that male embryos did not reach the DC stage. This might apply particularly to embryos in which Dlic depletion was mediated by an early anti-GFP nanobody expression driven by *daGal* or *actinGal4*. The use of a fluorescent X-chromosome balancer could give an answer to this.

Yet another reason for a missing DC phenotype might be that both P-element insertions do not cause a complete Dlic loss of function, thus remaining Dlic activity allows normal DC progression. Imprecise excision of the P-element insertions could result in stronger mutant alleles. Alternatively, Dlic function is simply not required for DC.

So far, not much is known about Dlic function during *Drosophila* embryogenesis. During the formation of the oocyte, however, it has been shown that Dlic is required for all known Dhc64 functions. Alike Dhc64, Dlic localises to the oocyte posterior and is needed for oocyte specification. Both components are also required for spindle orientation in mitotic germline cysts. Furthermore, it was suggested that the heavy chain, intermediate chain and light intermediate chain are more stable once incorporated into the dynein complex in Drosophila S2 cells (Mische et al., 2008). Although, dynein is involved in transporting and anchoring cargoes at the posterior pole during oocyte formation (Januschke et al., 2002; Duncan & Warrior, 2002), such dynein functions might likely differ from cortical dynein functions involved in force generation. One could hypothesise that cortical dynein function requires different dynein subunits, and thus Dlic might not be needed for a dynein function at the cortex.

Furthermore, during early embryonic *C. elegans* development, Dlic was shown to be needed for mitosis. As Dhc localisation was not affected during mitosis in *Dlic* mutant embryos, it was suggested that Dlic has a specific function during mitosis,

which is not dependent on Dhc. Moreover, meiotic spindle formation is not affected in *C. elegans Dlic* mutants, whereas *Dhc* mutants fail to form spindles (Yoder & Han, 2001). These results indicate that Dlic is not required for all Dhc functions in *C. elegans*, similar might apply for *Drosophila*. Thus, one could speculate that Dlic has no role in a presumably dynein driven zipping force during DC.

3.4 Dynactin does not seem to be required for the zipping process

Another way to examine dynein function during zipping, was to analyse components of the dynactin complex. Dynactin, also known as the dynein activator complex, can regulate dynein activity and is required for many dynein functions. It consists of several subunits, of which p150 Glued is the largest and was shown to be essential for dynactin function. Moreover, it directly binds dynein (reviewed in Schroer, 2004). The Drosophila *Glued* is the functional homologue of the vertebrate p150, thus the name p150 Glued (Waterman-Storer & Holzbaur, 1996).

To assess the function of dynein/dynactin during DC I examined two fly lines, each expressing a dominant-negative variant of Glued, dnGl84 and dnGl96B (Allen et al., 1999). Both lines express the $Glued^1$ mutation under the control of the UAS promoter. $Glued^1$ was shown to be a dominant mutation, which results in a truncated protein product that "poisons" normal dynactin activity (Plough & Ives, 1935; Harte & Kankel, 1982; Swaroop et al., 1985; Fan & Ready, 1997).

I overexpressed UAS-dnGl84 and UAS-dnGl96 using the *enGal4* driver. Such embryos did not show any closure defects. As the dominant-negative effect of Glued has been shown to be dosage dependent (Swaroop et al., 1985), I overexpressed UAS-dnGl84 in a heterozygous $Glued^1$ mutant background. The only effect we observed in DC stage embryos, however, were reduced zipping speeds of individual engrailed cell stripes, but no full arrest of closure. As $Glued^1$ heterozygosis revealed similar zipping speeds compared to wild-type embryos, the observed effect might be indeed the result of a dosage-dependent dominant-negative effect of Glued. Hence, to increase a putative phenotype, one could use a stronger Gal4 driver for UAS-dnGl84 expression and in addition combine it with a $Glued^1$ homozygous mutant. This might cause sufficient "poison" Glued protein to interfere with the wild-type Glued protein. However, homozygous $Glued^1$ mutants develop beyond DC and die at first instar larval stage (Harte & Kankel, 1982; Swaroop et al., 1986; Waterman-Storer & Holzbaur, 1996), indicating that maternal contribution supports embryonic development. Therefore, high levels of abnormal $Glued^1$ gene product might be needed to interfere with the maternally and zygotically produced wild-type Glued

protein.

To further investigate a possible role of dynactin during zipping, I overexpressed another subunit of the dynactin complex, p50 dynamitin. Overexpression of dynamitin was shown to inhibit dynein function. Dynamitin, however, does not inhibit dynein directly but instead causes the disassembly of the dynactin complex (Melkonian et al., 2007). Dynamitin overexpression driven by the epidermis-specific *pnrGal4* in heterozygous *Dhc 4-19* mutant embryos caused reduced closure speeds, but did not appear to affect zipping. In heterozygous *Dhc 4-19* mutant embryos alone, closure speed was not affected. Although we observed a decrease in closure speed, these results do not appear to support dynein function during zipping. However, experiments with enhanced sensitisation of the genetic background combined with dynamitin overexpression and dominant-negative Glued expression might give further insights into dynactin-dependent dynein function in DC.

So far, dynactin has been shown to be essential for a broad range of cellular functions of cytoplasmic dynein (reviewed in Schroer, 2004). However, there is not much known if dynactin function is at all required for dynein in order to exert pulling forces on shrinking MTs. Yet, several studies have shown, that dynactin colocalises with dynein at the cell cortex (McGrail & Hays, 1997; Yang et al., 2014; Woodard et al., 2010; Crowder et al., 2015; Fujita et al., 2015). Furthermore, it was suggested that dynactin is needed for the cortical anchoring of dynein in *S. pombe* during meiotic nuclear oscillations and in *C. elegans* oocytes and embryos during meiotic and mitotic spindle orientation (Niccoli et al., 2004; Fujita et al., 2015; Skop & White, 1998; Crowder et al., 2015). In these systems cortical dynein generates pulling forces by interacting with MT plus ends. Yet, disrupting dynactin function during DC did not affect the zipping process. Thus, our results do not appear to support an essential function for dynein during zipping in DC. However, cortical anchoring of dynein might be independent of dynactin in this process.

3.5 CiliobrevinD impairs zipping, but also affects amnioserosa cell pulsing

As we were unable to clearly identify a role for dynein in zipping by genetic means, drug injections were performed in an alternative attempt to inhibit dynein function. The recently discovered specific dynein inhibitor CiliobrevinD was shown to efficiently block dynein (Firestone et al., 2012). Until now, the use of CiliobrevinD to inhibit dynein function was only demonstrated in cell culture experiments (reviewed in Roossien et al., 2015). Hence, I tested its efficiency in syncytial embryos.

During this stage of development embryos undergo several rounds of mitotic divisons, which require dynein function. CiliobrevinD caused mitotic defects such as multipolar spindle arrays or free centrosomes in the living embryo. A similar effect was seen in *Dhc64* mutants (Robinson et al., 1999), thus implying that CiliobrevinD can indeed block dynein function in intact *Drosophila* embryos.

In DC stage embryos, CiliobrevinD injection led to a variety of phenotypes such as slowed or arrested zipping, or the expansion and subsequent rupturing of embryonic tissue, which was often seen during early zipping stages. CiliobrevinD injection did not, however, always cause a DC phenotype, as there were embryos which zipped normally. Furthermore, some DMSO control embryos showed similar phenotypes as the ones caused by CiliobrevinD injection, however such phenotypes occurred seldom compared to the far more frequent and generally more severe occurrence of phenotypes in CiliobrevinD-treated embryos. This indicates that CiliobrevinD application is efficient and dynein function seems to be required during DC. That DMSO, the most commonly used solvent for drug injection experiments, appears to affect DC progression too, stresses the importance of control injections with the solvent alone.

The variety of CiliobrevinD phenotypes might be a consequence of the injection procedure. Embryos were injected posteriorly and anteriorly into the yolk cell. However, as the yolk cell is a highly viscous system, the effect of the drug might differ if released close to the amnioserosa surface or more towards the bottom of the yolk cell. Thus, drug release at the bottom of the yolk cell likely has little or no effect on zipping as the diffusion of the drug might be rather slow and not reach the epidermal tissue on time to cause an effect, whereas a release closer to the amniosresoa surface might lead to a faster and stronger effect on zipping. In addtion, the injected volume likely varied due to manually applied pressure on the syringe and different sized openings of each injection needle, although the applied concentrations were equal. To improve the injection performance, an automated or semi-automated injection process could be helpful. Furthermore, one could also add a fluorescent dye to the injection mix, which would allow one to observe the diffusion of the drug while imaging and, hence, monitor whether CiliobrevinD acts locally or globally.

Moreover, CiliobrevinD-mediated dynein inhibition did not seem to affect exclusively the zipping process. Embryos, in which specifically zipping is impaired, show an elongated, abnormally narrow dorsal hole as a result of an absent zipping process but normal epithelial sheet convergence. Such a phenotype was rarely observed in CiliobrevinD-injected embryos. This suggests, that CiliobrevinD might also affect

other tissues. This is to be expected, as drug injections often cause global effects. Both normal, and a partial or full arrest of, amnioserosa cell pulsing (the driving force for epithelial sheet convergence) were seen in CiliobrevinD-treated embryos, in which zipping stopped or the embryonic tissue expanded and eventually ruptured. Thus, the observed phenotypes are not a consequence of defective amnioserosa cell pulsing, however, dynein inhibition seems to have some effect on the amnioserosa tissue. In CiliobrevinD-treated embryos in which zipping was slowed down or progressed normal, as well as in DMSO control embryos, amnioserosa cell pulsing was normal. Due to the varying effects of CiliobrevinD it is not possible to determine an explicit role for dynein during DC. Yet, it seems that not only zipping is affected, but also apical constriction of amnioserosa cell pulsing. Therefore, it is essential to study a dynein mutant during DC.

3.6 Methods to overcome dynein maternal contribution during dorsal closure

3.6.1 N-terminal tagging of Dhc64 seems to generate a dominant-negative variant of Dhc64

The main obstacle to study dynein function during DC using mutants is maternal contribution, which is sufficient to complete embryogenesis. The same applies when using RNAi against *Dhc64*. If maternally provided proteins are stable, depletion of newly produced mRNAs does not have a significant effect. Other approaches to interfere with dynein function, like dominant-negative expression of Glued, or dynamitin overexpression, are widely used as they disrupt the dynactin complex and hence block dynein function. These approaches did not produce a phenotype during DC, thus speaking against a role of dynein in this process. It is possible, however, that dynein acts independently of dynactin in DC. To shed more light on a possible role for dynein in force generation during zipping, we have to study Dhc64 function specifically during this process. Therefore, it is essential to overcome Dhc64 maternal contribution.

There are several methods that can mediate an acute protein knockdown, which I have described in Section 1.5.2. An acute protein knockdown does not only degrade newly produced proteins, but also proteins provided by maternal contribution. Furthermore, it can be mediated in a time- and tissue-specific manner, which allows studying the function of a protein during a specific process. To perform such a protein knockdown of Dhc64, I had to generate several different transgenes for different

protein depletion methods, which rescue a homozygous *Dhc64* mutant.

I generated an N-terminal GFP-tagged Dhc64 construct for the deGradFP system, in which protein depletion is mediated by the anti-GFP nanobody recognising a GFP-tagged protein and targeting it for degradation. For the TIPI (TEV protease induced protein inactivation) approach, I generated a transgene containing the TEV cleavage site as well as the N-Degron with an N-terminal phenylalanine, followed by a GFP tag and the genomic *Dhc64* sequence. Upon TEV expression, TEV cleavage unmasks the phenylalanine, and Dhc64 will be targeted for degradation. For blue light mediated protein inactivation, the generated construct contained the genomic *Dhc64* sequence, which was tagged N-terminally with the plant cryptochrome Cry2 and RFP. Upon blue light illumination Cry2 leads to the formation of photobodies, and thus likely to the aggregation and inactivation of the target protein. All generated transgenes contained an attB site for ϕC31 integrase mediated site-specific recombination. As every construct contained the whole genomic *Dhc64* sequence, the constructs were very large ($28 - 30kb$). Unfortunately, none of the injected embryos gave rise to a transgenic fly for any of the generated transgenes. Although high numbers of embryos were injected and different DNA concentrations were applied, the embryonic survival rate was very low. As transcription of injected constructs starts even before integration, we concluded that the N-terminal tagging was causing a dominant-negative effect and therefore, we did not obtain a viable fly with an integrated transgene. Yet, the constructs generated for the deGradFP and the TIPI system were successfully expressed in *Drosophila* S2 cells, showing that a tagged Dhc64 protein can be expressed.

The N-terminal tail of the dynein heavy chain has binding sites for other structural and regulatory components of the dynein complex as well as docking sites for cargoes (Schiavo et al., 2013). As N-terminally modified Dhc64 likely competes with the wild-type protein to form the dynein complex, one could speculate that this modified Dhc64 does not allow a proper assembly of the complex, and thus causes a non-functional dynein complex. Since dynein is needed in early embryogenesis (Robinson et al., 1999), a dominant-negative effect of the injected dynein construct might therefore lead to early lethality. As dynein function is intensively studied in *Drosophila*, it is surprising that there is no tagged version of Dhc64 available. This leads to the assumption that tagging Dhc64 is not trivial.

However, searching the literature, I found that the organisms in which a tagging of dynein heavy chain, either N- or C-terminally is possible, are fungi, e.g. *S. pombe* (Yamamoto et al., 1999), *S. ceravisiae* (Markus & Lee, 2011), *Aspergillus nidulans*

(Xiang et al., 2000) or *Ustilago maydis* (Schuster et al., 2011). Morever, GFP-tagged Dhc can also be expressed in different cultivated cells, e.g. HeLa (Splinter et al., 2012) Yet, I could not find higher eukaryotes which have been described to express GFP-tagged Dhc.

It was not possible to perform an acute protein knockdown of Dhc64 during DC, as an N-terminally modified Dhc64 likely causes a dominant-negative effect during embryogenesis. Thus, to study dynein function during DC, we decided to express such a dominant-negative variant of Dhc64, which would then interfere with the wild-type Dhc64. To avoid early dominant-negative effects, I cloned the N-terminal GFP-tagged *Dhc64* sequence into vector containing a UAS promoter. As the UAS promoter would control the expression of the GFP-tagged Dhc64, we expected the tagged Dhc64 to be silent until its expression would be induced. To ensure strong expression of this presumably dominant-negative variant of Dhc64, the vector contained ten UAS sites for Gal4 transcriptional activators, as described in Pfeiffer et al. (2012). For stable integration into the fly genome using the ϕC31 integrase system, this construct contained an attB site. Injected embryos, however, had a low survival rate, which remained even in a second injection round where the DNA concentration was reduced. A reason for this is likely a leaky expression of the UAS controlled GFP-tagged Dhc64, which causes a dominant-negative effect. Such a leaky expression can be the result of a position effect of the landing site. The chromatin environment can influence the landing sites, and thus the genomic landing site might not work well for some transgenes (Markstein et al., 2008; Pfeiffer et al., 2010). To overcome this, one could try to use different landing sites, which might cause less leaky expression of the transgene. Alternatively, introducing a stop-cassette, which prevents unwanted early expression of a modified Dhc64 could overcome the problem of leaky transgene expression. Using the FLP/FRT system the stop-cassette could be controlled in a time- and tissue-specific manner. However, transient expression of this transgene during DC resulted in mosaic expression of GFP-tagged Dhc64 in the dorsal epidermis and revealed normal zipping progression. As only few cells expressed the transgene, it may not be sufficient to interfere with the zipping process.

I generated another *Dhc64* construct, which was cloned into the 10xUAS vector. This *Dhc64* did not have an N-terminal modification, but a mutated MTBD. Highly conserved prolines within the MTBD domain were substituted with alanine. As these prolines are thought to introduce kinks into the α-helices, which are a part of the MTBD, we expect that an alanine substitution will cause structural impairments

that will not allow dynein to bind to MTs. This transgene is yet to be injected, however it might give similar results as the UAS transgene described earlier.

3.6.2 A tool to generate conditional *Dhc64* mutants

The recently established CRISPR/Cas9 system allows precisely targeted changes to be made to the genome in *Drosophila* in an efficient and reliable manner. Gratz et al. (2013a) have successfully used this system to replace the *yellow* gene with an attP site. Using a similar strategy, I planned to introduce an attP site into the endogenous Dhc64 locus, which would also cause the deletion of the first exon coding for Dhc64. A successful introduction would allow one to reintroduce an N-terminally modified exon 1, and thus various methods could be used for Dhc64 protein depletion depending on the N-terminal modification. I used an ssODN containing a minimal attP site flanked by $60nt$ homology arms. Embryos, with Cas9 expression restricted to the germline, were injected with a DNA mix containing the two gRNA plasmids and the ssODN. As the resulting embryonic survival rate was extremely low and no successful CRISPR event was scored in adult flies, early lethality might have occurred. This early lethality can be a consequence of a Cas9-induced double-strand break that has been repaired by homologous recombination during which exon 1 was replaced with an attP site on both homologous chromosomes. To avoid Cas9-induced DNA cleavage of both strands, one could introduce a balancer chromosome into the *nos-cas9* stock, in which the sequence does not match the identified CRISPR target sites. This sequence should differ from the CRISPR target sites in such a way that Cas9 cannot recognise the target sequence and thus only induces a single-strand break in the chromosome not coming from the balancer. An alternative explanation for the absence of a successful CRISPR event might be that instead of homology directed repair (HDR), non-homologous end joining (NHEJ) occurred at the cut sites, and thus might have caused a dominant-negative Dhc64 variant leading to early lethality. Therefore, a modified CRISPR/Cas9 strategy for manipulation of the *Dhc64* gene might be more efficient. Instead of using an ssODN as a homology donor for the subsequent HDR after Cas9-induced DNA cleavage, a double-stranded homology donor (dsHD) has proven to be an ideal template for HDR. This dsHD carries in addition a DsRed marker, whose expression is controlled by an eye-specific enhancer and therefore allows easy screening for DsRed positive eyes and thus a successful CRISPR event. Using this CRISPR/Cas9 strategy, it was possible to successfully replace *zipper*, which encodes myosin II heavy chain, with an attP site (Fürst, 2015).

I used a similar strategy to introduce FRT sites into introns flanking two small exons (exon 10 and 11) of the MTBD of *Dhc64*. A successful integration of such FRT sites would allow the generation of conditional dynein mutants using the FLP/FRT system. Two different DNA concentrations were used for injection: $700ng/\mu l$, which was recommended by Gratz et al. (2014); and a lower one of $240ng/\mu l$, to have a possible increased embryonic survival rate. Each injection mix contained the dsHD, carrying the modified sequence coding for the MTBD, and the gRNAs. The survival rate of embryos with the lower injected DNA concentration was double that of embryos injected with the higher concentration. However, this did not affect the percentage of obtained transgenic flies. About 10% of transgenic flies were scored for each applied injection mix. Thus, the amount of injected DNA affects the initial embryonic survival rate, however, it does not affect CRISPR/Cas9 efficiency.

As a next step, we will need to confirm the sequence of the integrated donor as well as its integration site. The efficiency of this newly established tool to generate *Dhc64* conditional mutants could be tested during early mitotic divisions in the syncytial embryo for which dynein function is required (Robinson et al., 1999). Once we can show that dynein function can be perturbed using this system, it will be a unique tool to study dynein function during *Drosophila* development.

3.6.3 Microtubules tethering to the cortex

MTs have been suggested to generate the zipping force during DC (Eltsov et al., 2015). During zipping, interacting LE cells generate single lamellar overlaps after initial contacts have been made by filopodia. These overlaps subsequently shorten, and thus likely generate the zipping force. As these overlap regions are filled with MTs, and actin bundles are absent, MTs are prime candidates to generate the force necessary for zipping. Within the shortening lamellar overlap, the shrinking ends of MTs are situated end-on at putative cell-cell adhesion sites. This indicates that these MTs do not freely depolymerise, but are tethered to the adhesion sites, where they might interact with cortical dynein (Eltsov et al., 2015). However, not much is known about how MTs are organised at the distal end of the cell. It is likely that MTs in this location are also tethered to the cortex of the cell, which would enable efficient force transmission. The anti-parallel organisation of MTs along the apical cell cortex throughout the cell supports such a hypothesis. Cortical interaction of MTs in the distal part of the cell might also be mediated by dynein, but other cortical anchors are conceivable. The presence of MT-cortical dynein interactions however, would suggest the same force generating mechanism as in the proximal

part of the cell. This is reminiscent of the asymmetric spindle positioning in the *C. elegans* one cell stage embryo, where cortical dynein is found at the anterior as well as at the posterior end of the cell, exerting pulling forces. As there are more dynein activators concentrated at the posterior end than at the anterior end of the cell, a greater net pulling force towards the posterior end ensues (Gönczy et al., 1999; Grill et al., 2001, 2003; Park & Rose, 2008). A similar mechanism would be conceivable in LE cells to facilitate zipping of the two leading edges. Alternatively, dynein can also interact with another cortical anchor, which would not lead to MT shrinkage and, consequently, pulling forces towards the distal end of the cell. Such a mechanism would cause shrinkage of the leading edge, as MTs at this location are parallel. Yet, shrinkage of the entire cell would be hindered by the anti-parallel organisation of MTs. Jankovics & Brunner (2006) observed that anti-parallel MT ends are associated with the apical cell cortex. It is likely, that these anti-parallel MTs are cross-linked throughout the cell. In addition, MTs might also be connected to the cell cortex via apically anchored MT motors, which the taxol experiments of this work suggested.

In conclusion, MTs are likely candidates for the generation of the zipping force. However, the mechanism is still unknown but could involve force generation at the distal ends of the LE cells. Electron tomography experiments have been started by a lab colleague, Mandy Börmel, to further investigate MT organisation at the distal end of LE cells during zipping.

3.6.4 Cortical attachment of dyenin

Alternatively, to unveil a role for cortical l during zipping, examining proteins involved in dynein attachment to the cortex might give further insights. Studies indicate that cortical attachment of dynein is driven by conserved machinery. A ternary complex (LIN-5/GPR-1/2/Gα in *C. elegans* and NuMA/LGN/Gαi in *Homo sapiens*) is involved in mediating dynein attachment to the cortex (Kotak & Gönczy, 2013). The *Drosophila* Mushroom body defect (Mud) has been proposed to be a functional orthologue of *C. elegans* LIN-5 and mammalian NuMA (Siller et al., 2006). During asymmetric spindle positioning in *Drosophila* neuroblasts dynein generates pulling forces on astral MTs. Cortical attachment of dynein involves the Mud/Pins/Gα protein complex (Yu et al., 2005). It was shown that Mud associates with cytoplasmic dynein, however, how such an interaction is mediated, remains unclear (Lu & Johnston, 2013). Although, a recent study suggests that Mud associates with the dynein light chain subunit Ctp (Cut up; Wang et al., 2011). Hence, Mud

helps to link the dynein motor complex to the cortically polarised Pins (Partner of Inscuteable; Lu & Johnston, 2013). The same complex might also regulate dynein attachment in LE cells during DC.

3.6.5 Alternatives for dynein-independent zipping force generation

Based on previous studies, there is every indication that cortical dynein interacts with MTs and thus generates the zipping force during DC, as it seems to be an evolutionarily conserved mechanism. However, an alternative to a dynein-mediated zipping force could be conceivable, especially considering that here cortical dynein would act in a specialised developmental process rather than several general cell biological processes in which its function was described so far. Dyneins are not the only minus-end directed MT motors. Members of the kinesin-14 family have also been described to be minus-end-directed MT motor proteins (Miki et al., 2005). The *Drosophila ncd* gene was shown to encode a minus-end directed kinesin (McDonald et al., 1990; Walker et al., 1990). Ncd controls mitotic spindle length by generating pulling forces on the overlapping antiparallel MTs in the spindle midzone (Sharp et al., 2000a). Yet, there are no processes known, which involve cortical anchored Ncd. However, the yeast minus-end directed kinesin, Karp3, was shown to anchor at the cell cortex of the budding yeast shmoo tip to interact with depolymerising MTs (Maddox et al., 2003). Thus, it is conceivable that the zipping force could be generated by a minus-end directed kinesin during DC.

Alternatively, it might be possible, that members of the kinesin-8 or kinesin-13 family play a role in zipping. Although these kinesin families are plus-end directed MT motors, they have been shown to depolymerise MT plus ends (Howard & Hyman, 2007). Kip3p, a yeast kinesin-8 was shown to be required for cortical interactions with MTs (Gupta et al., 2006). Thus, one could speculate that such a depolymerising kinesin is also involved in generating pulling forces which are required for the zipping process. Thereby, a depolymerising kinesin might move to the MT plus end, where it promotes MT shrinkage upon cortical contact and thus providing a pulling force. Yet, such a mechanism would also require a cortical receptor to keep MTs attached during depolymerisation.

3.7 Conclusion

Within this work, I tested the hypothesis that cortical dynein pulls on MTs, thereby generating a zipping force during one of the final phases of DC. However, the ob-

tained results do not unambiguously indicate a function for dynein during zipping. Although it is clearly evident that dynamic MTs are essential for normal zipping progression, an interaction between these MTs and cortical dynein needs further investigation.

Studying dynein during DC has proven to be challenging. One of the main obstacles in studying dynein function using mutants is maternal contribution, which is sufficient for embryonic development. The injection of CiliobrevinD, a recently discovered drug that inhibits dynein specifically, caused global effects on dorsal closure, and thus it remains difficult to assess dynein function exclusively during zipping.

The development of a unique tool, which may help to answer if dynein is involved in generating the zipping force has begun. I used the recently developed CRSIPR/-Cas9 technique to generate conditional *Dhc64* mutants. Using the FLP/FRT system will allow us to mediate the excision of two exons of the endogenous *Dhc64*, which code for the MTBD. As this excision can be controlled in a time- and tissue-specific manner, it will not only allow studying Dhc64 function during DC but also during other developmental processes.

A zipping force mediated by cortical dynein and MTs would suggest a function for dynein in tissue morphogenesis and could reveal a conserved mechanism driving tissue fusion in all embryogenesis as well as in wound healing.

4 Results: Part 2

4.1 Screens to identify molecules mediating cell-cell recognition during zipping

At the dorsal closure stage, the epithelium is patterned into repetitive segments consisting of stripes of cells with defined positional identity (St Johnston & Nüsslein-Volhard, 1992; Kornberg & Tabata, 1993; Martinez-Arias & Lawrence, 1984; Rivera-Pomar & Jãckle, 1996). Perfect matching of cells with identical positional identity within the two opposing epithelial sheets thus seems of fundamental importance for proper dorsal closure. However, little is known about the molecular basis of cell-cell recognition in dorsal closure. To identify recognition molecules, I performed a forward genetic screen for dominant mutations. In a second approach, I tested some candidates that are known to function as recognition molecules in other processes such as axon guidance.

4.1.1 Forward genetic screen: EMS mutagenesis

To identify genes regulating cell-cell recognition, I performed a forward genetic screen using EMS (ethyl methanesulfonate) mutagenesis (Lewis & Bacher, 1968). EMS is the most commonly used mutagen for forward mutagenesis screens in *Drosophila*. The ethyl group of EMS reacts with the guanine in the DNA resulting in the formation of the abnormal base O6-ethylguanine. During DNA replication the O6-ethyulguanine pairs with thymine instead of cytosine. The main EMS-induced mutations will comprise GC $\rightarrow$ AT transitions, which can form missense or non-sense codons or destroy splice sites. Occasionally, other DNA lesions such as transversions, deletions and frameshifts are also observed (Bentley et al., 2000; Pastink et al., 1991). Most importantly, such point mutations can generate mild gain of function mutations that manifest dominant or haploinsufficient phenotypes in heterozygosity, which can easily be screened for in the first generation (F1) emerging from treated fly germ cells.

For EMS mutagenesis I used a $white^{1118}$ (w^{1118}) fly strain (Figure 31). Prior to EMS mutagenesis, chromosomes II and III of this fly strain were isogenised to eliminate possible existing lethal mutations. Males were treated with a $25mM$ dose of EMS and then crossed to untreated females of the same strain. Following this, I screened adult flies of the F1 generation that exhibited defects in the thorax and/or abdominal segmentation. The reasoning behind this was that mild gain of function

mutations causing cell mismatching defects in dorsal closure, would similarly do so in related tissue sealing processes as occur in large number in the pupae where the larval imaginal discs expand and fuse with each other or generate the adult fly. In particular, thorax closure and abdominal epidermis closure, both morphogenetic events, in which movement and fusion of epithelial cells occur (Ninov et al., 2007), can be easily screened for defects. Obviously, strong gain of function mutations causing lethality before adulthood will be missed using this strategy.

In total I screened approximately 111,000 flies. Those ones that displayed defects in abdominal segment matching were crossed once again with w^{1118} flies and the F2 generation was analysed to see if possible mutations were propagated to the next generation. The chance of having false positives is high, as EMS mutagenesis also causes somatic mutations or germ-line mosaics. Thus, mutant F1 progeny yields a mixture of F2 progeny carrying the new allele or the phenotype does not propagate at all. I found three candidates, which still displayed segmentation defects in the abdomen in the F2 (Figure 32). In two of them the mutant phenotype was visible in 41% and 45% of all the progeny, respectively. This indicates that these two candidates carry a dominant mutation, as the expected ratio between wild-type files and flies exhibiting the phenotype would be 1:1 unless the mutation causes increased lethality. In the third mutant only females were affected. About 37% of females showed defects in the abdomen. Yet, males did not show any phenotpye. This suggests, that the EMS-induced mutation is X-chromosome linked and causes male lethality. The most interesting phenotype was that of mutant 1, which displayed a dorsal gap mostly in the upper two segments of the abdomen (Figure 32B). These phenotypes were similar to those of flies that fail to complete abdominal closure (Sekyrova et al., 2010). The other two mutants exhibited raggedly incomplete or defective tergites, which in turn resulted in partially eliminated bristles and hairs (Figure 32B and C). To establish stable fly stocks and for chromosome mapping of the mutation, these candidates were further crossed with flies carrying a multi-balancer for chromosomes 2 and 3. The penetrance of the phenotype dropped drastically in the progeny from these crosses (Table 6). For mutant 1, only 7% of the progeny displayed the phenotype. Moreover, screening of the w^{1118} stock itself revealed that in about 4% of the flies, abdominal segmentation defects occur.

These results suggest that the observed phenotypes after EMS mutagenesis are caused by a w^{1118} sensitised background. Thus, we were unfortunately not able to isolate the mutant phenotypes. To find molecules mediating cell-cell recognition during zipping in dorsal closure another screen should be performed. An alter-

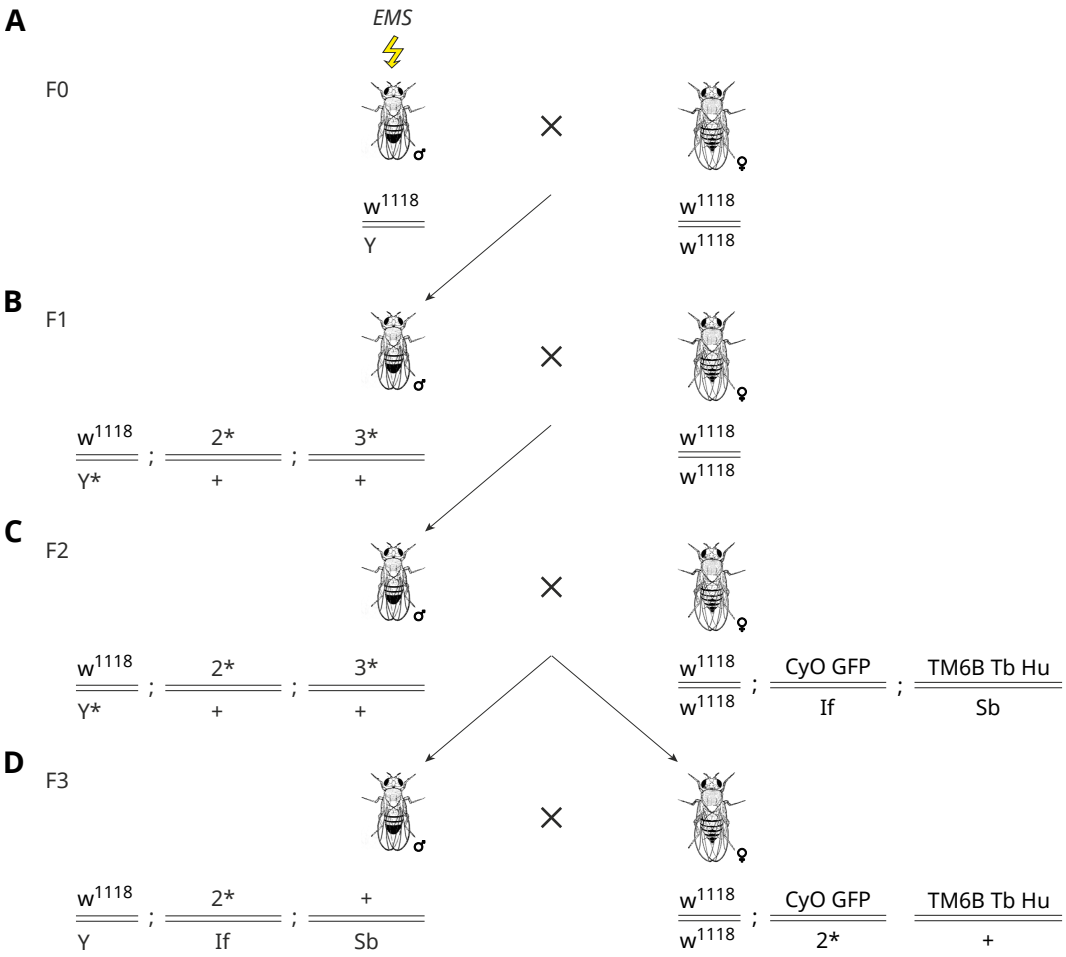

Figure 31: Scheme of EMS screen to isolate dominant mutations to find candidates mediating cell-cell recognition.
(A) EMS Mutagenesis of w^{1118} males and mass mate to w^{1118} virgins. **(B)** Screen F1 progeny for flies showing a phenotype in abdomen or thorax and cross individually with w^{1118} virgins to eliminate false-positives. **(C)** Cross flies of F2 progeny showing the phenotype with flies carrying a multi-balancer stock. **(D)** To establish a stock, cross flies of F3 progeny exhibiting the phenotype and dominant markers once again with virgins carrying a multi-balancer.

Table 6: EMS screen results

Total no. of flies screened	Candidates found	Phenotype occurence in w^{1118} background	Phenotype occurence in different genetic background
111000	Mutant 1	45% (males and females)	7%
	Mutant 2	41% (males and females)	8%
	Mutant 3	38% (only females)	15%

native to an EMS screen could be insertional mutagenesis in which disruption of genes is caused by transposable elements. Yet, one could also use a deletion library and screen for phenotypes showing abdominal segmentation defects and then use radiation to detect the affected gene at DNA level.

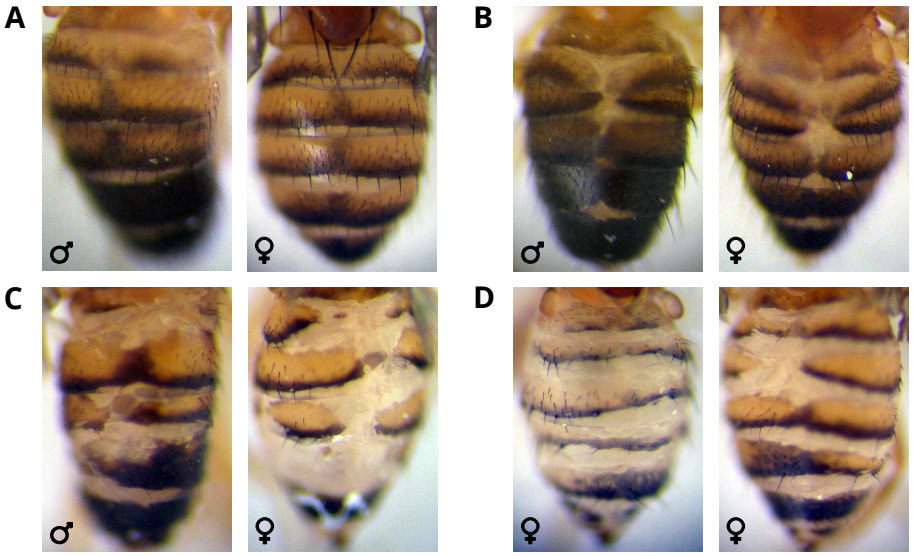

Figure 32: Candidates found in EMS screen.
(A) Abdomen of wild-type flies. **(B)** Mutant 1 showing dorsal gap in the upper part of the abdomen. **(C)** Mutant 2 showing defective tergites and missing partially bristles and hairs in the abdomen. **(D)** In mutant 3 only females are affected; showing a similar phenotype as mutant 2.

4.1.2 Candidate-based screen: Testing involvement of axon guidance molecules during dorsal closure

To identify molecules that are involved in cell-cell matching during zipping, I have performed an EMS mutagenesis screen for dominant mutations exhibiting defects in abdominal segmentation or the thorax. Unfortunately, as shown in the previous section, the screen was not successful. Thus, we decided to analyse ephrins and

semaphorins which are involved in axon guidance. These candidates seemed to be particularly promising since recent findings have shown an important role for these proteins also during ventral enclosure in *Caenorhabditis elegans*, a developmental process analogous to dorsal closure (Martín-Blanco & Knust, 2001). The ephrin (Eph) receptor, which is a receptor tyrosine kinase (RTK), was shown to be involved in epidermal cell migration to the ventral midline during ventral enclosure in *C. elegans*. In the Eph receptor null mutant *vab-1*, the ventral gap either does not close or leads to misalignments of opposing epidermal cells along the ventral midline. Furthermore, in the semamophrin mutant *mab-20*, misalignment occurs between opposing epithelial cells and ectopic contacts between neighbouring cells are formed (Ikegami et al., 2012; Roy et al., 2000). Based on these findings, we were interested if the same proteins may play a role in cell-cell recognition during dorsal closure in *Drosophila*.

4.1.2.1 Components of the ephrin signalling pathway and semaphorins do not seem to be involved in the cell-cell recognition process

To study possible functions of the axon guidance molecules, like components of the ephrin signalling pathway or semaphorins in dorsal closure, I analysed loss-of-function mutations of these candidates . In contrast to vertebrates, there is only one gene coding for the Eph receptor in *Drosophila*. I examined a fly strain carrying a homozygous Eph receptor loss-of-function mutation (Eph^{x652}) (Boyle et al., 2006). In addition, the flies carried the cytoskeletal marker mCherry-Moesin as a live-marker for actin imaging. As mCherry-Moesin is regulated by a UAS promoter, I used engrailed-Gal4 (enGal4) to drive its expression in epidermal cell stripes with each stripe comprising 4 engrailed-expressing cells (Figure 33A). Thus, we could easily monitor misalignment occurring along the dorsal midline due to possible cell-cell recognition defects. Analysis of the homozygous Eph^{x652} mutant revealed defects during dorsal closure in about 18% of embryos. Yet, misalignment occurred very rarely and the most prominent phenotype was puckering, indicating a zipping delay (Figure 33B and C). Furthermore, I examined another component of the ephrin signalling pathway, the ephexin, a Rho-type guanine nucleotide exchange factor (Rho-GEF), which binds directly to the Eph receptor (Frank et al., 2009). To study ephexin function in dorsal closure, I analysed homozygous mutant embryos. The ephexin mutant ($\text{exn}^{EY\Delta 50}$) was generated by imprecise excision of a P-element leading to a putative null allele (Frank et al., 2009). I observed similar mutant

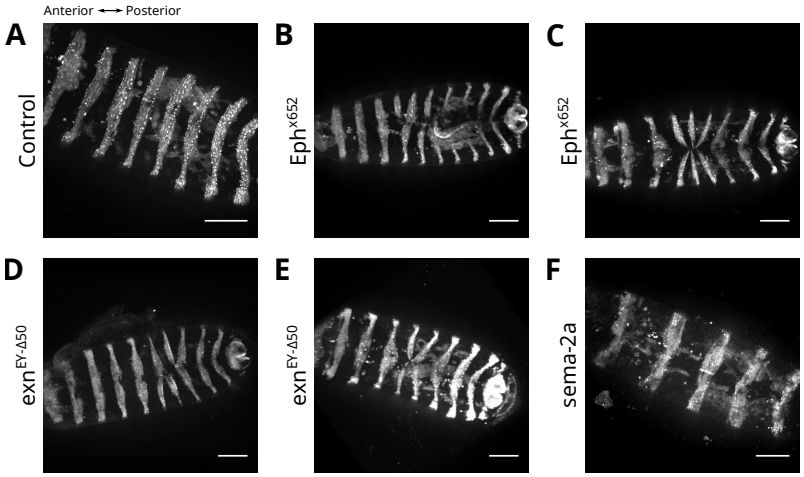

Figure 33: Phenotypes of Eph receptor, ephexin and sema-2a mutants in dorsal closure.
(A-F) Images showing embryos expressing mCherry-Moesin in engrailed stripes (except (F) in paired stripes) after completion of dorsal closure. **(A)** Wild-type embryo. **(B)** Homozygous Eph^{x652} mutant showing misalignment of middle stripes along the dorsal midline. **(C)** Homozygous Eph^{x652} mutant showing puckering phenotype. **(D)** Homozygous exn$^{EY\Delta 50}$ mutant showing misalignment. **(E)** Homozygous exn$^{EY\Delta 50}$ showing puckering phenotype. **(F)** Homozygous sema-2a mutant displaying no defects. Scale bars: 50μm.

phenotypes as with the Eph receptor mutant. Most embryos completed closure without any defects, with 13% showing phenotypes, of which the most prominent was puckering (Figure 33D and E). Analysis of enGal4, UAS-mCherry-Moesin control embryos revealed 7% of embryos with similar defects as those found in homozygous ephexin and Eph receptor mutants. These data suggests that the Eph receptor and ephexin do not play a role in cell-cell recognition during dorsal closure. Moreover, homozygous mutants are viable, thus the Eph receptor does not seem to be required for *Drosophila* development. It was suggested, however, by Tsuda et al. (2008) that the Eph deletion is not a complete null, thus further analysis is necessary.

Lastly, I analysed semaphorins, which, like components of the ephrin signalling pathway, are involved in axon guidance. In *Drosophila* there are five different semaphorins, which are either transmembrane or secreted proteins: sema-1a, sema-1b and sema-5c (transmembrane) and sema-2a and sema-2b (secreted). As sema-2a is the *Drosophila* homolog of *C. elegans* mab-20, which was shown to be required for cell-cell recognition during ventral enclosure (Ikegami et al., 2012), I analysed embryos carrying a homozygous sema-2a loss-of-function mutation and the marker pairedGal-UAS-mCherry-Moesin. Similar to enGal4, pairedGal4 (prdGal4) drives mCherry-Moesin expression in stripes, but there are fewer prd-stripes than en-stripes. Homozygous sema-2a mutants did not show any dorsal closure pheno-

type (Figure 33F). We cannot, however, exclude that maternally provided sema-2a mRNA or protein might mask a possible phenotype. Thus, to study sema-2a function exclusively during dorsal closure, a tissue-specific sema-2a protein knockdown has to be performed. Further, we cannot exclude, that one of the other semaphorins may play a role in cell-cell recognition during dorsal closure. While only little is known about the biological function of sema-1b and sema-5c in *Drosophila*, sema-1a has been shown to be implicated in several axon guidance functions during *Drosophila* development (Yu et al., 1998; Cafferty et al., 2006; Godenschwege et al., 2002). During *C. elegans* development sema-1a is required for correct epidermal cell positioning and adhesion during morphogenesis (Ginzburg et al., 2002). Moreover, only recently it has been shown that sema-2b is required for axon guidance of a subset of embryonic neurons (Emerson et al., 2013). Therefore, it would be interesting to examine the function of the remaining semaphorins during dorsal closure.

5 Discussion: Part 2

5.1 EMS screen

As part of this work I attempted to find the underlying mechanisms and the molecules mediating cell-cell recognition during dorsal closure. During the dorsal closure stage, the epithelium is patterned into repetitive segments that consists of stripes of cells with a defined positional identity. Thus, it seems of fundamental importance that during zipping precise matching of opposing leading edge cells with identical positional identity takes place, as imprecise fusion would otherwise disrupt such patterning. Indeed, the alignment of the epithelial sheets occurs with high accuracy resulting in a perfectly established pattern across the fusion seam even at single cell resolution. To achieve this, each cell in the leading edge must recognise and specifically fuse with its correct partner form the opposing epithelial sheet.

To find molecules that are involved in regulating cell-cell recognition during dorsal closure, I have performed an EMS screen to find mild gain of function mutations causing cell-mismatching defects during dorsal closure. To facilitate the screening process, I looked for mismatching defects in the thorax and abdominal epidermis of adult flies, which are related tissue-sealing processes in which movement and fusion of epithelial cells occur. I found three candidates, of which one was particularly promising, as it displayed a similar phenotype to mutants that fail to complete abdominal closure. However, it was not possible to isolate the mutants, as the phenotypic penetrance vastly decreased once trying to establish fly stocks. Thus, the w^{1118} stock, which we used for mutagenesis turned out to provide a sensitised background for abdominal defects. In addition, a low percentage of non-mutagenised w^{1118} flies exhibited defects in the abdomen. A repetition of such a screen using a different fly stock might be worthwhile as it is faster and less tedious than F2 screens. Alternatively, one could also use a deletion library and screen for phenotypes with abdomen or thorax defects.

5.2 Role of axon guidance proteins

Since the EMS screen was not successful, I examined the Ephrin receptor and its direct interaction partner Ephexin, as well as semaphorins, which function in axon guidance. Such guidance proteins often act as repellents or attractants and thus may also have a role in cell-cell recognition during dorsal closure. Moreover, these molecules were shown to be required for correct alignment of cells along the ventral

midline during *C. elegans* ventral enclosure, a morphogenetic process with analogy to dorsal closure (Martín-Blanco & Knust, 2001). During dorsal closure, Ephrin receptor and Ephexin loss of function mutants rarely showed defects. In most embryos, correct alignment along the dorsal midline was observed and in some embryos a puckering phenotype indicating a zipping delay. Yet a mismatch between segments was hardly ever observed. In a low number of control embryos, a puckering phenotype was also observed. Both, the Eph receptor and Ephexin do not seem to be involved in cell-cell recognition during dorsal closure. Furthermore, it appears that the Eph receptor, which is encoded by a single gene, is dispensable for all of *Drosophila* development, as homozygous mutants are viable. This, however, seems highly unlikely, as Eph receptors play key roles in the organisation of many tissues in most organisms. It was suggested by Tsuda et al. (2008) that the analysed mutant might not be a complete null. Thus, a function for the Eph receptor in cell-cell recognition cannot be excluded and needs further analysis. Furthermore, in *C. elegans* the Eph receptor Vab-1 is required for proper ventral epidermal enclosure (Ikegami et al., 2012).

Recently, the Eph receptor has been suggested to be required to maintain a straight boundary between anterior and posterior compartments in *Drosophila* imaginal discs. A role for Eph receptors and their ligands, the ephrins, to maintain such boundary formation, has also been described in the vertebrate hindbrain. There, the lack of cells mixing across segment boundaries depends on the interaction between Eph receptors and their ligands, which are expressed in a complementary manner in alternate segments (Wilkinson, 2001). Also, at dorsal closure stage the embryo is patterned into segments, with segments being divided into anterior (A) and posterior (P) compartments (Dahmann & Basler, 2000; Larsen et al., 2003). During zipping, A-compartments match with A-compartments, while P-compartments match with P-compartments. But these recognition events are not segment-specific, as fusion can occur between matching compartments from different segments, which was described by Millard & Martin (2008) and also observed by a former postdoc Nadia Dubé in a dominant-negative Cdc42 mutant. Hence, the Eph receptor might have a role in maintaining boundaries between compartments and a possible function during cell-cell recognition in dorsal closure.

Other promising candidates for cell-cell recognition are the semaphorins, which are involved in axon guidance, but have also been shown to play a role in *C. elegans* ventral enclosure. The *C. elegans* semaphorin-2a, Mab-20, is required to prevent ectopic contacts of leading edge cells, thus acting as a repellent, during

ventral enclosure (Roy et al., 2000). There are five different semaphorins described in *Drosophila*, which are either secreted or transmembrane proteins (Yazdani & Terman, 2006). Analysis of the semaphorin loss of function mutant *sema-2a* did not cause mismatching defects along the dorsal midline. This might indicate, that Sema-2a is not involved in the regulation of cell-cell recognition during dorsal closure. However, we cannot exclude maternally contributed Sema-2a protein, which might mask a possible phenotype. The role of the remaining semaphorins in cell-cell recognition during dorsal closure should also be investigated.

Although no cell-cell recognition defects were observed, axon guidance molecules remain interesting candidates to be investigated during dorsal closure. As such molecules can act in an attractive or repulsive manner, a possible mechanism could be that filopodia express different ligands and receptor molecules with repelling and attracting functions. Filopodia of leading edge cells of segments with different identities would interact in a repelling manner, while filopodia of leading edge cells with the same segment identity would be attracted to each other. Furthermore, zipping cells contact also filopodia of neighbouring cells of the same segment without effect (Jacinto et al., 2000). Thus, the adhesion of neighbouring cells might be prohibited by molecules that also function as repellents, but this repelling must be overruled when the equivalent "neighbour" from the other side is encountered. However, an additional level of control is needed, as cells still need to sort out the right partner, once the initial contacts between identical segments are made. Furthermore, a similar mechanism might apply for the interaction of leading edge filopodia and filopodia of amnioserosa cells. While searching for their matching partner in the opposing epithelial sheet, leading edge filopodia scan the tissue above the amnioserosa and make contacts with filopodia of amnioserosa cells. An alternative to axon guidance molecules regulating cell-cell recognition might be differential expression of cell adhesion molecules on the cell surface, which occurs during cell sorting (Niessen et al., 2011).

5.3 Conclusion

Further experiments are required to find the underlying mechanisms mediating cell-cell recognition during dorsal closure. Unveiling the molecular basis for cell-cell recognition during dorsal closure, would also have implications for many other processes during embryogenesis, where epithelial sheets must precisely zipper up a hole or fuse together epithelial sheets to form the correct aligned closure seam. This may also further our understanding of cellular homing, a behaviour found, for example,

in metastatic cancer cells that preferentially home in on specific tissues and cellular environments.

6 Materials and Methods

6.1 Fly stocks and crosses

All *Drosophila melanogaster* strain genotypes reported in the text or shown in the figures are listed in Table 7. The original stocks are listed in Table 8. All fly stocks were kept, handled and crossed using standard genetic practices.

Flies carrying homozygous lethal alleles were kept with balancer chromosomes. The most frequently used balancers were: FM7, KrGal4, UAS-GFP; CyO, KrGal4, UAS-GFP; TM3, Ser, Sb, sqh-mCherry; TM3, KrGal4, UAS-GFP; TM3 Ser pAct-GFP; TM6B, Tb, Hu; TM3, Sb; TM3, Ser.

6.2 Confocal microscopy

For live-imaging, embryos were collected and aged at $21 - 25°C$, dechorionated with 50% hypochlorite for $3 - 4min$, aligned and transferred onto glass cover slip with glue. To prevent dehydration, embryos were covered with Voltalef Halocarbon oil 10S (Sigma-Aldrich). Embryos were imaged at $23 - 25°C$ using spinning-disk confocal microscopes (Zeiss Axio Observer Z1 or custom-modulated Leica DM IRBE) equipped with iXon3/888 cameras and controlled by ANDOR IQ software. Objectives used: 20X, 25X, 40X, 63X and 100X. Usually, Z-planes were acquired every $0.5 - 2\mu m$ and maximum-intensity Z projections were analysed.

6.3 Image processing and analysis

Image processing and maximum intensity Z-projections were done using the image analysis software ImageJ and the programming language R. All statistical tests were performed with R.

Average closure speed of embryo: The average dorsal closure speed of embryos was measured as depicted in Figure 34. The speed measurements were calculated by dividing the distance between the anterior and posterior canthi at the start of imaging by the total closure time. For comparison with other calculations and in order to give an average speed value for a single canthi, this value was divided by two. In previous measurements we found that zipping progression does not occur faster at a specific canthus, but the speed of the canthi seems to vary between them. Only embryos with an initial length of at least $100\mu m$ were considered, as it was observed that speeds accelerate considerably in the last moments of closure.

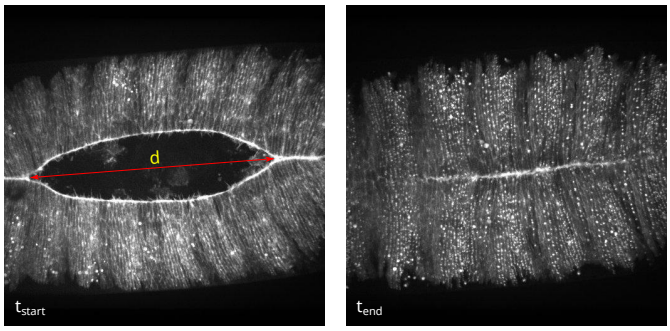

Figure 34: Average embryo closure speed measurement.
The length d represents the distance between anterior and posterior canthi at the beginning of imaging in μm. The total closure time is given by $t_{end} - t_{start}$.

Independent closure speed of canthi: In order to determine the independent closure speeds of the anterior and posterior canthi, a modified analysis was performed (Figure 35). In addition to recording the coordinates of the two canthi every 10 minutes, the position of the closure point of the leading edge was also recorded. This point was identified as the location on the leading edge which closes last. For this reason, the measurement process started at the time of complete closure, and worked backwards until the start of the movie was reached. From these three coordinates, the theoretical middle of the whole dorsal opening could be calculated. The movement of the anterior and posterior canthi was determined relative to this middle position independently, instead of to each other, thus allowing the difference in speeds from each side to be quantified. Average speeds over the whole closing process were then calculated, as well as detailed plots of canthi movement, as shown, for example, in Figure 27A.

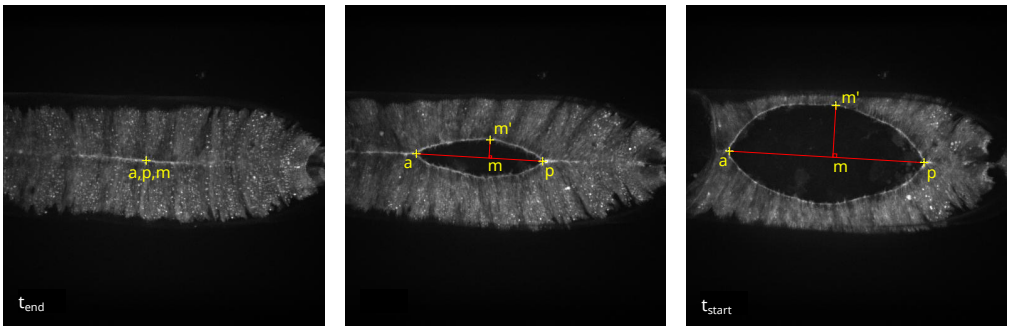

Figure 35: Independent closure speed of canthi.
The position of the anterior canthus (a), posterior canthus (p) and closure point on the leading edge (m') were measured every 10 minutes, starting at time of complete closure and working backwards. The theoretical midpoint of the dorsal opening (m) is defined as the intersection of the anterior-posterior canthi line and a line at 90° contacting the closure point of the leading edge (shown in red). The speed of the anterior canthus is thus calculated based on the distance $m - a$, and the posterior speed based on the distance $m - p$.

Kymographs: To analyse microtubule dynamics, kymographs were made using ImageJ. For this, a boxed region within the epidermis was selected and plotted over time showing the dynamics of EB1 movement.

Statistical analysis: Standard statistical tests were used to determine the significance of the analysed data. To test the type of distribution of data, the Shapiro-Wilks test was first performed. Data sets with a p-value greater than 0.05 were considered normally distributed.

If normally distributed data, an un-paired t-test was used to determine the statistical significance of the relationship between two data sets. If not normally distributed, the Mann-Whitney-Wilcoxon (Mann-Whitney U) test was applied.

In graphs, the statistical significance of data sets compared to the control data was represented by a number of asterisks, with a higher number of asterisks representing a more significant relationship. For both the t-test and Mann-Whitney U test, the number of asterisks were based on the following p-values:

* $p - value \leq 0.05$

** $p - value \leq 0.01$

*** $p - value \leq 0.005$

6.4 Laser incision experiments

Laser incision experiments were performed on a spinning disc confocal microscope (Zeiss Axio Observer Z1) equipped with a MicroPoint pulsed nitrogen pumped dye

laser ($5ms$ pulse width, $10Hz$, $\lambda = 435nm$; Andor Technology). Objectives used: 100X.

6.5 FRAP

FRAP experiments were done on a Zeiss LSM710 microscope using Zen software. Taxol-treated and wild-type embryos expressing *pnrGal4*/UAS-tubulinGFP were used for this experiment. ImageJ software was used to calculate the mean intensity of the images in the area of bleaching, as well as both the total embryo area and the background. The intensity over time in the region of interest was determined after subtracting average background values, and normalised in order to allow comparison between different experiments. The measurements were done according to Bancaud et al. (2010).

6.6 Injections of taxol and CiliobrevinD

For all injections, embryos were desiccated for $10-15min$, prior to covering embryos with Halocarbon oil. Injections were carried out at the upright Zeiss Axiovert X35 microscope using Narishige MO-11 injection manipulator. To generate injection needles, boro-silicate capillaries (GC100TF-10, Harvard Instruments) were pulled using the Narishige needle puller PN-3 (Narishige Scientific Instrument Lab, Japan). To open the needles, the tip was broken against a glass slide and fluid was expelled using an air syringe. For taxol and DMSO injections, compounds were injected posteriorly into the yolk of dorsal closure stage embryos. For CiliobrevinD, DMSO and water injections, compounds were injected posteriorly or anteriorly into the yolk in the middle of the dorsal opening or close to anterior or posterior canthi. Embryos were imaged within $5-10min$ after injection. Both, taxol and CiliobrevinD (Xcessbio) were dissolved in DMSO. The injected concentrations fort both compounds were $10mM$.

6.7 Immunofluorescence staining

Fixation: Embryos expressing armadillo-GFP were dechorionated in 50% hypochlorite and washed several times with water on a membrane filter. Embryos were transferred into an Eppendorf tube containing $500\mu l$ heptane and an equal volume of 37% formaldehyde (mixed before adding embryos) and incubated for $40min$ at room temperature. Then the lower aqueous phase was removed. Using a glass pipette, embryos were transferred into a plastic Petri dish and the remaining hep-

tane was allowed to evaporate. Next PBS was added. Using fine forceps or a needle, the vitalline membrane of the embryos was removed. After devitellinisation, PBS was removed and PBT (PBS + 0.1% Triton X-100) was added. Subsequently, the embryos were transferred into an Eppendorf tube. Embryos were washed about three times with PBT.

Blocking: Blocking solution was added (PBS + 0.05% Trition X-100, 1% BSA, 5% normal goat serum (NGS)) and Eppendorf tubes were rotating for $1-2$ hours at room temperature.

Staining: After removal of blocking solution, embryos were incubated for $3-4$ hours with mouse anti-dynein heavy chain antibodies (2C11-2, Developmental Studies Hybridoma Bank) diluted in 1:2.5 blocking buffer and chicken anti-GFP (abcam), diluted 1:250 in blocking buffer. After seven $15min$ washing steps with PBT, embryos were incubated for 2 hours with Alexa-Fluor 647 goat anti-mouse (Invitrogen) and Alexa-Fluor 488 goat anti chicken antibody (Invitrogen), each diluted 1:300 in blocking buffer, which was followed by the same washing step as before.

Mounting: Most of the PBT solution was removed and embryos were transferred onto a glass slide. The remaining liquid was removed using a pipette. A few drops of mounting medium (80% Glycerol, 0.1M Tris-HCl pH 7.5, 0.1% DABCO (1,4-Diazabicyclo[2.2.2]octan)) were added and a coverslip was placed on top and incubated over night at $4°C$. Fixed embryos were imaged with the Zeiss LSM710 (Zen software).

6.8 Generation of transgenes for acute protein knockdown

The pDhc+ vector containing the the full length genomic Dhc64 is a gift from T. Hays (described in Gepner et al. (1996)). To generate plasmids for the various protein depletion approaches, the N-terminus of Dhc64 was modified. For this, pDhc+ was linearised with AgeI and Swa1 restriction enzymes. A modified N-terminal Dhc64 fragment with Age1 and Swa1 overhangs for generating a GFP-, TIPI- and Cry2-tagged Dhc64 was cloned into the linearised pDhc+ vector using the Gibson Assembly Kit (New England Biolabs). The N-terminally modified Dhc64 constructs in pDhc+ were excised using NotI restriction enzymes and cloned into pWBattB, which was linearised with NotI restriction enzymes and the final plasmids were generated. The strategy how Dhc64 was modified is described in the next sections.

6.8.1 Generation of *Dhc64* transgene for deGradFP

To generate GFP-tagged Dhc64, the following strategy was used:

1. GFP was amplified from pJFRC81 by PCR with primers OMA31 (with Dhc64 overhang) and OMA32 (with Happy Linker (HL) and Dhc64 overhang).
2. Start of Dhc64 coding sequence until Swa1 site was amplified from pDhc+ with primers OMA34 (with HL overhang) and OMA33.
3. Products of OMA31/OM32 and OMA34/OMA33 were fused together with primers OMA31 and OM33 to generate a GFP-HL-start of Dhc64 fragment ($1412bp$).
4. Dhc64 flanking sequence containing AgeI site was amplified with primers OMA38 and OMA39 (with GFP overhang).
5. The fragment frow AgeI to SwaI containing the GFP-tagged Dhc64 fragment was amplified with primers OMA38 AND OMA41. The final fragment ($1799bp$) had $\sim 20-30bp$ overlapping overhangs needed for Gibson assembly.

6.8.2 Generation of *Dhc64* transgene for TIPI

To generate TIPI (M = methionine/ F = phenylalanine)-tagged Dhc64, the following strategy was used:

1. TIPI-tag was amplified from TIPI-(M/F)-Sqh plasmids (made by L. Pasakarnis) by PCR with primers OMA35 (with Dhc64 overhang) and OMA36 (with GFP overhang) and GFP-tag for was amplified with primers OMA 37 (with TIPI overhang) and OMA32.
2. TIPI-tag and GFP tag were fused togehter using primers OMA35 and OMA32.
3. Products of OMA35/OMA32 and OMA33/OMA34 were fused togehter with primers OMA35 and OMA33 to generate TIPI-GFP-HL-start of Dhc64 ($1751bp$).
4. Dhc64 flanking sequence containing AgeI site was amplified with primers OMA38 and OMA40 (with TIPI overhang).
5. The fragment frow AgeI to SwaI containing the TIPI-tagged Dhc64 fragment was amplified with primers OMA38 and OMA41. The final fragment ($2144bp$) had $\sim 20-30bp$ overlapping overhangs needed for Gibson assembly.

6.8.3 Generation of *Dhc64* transgene blue light-induced protein inactivation

To generate Cry2-RFP-tagged Dhc64, the following strategy was used:

1. CRY2-HL was amplified from pTWBattB-CRY2-tRFP-Sqh (made by L. Pasakarnis) with primers OMA67 (with 3'UTR Dhc64 overhang) and CRY2-PacI (L. Pasakarnis) and RFP was amplified from pTWBattB-Pact-Dia-RFP-LOV2-cODC plasmid (made by W. Boll) with primers GIB-tagRFP-PacI and CRY2-PacI (L. Pasakarnis). HL was fused to the 5' end of RFP with primers GIB-tagRFP-PacI and OMA68 (with Dhc64 overhang).

2. The fragment containing AgeI restriction site in the flanking sequence of Dhc64 was fused with CRY2-HL with primers OMA38 and CRY2-PacI, resulting in 1987*bp* product.

3. The RFP-HL fragment was fused with a short fragment of Dhc64 coding sequence with the Swa1 site with primers GIB-tagRFP-PacI and OMA41, resulting in a 1373*bp* product.

Both final fragments had $\sim 20 - 30bp$ overlapping overhangs needed for Gibson assembly.

6.9 Generation of *Dhc64* transgene in attB containing vector

To generate pMA-attB-Dhc64, I used the following strategy:

The genomic Dhc64 sequence including 5' and 3' UTR (total 19.4*kb*) was cut out from pDhc+ using NotI restriction enzymes and ligated into a NotI linearised pWBattB vector to generate pMA-attB-Dhc64.

6.10 Generation of dominant-negative variant of *Dhc64*

To generate pMA-UAS-EGFP-Dhc64, the following strategy was used:

1. A short fragment containing GFP and a part of Dhc64 until 83*bp* downstream of the Swa1 site was amplified by PCR from pMA-attB-EGFP-Dhc64 with primers OMA91 (containing a Syn21 and NotI site in the overhang) and OMA104 (containing Xba1 site), resulting in a 1521*bp* product. This product was then digested with NotI and XbaI and ligated into pJFRC81-10xUAS-IVS-Syn21-p10, which was before linearised with NotI and XbaI.

2. The pMA-attB-Dhc64 plasmid was digested with SwaI and XbaI to isolate a SwaI/XbaI Dhc64 fragment of 4982*bp* and a XbaI/XbaI Dhc64 fragment of 12782*bp*.

3. Next the intermediate vector (see point 1) was linearised using SwaI and XbaI restriction enzymes and ligated with the SwaI/XbaI 4982*bp* Dhc64 fragment. This intermediate vector was in turn linearised with XbaI and ligated with the 12782*bp* Dhc64 fragment to generate the final plasmid pMA-UAS-EGFP-Dhc64.

To generate pMA-UAS-Dhc64 (mutated MTBD) four prolines lying within the MTBD were changed to alanine. For this, the nucleotides coding for these prolines were changed to code for alanine (CCG → GCC). The following strategy was used:

1. Excision of GFP of previously generated pMA-UAS-EGFP-Dhc64 plasmid using NotI and SwaI restriction enzymes. Then replace the missing *Dhc64* sequence with a PCR product amplified with primers OMA116 and OMA41 from *pDhc+* plasmid using Gibson assembly kit. This resulted in the intermediate plasmid pMA-UAS-Dhc64.

2. The fragment coding for the mutated MTBD was generated by several fragments amplified by PCR. Product 1 (4144*bp*) was amplified with primers OMA115 (overlapping region containing BbvCI restriction site) and OMA 111 (exchanging CCG to GCC).

3. Product 2 (1200*bp*) was amplified with primers OMA105 (overlapping with OMA111) and OMA106 (changing 2 consecutive CCG to GCC).

4. Product 3 (789*bp*) was amplified with primers OMA112 (overlapping with OMA106) and OMA110 (changing the fourth CCG to GCC).

5. Product 4 (3911*bp*) was amplified with primers OMA109 (overlapping with OMA110) and OMA108 (overlapping region containing Bsu36I restriction site).

6. Product 3 and 4 were fused together using primers OMA112 and OMA108 to generate a 4652 bp product 5.

7. Overlapping overhang for each product were extended, product 1 with primers OMA178 and OMA179, product 2 with primers OMA180 and OMA106 and for product 5 with primers OMA181 and OMA182.

8. To insert the mutated MTBD fragments, the pMA-UAS-Dhc64 was cut with BbvCI and Bsu36I restriction enzymes, creating a *16375 bp* vector backbone.

9. The pMA-UAS-Dhc64 with the mutated MTBD was assembled using Gibson assembly kit.

6.11 S2 cell transfection

Schneiders S2 cells were kept in Schneiders Drosophila Medium (Gibco Life Technologies) supplemented by 10% fetal calf serum (FCS). Transient transfection with plasmids was performed according to FuGENE (Promega Corporation) cell transfection protocol. S2 cells were grown for 24 hours in 6-well dishes (MatTek Corporation), transfected with total of $2\mu g$ DNA and imaged 72 hours later with custom-modulated Leica DM IRBE spinning-disk confocal microscope. For imaging 8-well dishes (MatTek Corporation) with a glass bottom were used, which were previously coated with LectinConA ($1mg/\mu l$).

Transfected plasmids:
pMA-attB-EGFP-Dhc64 ($2\mu g$)
pMA-attB-TEV-Degron-Dhc64 ($2\mu g$)
pMA-UAS-EGFP-Dhc64, pWB-tubulinGal4 ($1\mu g$ each)

6.12 Generation of plasmids for CRISPR/Cas9 to introduce FRT sites flanking the MTBD of Dhc64

CRISPR/Cas9 genome engineering was performed according to the protocols on flyCRISPR (Gratz et al., 2014), http://flycrispr.molbio.wisc.edu/) and CRISPR fly design (Port et al., 2014), http://www.crisprflydesign.org/protocols/).

6.12.1 Generation of guideRNA plasmids

CRISPR target sites were identified using the CRISPR optimal target finder (http://tools.flycrispr.molbio.wisc.edu/targetFinder/).

CRISPR target site 1: cctggagtcggtctgcgagctgc
CRISPR target site 2: ccgcactgaatatctttccaatc

Next, two plasmids were generated, each containing the target sequence followed by the gRNA core. For this, annealed oligos each containing CRISPR target site and BbsI restriction overhang were ligated into linearised pCFD3-dU6:3gRNA (Addgene ID: 49410) vector. Correct sequence was confirmed by sequencing.

6.12.2 Generation of double-stranded homology donor

To introduce FRT sites into the Dhc64 locus flanking the MTBD, a double-stranded homology donor for HDR was generated (dsHD) using Gibson assembly kit.

1. Amplification of first part of homology arm 1 (HR1) using primers OMA157 (with overhang into pHD-DsRed vector) and OMA144 (introducing two nucleotides into exon 9 of Dhc64 to code for an otherwise missing alanine after excision of exon 10 and 11)

2. Amplifying second part of HR1 and exchanging nucleotides in PAM site of CRISPR target site 1 to avoid Cas9 cleavage after HDR. Nucleotides will code for the same amnio acid. This fragment was amplified using primers OMA132 and 0MA136 (changing PAM site).

3. Amplifying 3' end of HR1 first part of intron inbetween exon 9 and 10 with primers OMA145 and 0MA147 (with FRT1 site overhang)

4. Introducing FRT1 into intron by PCR using primers OMA155 (contains FRT1) and OMA162 (with loxP overhang).

5. Amplifying loxP-DsRed-loxP from pHD-DsRed (Addgene ID: 51434) using primers OMA149 and OMA151 (both with Dhc64 overhang).

6. Deleting first two nucleotides of exon 10, as these were added to exon 9 to code for alanine. This fragment from the second loxP site unti start of exon 10 was amplified with primers OMA152 and 150.

7. Introducing FRT2 into the intron situated inbetween exon 11 and 12 using primers OMA143 (start of exon 10) and OMA156 (overhang FRT2).

8. Amplifying sequence from FRT2 to CRISPR target site 2, of which PAM site has to be mutated to avoid Cas9 cleavage after HDR. This fragment was amplified with primers OMA161 and OMA154 (changing PAM site).

9. Amplifying HR1 using primers OMA138 and OMA158 (with overhang into pHD-DsRed vector)

10. Amplifying vector backbone of pHD-DsRed with primers OMA159 (with HR1 overhang) and OMA160 (with HR2 overhang)

11. From these ten PCR products, three final products were generated: product 1 amplified with OMA159/160 (2720*bp*), product 2 amplified with OMA151/157 (2526*bp*) and product 3 amplified with OMA152/158 (2736*bp*).

12. Using the Gibson assembly kit, the final plasmid pHD-HR1-FRT1-DsRed-FRT2-HR2-Dhc64 (7982*bp*) was created.

6.12.3 Injection of plasmids

For injection the *nos-cas9* fly strain was used. Embryos were injected following the standard injection protocol.

6.13 Plasmid maxi-preparations

For all plasmids, maxi-prepartions were performed using NucleoBlond PC 500 DNA purification kit (Macherey-Nagel). DNA concentrations were determined by NanoDrop (Witec AG).

6.14 EMS mutagenesis

Isogenised male flies (w^{1118}) which were not older than $4-5$ days were starved for 6 hours before EMS mutagenesis. For EMS mutagenesis a Kimwipe paper (Kimtech Science 7102) was put in each glass bottle and $1ml$ of EMS/sucrose ($25mM$ EMS in 1% sucrose) solution was dropped onto the Kimwipe paper. About 100 male flies were then added to each EMS containing bottle and incubated for 18 hours. After the incubation, flies were transferred into new bottles containing food and yeast and were allowed to recover for one day. Leftover EMS solution was inactivated by adding $1M$ NaOH and thioglycolic acid. The next day, the mutagenised male flies were crossed to 150 virgin females of the same strain for 4 days. The F1 generation was screened for phenotypes.

List of Figures

List of Tables

References

Abbott, B. D. (2010). The etiology of cleft palate: a 50-year search for mechanistic and molecular understanding. *Birth Defects Research Part B: Developmental and Reproductive Toxicology*, *89*(4), 266–274.

Adames, N. R., & Cooper, J. A. (2000). Microtubule interactions with the cell cortex causing nuclear movements in saccharomyces cerevisiae. *The Journal of cell biology*, *149*(4), 863–874.

Akhmanova, A., & Hoogenraad, C. C. (2005). Microtubule plus-end-tracking proteins: mechanisms and functions. *Current opinion in cell biology*, *17*(1), 47–54.

Allen, M. J., Shan, X., Caruccio, P., Froggett, S. J., Moffat, K. G., & Murphey, R. (1999). Targeted expression of truncated glued disrupts giant fiber synapse formation in drosophila. *The Journal of neuroscience*, *19*(21), 9374–9384.

Bachmair, A., Finley, D., & Varshavsky, A. (1986). In vivo half-life of a protein is a function of its amino-terminal residue. *Science*, *234*(4773), 179–186.

Bancaud, A., Huet, S., Rabut, G., & Ellenberg, J. (2010). Fluorescence perturbation techniques to study mobility and molecular dynamics of proteins in live cells: Frap, photoactivation, photoconversion, and flip. *Cold Spring Harbor Protocols*, *2010*(12), pdb–top90.

Bassett, A. R., & Liu, J.-L. (2014). Crispr/cas9 and genome editing in drosophila. *Journal of Genetics and Genomics*, *41*(1), 7–19.

Bentley, A., MacLennan, B., Calvo, J., & Dearolf, C. R. (2000). Targeted recovery of mutations in drosophila. *Genetics*, *156*(3), 1169–1173.

Bischof, J., Maeda, R. K., Hediger, M., Karch, F., & Basler, K. (2007). An optimized transgenesis system for drosophila using germ-line-specific φc31 integrases. *Proceedings of the National Academy of Sciences*, *104*(9), 3312–3317.

Boyle, M., Nighorn, A., & Thomas, J. B. (2006). Drosophila eph receptor guides specific axon branches of mushroom body neurons. *Development*, *133*(9), 1845–1854.

Brand, A. H., & Perrimon, N. (1993). Targeted gene expression as a means of altering cell fates and generating dominant phenotypes. *development*, *118*(2), 401–415.

Brouns, S. J., Jore, M. M., Lundgren, M., Westra, E. R., Slijkhuis, R. J., Snijders, A. P., Dickman, M. J., Makarova, K. S., Koonin, E. V., & Van Der Oost, J. (2008). Small crispr rnas guide antiviral defense in prokaryotes. *Science*, *321*(5891), 960–964.

Burgess, S. A., Walker, M. L., Sakakibara, H., Knight, P. J., & Oiwa, K. (2003). Dynein structure and power stroke. *Nature*, *421*(6924), 715–718.

Burkhardt, J. K., Echeverri, C. J., Nilsson, T., & Vallee, R. B. (1997). Overexpression of the dynamitin (p50) subunit of the dynactin complex disrupts dynein-dependent maintenance of membrane organelle distribution. *The Journal of cell biology*, *139*(2), 469–484.

Cafferty, P., Yu, L., Long, H., & Rao, Y. (2006). Semaphorin-1a functions as a guidance receptor in the drosophila visual system. *The Journal of neuroscience*, *26*(15), 3999–4003.

Campos-Ortega, J. A., & Hartenstein, V. (2013). *The embryonic development of Drosophila melanogaster*. Springer Science & Business Media.

Carter, A. P. (2013). Crystal clear insights into how the dynein motor moves. *Journal of cell science*, *126*(3), 705–713.

Carter, A. P., Garbarino, J. E., Wilson-Kubalek, E. M., Shipley, W. E., Cho, C., Milligan, R. A., Vale, R. D., & Gibbons, I. (2008). Structure and functional role of dynein's microtubule-binding domain. *Science*, *322*(5908), 1691–1695.

Casso, D., Ramırez-Weber, F.-A., & Kornberg, T. B. (1999). Gfp-tagged balancer chromosomes for drosophila melanogaster. *Mechanisms of development*, *88*(2), 229–232.

Caussinus, E., Kanca, O., & Affolter, M. (2012). Fluorescent fusion protein knockout mediated by anti-gfp nanobody. *Nature structural & molecular biology*, *19*(1), 117–121.

Ciechanover, A. (1998). The ubiquitin–proteasome pathway: on protein death and cell life. *The EMBO journal*, *17*(24), 7151–7160.

Copp, A. J., Brook, F. A., Estibeiro, J. P., Shum, A. S., & Cockroft, D. L. (1990). The embryonic development of mammalian neural tube defects. *Progress in neurobiology*, *35*(5), 363–403.

Crowder, M. E., Flynn, J. R., McNally, K. P., Cortes, D. B., Price, K. L., Kuehnert, P. A., Panzica, M. T., Andaya, A., Leary, J. A., & McNally, F. J. (2015). Dynactin-dependent cortical dynein and spherical spindle shape correlate temporally with meiotic spindle rotation in caenorhabditis elegans. *Molecular biology of the cell*, *26*(17), 3030–3046.

Dahmann, C., & Basler, K. (2000). Opposing transcriptional outputs of hedgehog signaling and engrailed control compartmental cell sorting at the drosophila a/p boundary. *Cell*, *100*(4), 411–422.

Derry, W. B., Wilson, L., & Jordan, M. A. (1995). Substoichiometric binding of taxol suppresses microtubule dynamics. *Biochemistry*, *34*(7), 2203–2211.

Duffy, J. B. (2002). Gal4 system in drosophila: a fly geneticist's swiss army knife. *genesis*, *34*(1-2), 1–15.

Dujardin, D. L., Barnhart, L. E., Stehman, S. A., Gomes, E. R., Gundersen, G. G., & Vallee, R. B. (2003). A role for cytoplasmic dynein and lis1 in directed cell movement. *The Journal of cell biology*, *163*(6), 1205–1211.

Duncan, J. E., & Warrior, R. (2002). The cytoplasmic dynein and kinesin motors have interdependent roles in patterning the drosophila oocyte. *Current Biology*, *12*(23), 1982–1991.

Eltsov, M., Dubé, N., Yu, Z., Pasakarnis, L., Haselmann-Weiss, U., Brunner, D., & Frangakis, A. S. (2015). Quantitative analysis of cytoskeletal reorganization during epithelial tissue sealing by large-volume electron tomography. *Nature cell biology*, *17*(5), 605–614.

Emerson, M. M., Long, J. B., & Van Vactor, D. (2013). Drosophila semaphorin2b is required for the axon guidance of a subset of embryonic neurons. *Developmental Dynamics*, *242*(7), 861–873.

Fan, S.-S., & Ready, D. F. (1997). Glued participates in distinct microtubule-based activities in drosophila eye development. *Development*, *124*(8), 1497–1507.

Fernández, B. G., Arias, A. M., & Jacinto, A. (2007). Dpp signalling orchestrates dorsal closure by regulating cell shape changes both in the amnioserosa and in the epidermis. *Mechanisms of development*, *124*(11), 884–897.

Firestone, A. J., Weinger, J. S., Maldonado, M., Barlan, K., Langston, L. D., O'Donnell, M., Gelfand, V. I., Kapoor, T. M., & Chen, J. K. (2012). Small-molecule inhibitors of the aaa+ atpase motor cytoplasmic dynein. *Nature*, *484*(7392), 125–129.

Frank, C. A., Pielage, J., & Davis, G. W. (2009). A presynaptic homeostatic signaling system composed of the eph receptor, ephexin, cdc42, and ca v 2.1 calcium channels. *Neuron*, *61*(4), 556–569.

Franke, J. D., Montague, R. A., & Kiehart, D. P. (2005). Nonmuscle myosin ii generates forces that transmit tension and drive contraction in multiple tissues during dorsal closure. *Current biology*, *15*(24), 2208–2221.

Fujita, I., Yamashita, A., & Yamamoto, M. (2015). Dynactin and num1 cooperate to establish the cortical anchoring of cytoplasmic dynein in s. pombe. *J Cell Sci*, *128*(8), 1555–1567.

Fürst, D. (2015). *CRISPR/Cas9-mediated engineering of a temperature-sensitive zipper mutant to study dorsal closure in Drosophila*. Master's thesis, University of Zurich.

Garen, A., Miller, B. R., & Paco-Larson, M. L. (1984). Mutations affecting functions of the drosophila gene glued. *Genetics*, *107*(4), 645–655.

Gasiunas, G., Barrangou, R., Horvath, P., & Siksnys, V. (2012). Cas9–crrna ribonucleoprotein complex mediates specific dna cleavage for adaptive immunity in bacteria. *Proceedings of the National Academy of Sciences*, *109*(39), E2579–E2586.

Gee, M., & Vallee, R. (1998). The role of the dynein stalk in cytoplasmic and flagellar motility. *European biophysics journal*, *27*(5), 466–473.

Gee, M. A., Heuser, J. E., & Vallee, R. B. (1997). An extended microtubule-binding structure within the dynein motor domain. *Nature*, *390*(6660), 636–639.

Gepner, J., Li, M.-g., Ludmann, S., Kortas, C., Boylan, K., Iyadurai, S. J., McGrail, M., & Hays, T. S. (1996). Cytoplasmic dynein function is essential in drosophila melanogaster. *Genetics*, *142*(3), 865–878.

Gibbons, I., Garbarino, J. E., Tan, C. E., Reck-Peterson, S. L., Vale, R. D., & Carter, A. P. (2005). The affinity of the dynein microtubule-binding domain is modulated by the conformation of its coiled-coil stalk. *Journal of Biological Chemistry*, *280*(25), 23960–23965.

Gibbons, I., & Rowe, A. (1965). Dynein: a protein with adenosine triphosphatase activity from cilia. *Science*, *149*(3682), 424–426.

Gibbons, I. R. (1963). Studies on the protein components of cilia from tetrahymena pyriformis. *Proceedings of the National Academy of Sciences of the United States of America*, *50*(5), 1002–1010.

Gilbert, S. F. (2000). *Developmental biology.*, chap. 9 Early Drosophila development. Sinauer Associates, Sunderland MA, 6th ed.

Ginzburg, V. E., Roy, P. J., & Culotti, J. G. (2002). Semaphorin 1a and semaphorin 1b are required for correct epidermal cell positioning and adhesion during morphogenesis in c. elegans. *Development*, *129*(9), 2065–2078.

Godenschwege, T. A., Hu, H., Shan-Crofts, X., Goodman, C. S., & Murphey, R. K. (2002). Bi-directional signaling by semaphorin 1a during central synapse formation in drosophila. *Nature neuroscience*, *5*(12), 1294–1301.

Gönczy, P., Pichler, S., Kirkham, M., & Hyman, A. A. (1999). Cytoplasmic dynein is required for distinct aspects of mtoc positioning, including centrosome separation, in the one cell stage caenorhabditis elegans embryo. *The Journal of cell biology*, *147*(1), 135–150.

Gratz, S. J., Cummings, A. M., Nguyen, J. N., Hamm, D. C., Donohue, L. K., Harrison, M. M., Wildonger, J., & O'Connor-Giles, K. M. (2013a). Genome engineering of drosophila with the crispr rna-guided cas9 nuclease. *Genetics*, *194*(4), 1029–1035.

Gratz, S. J., Ukken, F. P., Rubinstein, C. D., Thiede, G., Donohue, L. K., Cummings, A. M., & O'Connor-Giles, K. M. (2014). Highly specific and efficient crispr/cas9-catalyzed homology-directed repair in drosophila. *Genetics*, *196*(4), 961–971.

Gratz, S. J., Wildonger, J., Harrison, M. M., & O'Connor-Giles, K. M. (2013b). Crispr/cas9-mediated genome engineering and the promise of designer flies on demand. *Fly*, *7*(4), 249–255.

Grill, S. W., GoÈnczy, P., Stelzer, E. H., & Hyman, A. A. (2001). Polarity controls forces governing asymmetric spindle positioning in the caenorhabditis elegans embryo. *Nature*, *409*(6820), 630–633.

Grill, S. W., Howard, J., Schäffer, E., Stelzer, E. H., & Hyman, A. A. (2003). The distribution of active force generators controls mitotic spindle position. *Science*, *301*(5632), 518–521.

Gupta, M. L., Carvalho, P., Roof, D. M., & Pellman, D. (2006). Plus end-specific depolymerase activity of kip3, a kinesin-8 protein, explains its role in positioning the yeast mitotic spindle. *Nature cell biology*, *8*(9), 913–923.

Harden, N. (2002). Signaling pathways directing the movement and fusion of epithelial sheets: lessons from dorsal closure in drosophila. *Differentiation*, *70*(4-5), 181–203.

Harte, P. J., & Kankel, D. R. (1982). Genetic analysis of mutations at the glued locus and interacting loci in drosophila melanogaster. *Genetics*, *101*(3-4), 477–501.

Harte, P. J., & Kankel, D. R. (1983). Analysis of visual system development in drosophila melanogaster: mutations at the glued locus. *Developmental biology*, *99*(1), 88–102.

Hays, T. S., Porter, M. E., McGrail, M., Grissom, P., Gosch, P., Fuller, M. T., & McIntosh, J. R. (1994). A cytoplasmic dynein motor in drosophila: identification and localization during embryogenesis. *Journal of cell science*, *107*(6), 1557–1569.

Hendricks, A. G., Lazarus, J. E., Perlson, E., Gardner, M. K., Odde, D. J., Goldman, Y. E., & Holzbaur, E. L. (2012). Dynein tethers and stabilizes dynamic microtubule plus ends. *Current Biology*, *22*(7), 632–637.

Herranz, H., & Morata, G. (2001). The functions of pannier during drosophila embryogenesis. *Development*, *128*(23), 4837–4846.

Höök, P., & Vallee, R. B. (2006). The dynein family at a glance. *Journal of cell science*, *119*(21), 4369–4371.

Howard, J., & Hyman, A. A. (2007). Microtubule polymerases and depolymerases. *Current opinion in cell biology*, *19*(1), 31–35.

Ikegami, R., Simokat, K., Zheng, H., Brown, L., Garriga, G., Hardin, J., & Culotti, J. (2012). Semaphorin and eph receptor signaling guide a series of cell movements for ventral enclosure in c. elegans. *Current Biology*, *22*(1), 1–11.

Jacinto, A., Wood, W., Balayo, T., Turmaine, M., Martinez-Arias, A., & Martin, P. (2000). Dynamic actin-based epithelial adhesion and cell matching during drosophila dorsal closure. *Current Biology*, *10*(22), 1420–1426.

Jacinto, A., Woolner, S., & Martin, P. (2002). Dynamic analysis of dorsal closure in drosophila: from genetics to cell biology. *Developmental cell*, *3*(1), 9–19.

Jankovics, F., & Brunner, D. (2006). Transiently reorganized microtubules are essential for zippering during dorsal closure in drosophila melanogaster. *Developmental cell*, *11*(3), 375–385.

Jansen, R., Embden, J., Gaastra, W., Schouls, L., et al. (2002). Identification of genes that are associated with dna repeats in prokaryotes. *Molecular microbiology*, *43*(6), 1565–1575.

Januschke, J., Gervais, L., Dass, S., Kaltschmidt, J. A., Lopez-Schier, H., Johnston, D. S., Brand, A. H., Roth, S., & Guichet, A. (2002). Polar transport in the drosophila oocyte requires dynein and kinesin i cooperation. *Current Biology*, *12*(23), 1971–1981.

Jiang, J., & Struhl, G. (1998). Regulation of the hedgehog and wingless signalling pathways by the f-box/wd40-repeat protein slimb. *Nature*, *391*(6666), 493–496.

Jinek, M., Chylinski, K., Fonfara, I., Hauer, M., Doudna, J. A., & Charpentier, E. (2012). A programmable dual-rna–guided dna endonuclease in adaptive bacterial immunity. *Science*, *337*(6096), 816–821.

Jordan, M. A., Toso, R. J., Thrower, D., & Wilson, L. (1993). Mechanism of mitotic block and inhibition of cell proliferation by taxol at low concentrations. *Proceedings of the National Academy of Sciences*, *90*(20), 9552–9556.

Kaltschmidt, J. A., Lawrence, N., Morel, V., Balayo, T., Fernández, B. G., Pelissier, A., Jacinto, A., & Arias, A. M. (2002). Planar polarity and actin dynamics in the epidermis of drosophila. *Nature cell biology*, *4*(12), 937–944.

Kapust, R. B., Tözsér, J., Fox, J. D., Anderson, D. E., Cherry, S., Copeland, T. D., & Waugh, D. S. (2001). Tobacco etch virus protease: mechanism of autolysis and rational design of stable mutants with wild-type catalytic proficiency. *Protein engineering*, *14*(12), 993–1000.

Kardon, J. R., & Vale, R. D. (2009). Regulators of the cytoplasmic dynein motor. *Nature reviews Molecular cell biology*, *10*(12), 854–865.

Karki, S., & Holzbaur, E. L. (1995). Affinity chromatography demonstrates a direct binding between cytoplasmic dynein and the dynactin complex. *Journal of Biological Chemistry*, *270*(48), 28806–28811.

Kennedy, M. J., Hughes, R. M., Peteya, L. A., Schwartz, J. W., Ehlers, M. D., & Tucker, C. L. (2010). Rapid blue-light-mediated induction of protein interactions in living cells. *Nature methods*, *7*(12), 973–975.

Kiehart, D. P., Galbraith, C. G., Edwards, K. A., Rickoll, W. L., & Montague, R. A. (2000). Multiple forces contribute to cell sheet morphogenesis for dorsal closure in drosophila. *The Journal of cell biology*, *149*(2), 471–490.

Kim, H., & Kim, J.-S. (2014). A guide to genome engineering with programmable nucleases. *Nature Reviews Genetics*, *15*(5), 321–334.

King, S. M. (2000). The dynein microtubule motor. *Biochimica et Biophysica Acta (BBA)-Molecular Cell Research*, *1496*(1), 60–75.

Kirschner, M., & Mitchison, T. (1986). Beyond self-assembly: from microtubules to morphogenesis. *Cell*, *45*(3), 329–342.

Kiyomitsu, T., & Cheeseman, I. M. (2012). Chromosome-and spindle-pole-derived signals generate an intrinsic code for spindle position and orientation. *Nature cell biology*, *14*(3), 311–317.

Kon, T., Mogami, T., Ohkura, R., Nishiura, M., & Sutoh, K. (2005). Atp hydrolysis cycle–dependent tail motions in cytoplasmic dynein. *Nature structural & molecular biology*, *12*(6), 513–519.

Koonce, M. P. (1997). Identification of a microtubule-binding domain in a cytoplasmic dynein heavy chain. *Journal of Biological Chemistry*, *272*(32), 19714–19718.

Koonin, E. V., & Makarova, K. S. (2013). Crispr-cas: evolution of an rna-based adaptive immunity system in prokaryotes. *RNA biology*, *10*(5), 679–686.

Kornberg, T. B., & Tabata, T. (1993). Segmentation of the drosophila embryo. *Current opinion in genetics & development*, *3*(4), 585–593.

Kotak, S., Busso, C., & Gönczy, P. (2012). Cortical dynein is critical for proper spindle positioning in human cells. *The Journal of cell biology*, *199*(1), 97–110.

Kotak, S., & Gönczy, P. (2013). Mechanisms of spindle positioning: cortical force generators in the limelight. *Current opinion in cell biology*, *25*(6), 741–748.

Kumar, N. (1981). Taxol-induced polymerization of purified tubulin. mechanism of action. *Journal of Biological Chemistry*, *256*(20), 10435–10441.

Laan, L., Pavin, N., Husson, J., Romet-Lemonne, G., Van Duijn, M., López, M. P., Vale, R. D., Jülicher, F., Reck-Peterson, S. L., & Dogterom, M. (2012a). Cortical dynein controls microtubule dynamics to generate pulling forces that position microtubule asters. *Cell*, *148*(3), 502–514.

Laan, L., Roth, S., & Dogterom, M. (2012b). End-on microtubule-dynein interactions and pulling-based positioning of microtubule organizing centers. *Cell Cycle*, *11*(20), 3750–3757.

LaMonte, B. H., Wallace, K. E., Holloway, B. A., Shelly, S. S., Ascaño, J., Tokito, M., Van Winkle, T., Howland, D. S., & Holzbaur, E. L. (2002). Disruption of dynein/dynactin inhibits axonal transport in motor neurons causing late-onset progressive degeneration. *Neuron*, *34*(5), 715–727.

Larsen, C. W., Hirst, E., Alexandre, C., & Vincent, J.-P. (2003). Segment boundary formation in drosophila embryos. *Development*, *130*(23), 5625–5635.

Lewis, E., & Bacher, F. (1968). Method of feeding ethyl methane sulfonate (ems) to drosophila males. *Dros. Inf. Serv*, *43*(193), 193.

Li, M.-g., McGrail, M., Serr, M., & Hays, T. S. (1994). Drosophila cytoplasmic dynein, a microtubule motor that is asymmetrically localized in the oocyte. *The Journal of Cell Biology*, *126*(6), 1475–1494.

Lu, M. S., & Johnston, C. A. (2013). Molecular pathways regulating mitotic spindle orientation in animal cells. *Development*, *140*(9), 1843–1856.

Maddox, P. S., Stemple, J. K., Satterwhite, L., Salmon, E., & Bloom, K. (2003). The minus end-directed motor kar3 is required for coupling dynamic microtubule plus ends to the cortical shmoo tip in budding yeast. *Current biology*, *13*(16), 1423–1428.

Makarova, K. S., Haft, D. H., Barrangou, R., Brouns, S. J., Charpentier, E., Horvath, P., Moineau, S., Mojica, F. J., Wolf, Y. I., Yakunin, A. F., et al. (2011). Evolution and classification of the crispr–cas systems. *Nature Reviews Microbiology*, *9*(6), 467–477.

Markstein, M., Pitsouli, C., Villalta, C., Celniker, S. E., & Perrimon, N. (2008). Exploiting position effects and the gypsy retrovirus insulator to engineer precisely expressed transgenes. *Nature genetics*, *40*(4), 476–483.

Markus, S. M., & Lee, W.-L. (2011). Regulated offloading of cytoplasmic dynein from microtubule plus ends to the cortex. *Developmental cell*, *20*(5), 639–651.

Martin, P., & Lewis, J. (1992). Actin cables and epidermal movement in embryonic wound healing.

Martin, P., & Parkhurst, S. M. (2004). Parallels between tissue repair and embryo morphogenesis. *Development*, *131*(13), 3021–3034.

Martin, P., & Wood, W. (2002). Epithelial fusions in the embryo. *Current opinion in cell biology*, *14*(5), 569–574.

Martín-Blanco, E., Gampel, A., Ring, J., Virdee, K., Kirov, N., Tolkovsky, A. M., & Martinez-Arias, A. (1998). puckered encodes a phosphatase that mediates a feedback loop regulating jnk activity during dorsal closure in drosophila. *Genes & development*, *12*(4), 557–570.

Martín-Blanco, E., & Knust, E. (2001). Epithelial morphogenesis: filopodia at work. *Current biology*, *11*(1), R28–R31.

Martinez-Arias, A., & Lawrence, P. A. (1984). Parasegments and compartments in the drosophila embryo. *Nature*, *313*(6004), 639–642.

McDonald, H. B., Stewart, R. J., & Goldstein, L. S. (1990). The kinesin-like ncd protein of drosophila is a minus end-directed microtubule motor. *Cell*, *63*(6), 1159–1165.

McGrail, M., Gepner, J., Silvanovich, A., Ludmann, S., Serr, M., & Hays, T. S. (1995). Regulation of cytoplasmic dynein function in vivo by the drosophila glued complex. *The Journal of cell biology*, *131*(2), 411–425.

McGrail, M., & Hays, T. S. (1997). The microtubule motor cytoplasmic dynein is required for spindle orientation during germline cell divisions and oocyte differentiation in drosophila. *Development*, *124*(12), 2409–2419.

Melkonian, K. A., Maier, K. C., Godfrey, J. E., Rodgers, M., & Schroer, T. A. (2007). Mechanism of dynamitin-mediated disruption of dynactin. *Journal of Biological Chemistry*, *282*(27), 19355–19364.

Miki, H., Okada, Y., & Hirokawa, N. (2005). Analysis of the kinesin superfamily: insights into structure and function. *Trends in cell biology*, *15*(9), 467–476.

Millard, T. H., & Martin, P. (2008). Dynamic analysis of filopodial interactions during the zippering phase of drosophila dorsal closure. *Development*, *135*(4), 621–626.

Mische, S., He, Y., Ma, L., Li, M., Serr, M., & Hays, T. S. (2008). Dynein light intermediate chain: an essential subunit that contributes to spindle checkpoint inactivation. *Molecular biology of the cell*, *19*(11), 4918–4929.

Müsch, A. (2004). Microtubule organization and function in epithelial cells. *Traffic*, *5*(1), 1–9.

Nguyen-Ngoc, T., Afshar, K., & Gönczy, P. (2007). Coupling of cortical dynein and gα proteins mediates spindle positioning in caenorhabditis elegans. *Nature Cell Biology*, *9*(11), 1294–1302.

Niccoli, T., Yamashita, A., Nurse, P., & Yamamoto, M. (2004). The p150-glued ssm4p regulates microtubular dynamics and nuclear movement in fission yeast. *Journal of cell science*, *117*(23), 5543–5556.

Niessen, C. M., Leckband, D., et al. (2011). Tissue organization by cadherin adhesion molecules: dynamic molecular and cellular mechanisms of morphogenetic regulation. *Physiological reviews*, *91*(2), 691–731.

Ninov, N., Chiarelli, D. A., & Martín-Blanco, E. (2007). Extrinsic and intrinsic mechanisms directing epithelial cell sheet replacement during drosophila metamorphosis. *Development*, *134*(2), 367–379.

Nüsslein-Volhard, C., Wieschaus, E., & Kluding, H. (1984). Mutations affecting the pattern of the larval cuticle indrosophila melanogaster. *Wilhelm Roux's archives of developmental biology*, *193*(5), 267–282.

Park, D. H., & Rose, L. S. (2008). Dynamic localization of lin-5 and gpr-1/2 to cortical force generation domains during spindle positioning. *Developmental biology*, *315*(1), 42–54.

Pasakarnis, L., Frei, E., Caussinus, E., Affolter, M., & Brunner, D. (2016). Tissue-specific, acute myosin 2 activity depletion dismisses current models of tissue force orchestration in dorsal closure. Submitted.

Pastink, A., Heemskerk, E., Nivard, M. J., van Vliet, C. J., & Vogel, E. W. (1991). Mutational specificity of ethyl methanesulfonate in excision-repair-proficient and-deficient strains of drosophila melanogaster. *Molecular and General Genetics MGG*, *229*(2), 213–218.

Peralta, X., Toyama, Y., Hutson, M., Montague, R., Venakides, S., Kiehart, D., & Edwards, G. (2007). Upregulation of forces and morphogenic asymmetries in dorsal closure during drosophila development. *Biophysical journal*, *92*(7), 2583–2596.

Pfeiffer, B. D., Ngo, T.-T. B., Hibbard, K. L., Murphy, C., Jenett, A., Truman, J. W., & Rubin, G. M. (2010). Refinement of tools for targeted gene expression in drosophila. *Genetics*, *186*(2), 735–755.

Pfeiffer, B. D., Truman, J. W., & Rubin, G. M. (2012). Using translational enhancers to increase transgene expression in drosophila. *Proceedings of the National Academy of Sciences*, *109*(17), 6626–6631.

Plough, H. H., & Ives, P. T. (1935). Induction of mutations by high temperature in drosophila. *Genetics*, *20*(1), 42.

Port, F., Chen, H.-M., Lee, T., & Bullock, S. L. (2014). Optimized crispr/cas tools for efficient germline and somatic genome engineering in drosophila. *Proceedings of the National Academy of Sciences*, *111*(29), E2967–E2976.

Port, F., Muschalik, N., & Bullock, S. L. (2015). Systematic evaluation of drosophila crispr tools reveals safe and robust alternatives to autonomous gene drives in basic research. *G3: Genes— Genomes— Genetics*, *5*(7), 1493–1502.

Reed, B. H., Wilk, R., & Lipshitz, H. D. (2001). Downregulation of jun kinase signaling in the amnioserosa is essential for dorsal closure of the drosophila embryo. *Current biology*, *11*(14), 1098–1108.

Reed, B. H., Wilk, R., Schöck, F., & Lipshitz, H. D. (2004). Integrin-dependent apposition of drosophila extraembryonic membranes promotes morphogenesis and prevents anoikis. *Current biology*, *14*(5), 372–380.

Reichhart, J., & Ferrandon, D. (1998). Green balancers. *Dros. Inf. Serv*, *81*, 201–202.

Riesgo-Escovar, J. R., & Hafen, E. (1997a). Common and distinct roles of dfos and djun during drosophila development. *Science*, *278*(5338), 669–672.

Riesgo-Escovar, J. R., & Hafen, E. (1997b). Drosophila jun kinase regulates expression of decapentaplegic via the ets-domain protein aop and the ap-1 transcription factor djun during dorsal closure. *Genes & Development*, *11*(13), 1717–1727.

Riesgo-Escovar, J. R., Jenni, M., Fritz, A., & Hafen, E. (1996). The drosophila jun-n-terminal kinase is required for cell morphogenesis but not for djun-dependent cell fate specification in the eye. *Genes & Development*, *10*(21), 2759–2768.

Rivera-Pomar, R., & Jãckle, H. (1996). From gradients to stripes in drosophila embryogenesis: filling in the gaps. *Trends in Genetics*, *12*(11), 478–483.

Robinson, J. T., Wojcik, E. J., Sanders, M. A., McGrail, M., & Hays, T. S. (1999). Cytoplasmic dynein is required for the nuclear attachment and migration of centrosomes during mitosis in drosophila. *The Journal of cell biology*, *146*(3), 597–608.

Rogers, S. L., Rogers, G. C., Sharp, D. J., & Vale, R. D. (2002). Drosophila eb1 is important for proper assembly, dynamics, and positioning of the mitotic spindle. *The Journal of cell biology*, *158*(5), 873–884.

Roossien, D. H., Miller, K. E., & Gallo, G. (2015). Ciliobrevins as tools for studying dynein motor function. *Frontiers in cellular neuroscience*, *9*.

Roy, P. J., Zheng, H., Warren, C. E., & Culotti, J. G. (2000). mab-20 encodes semaphorin-2a and is required to prevent ectopic cell contacts during epidermal morphogenesis in caenorhabditis elegans. *Development*, *127*(4), 755–767.

Schiavo, G., Greensmith, L., Hafezparast, M., & Fisher, E. M. (2013). Cytoplasmic dynein heavy chain: the servant of many masters. *Trends in neurosciences*, *36*(11), 641–651.

Schiff, P. B., Fant, J., & Horwitz, S. B. (1979). Promotion of microtubule assembly in vitro by taxol.

Schmidt, H., Gleave, E. S., & Carter, A. P. (2012). Insights into dynein motor domain function from a 3.3-å crystal structure. *Nature structural & molecular biology*, *19*(5), 492–497.

Schroer, T. A. (2004). Dynactin. *Annu. Rev. Cell Dev. Biol.*, *20*, 759–779.

Schuster, M., Lipowsky, R., Assmann, M.-A., Lenz, P., & Steinberg, G. (2011). Transient binding of dynein controls bidirectional long-range motility of early endosomes. *Proceedings of the National Academy of Sciences*, *108*(9), 3618–3623.

Sekyrova, P., Bohmann, D., Jindra, M., & Uhlirova, M. (2010). Interaction between drosophila bzip proteins atf3 and jun prevents replacement of epithelial cells during metamorphosis. *Development*, *137*(1), 141–150.

Sharp, D. J., Brown, H. M., Kwon, M., Rogers, G. C., Holland, G., & Scholey, J. M. (2000a). Functional coordination of three mitotic motors indrosophila embryos. *Molecular Biology of the Cell*, *11*(1), 241–253.

Sharp, D. J., Rogers, G. C., & Scholey, J. M. (2000b). Cytoplasmic dynein is required for poleward chromosome movement during mitosis in drosophila embryos. *Nature Cell Biology*, *2*(12), 922–930.

Siller, K. H., Cabernard, C., & Doe, C. Q. (2006). The numa-related mud protein binds pins and regulates spindle orientation in drosophila neuroblasts. *Nature Cell Biology*, *8*(6), 594–600.

Skop, A. R., & White, J. G. (1998). The dynactin complex is required for cleavage plane specification in early caenorhabditis elegans embryos. *Current biology*, *8*(20), 1110–1117.

Solon, J., Kaya-Copur, A., Colombelli, J., & Brunner, D. (2009). Pulsed forces timed by a ratchet-like mechanism drive directed tissue movement during dorsal closure. *Cell*, *137*(7), 1331–1342.

Spadaccini, R., Reidt, U., Dybkov, O., Will, C., Frank, R., Stier, G., Corsini, L., Wahl, M. C., Lührmann, R., & Sattler, M. (2006). Biochemical and nmr analyses of an sf3b155–p14–u2af-rna interaction network involved in branch point definition during pre-mrna splicing. *Rna*, *12*(3), 410–425.

Splinter, D., Razafsky, D. S., Schlager, M. A., Serra-Marques, A., Grigoriev, I., Demmers, J., Keijzer, N., Jiang, K., Poser, I., Hyman, A. A., et al. (2012). Bicd2, dynactin, and lis1 cooperate in regulating dynein recruitment to cellular structures. *Molecular biology of the cell*, *23*(21), 4226–4241.

St Johnston, D., & Nüsslein-Volhard, C. (1992). The origin of pattern and polarity in the drosophila embryo. *Cell*, *68*(2), 201–219.

Sternberg, S. H., Redding, S., Jinek, M., Greene, E. C., & Doudna, J. A. (2014). Dna interrogation by the crispr rna-guided endonuclease cas9. *Nature*, *507*(7490), 62–67.

Swaroop, A., Paco-Larson, M. L., & Garen, A. (1985). Molecular genetics of a transposon-induced dominant mutation in the drosophila locus glued. *Proceedings of the National Academy of Sciences*, *82*(6), 1751–1755.

Swaroop, A., Sun, J., Paco-Larson, M., & Garen, A. (1986). Molecular organization and expression of the genetic locus glued in drosophila melanogaster. *Molecular and cellular biology*, *6*(3), 833–841.

Tabata, T., Eaton, S., & Kornberg, T. B. (1992). The drosophila hedgehog gene is expressed specifically in posterior compartment cells and is a target of engrailed regulation. *Genes & development*, *6*(12b), 2635–2645.

Taxis, C., Stier, G., Spadaccini, R., & Knop, M. (2009). Efficient protein depletion by genetically controlled deprotection of a dormant n-degron. *Molecular systems biology*, *5*(1), 267.

Toyama, Y., Peralta, X. G., Wells, A. R., Kiehart, D. P., & Edwards, G. S. (2008). Apoptotic force and tissue dynamics during drosophila embryogenesis. *Science*, *321*(5896), 1683–1686.

Tsuda, H., Han, S. M., Yang, Y., Tong, C., Lin, Y. Q., Mohan, K., Haueter, C., Zoghbi, A., Harati, Y., Kwan, J., et al. (2008). The amyotrophic lateral sclerosis 8 protein vapb is cleaved, secreted, and acts as a ligand for eph receptors. *Cell*, *133*(6), 963–977.

Vale, R. D. (2003). The molecular motor toolbox for intracellular transport. *Cell*, *112*(4), 467–480.

VanHook, A., & Letsou, A. (2008). Head involution in drosophila: genetic and morphogenetic connections to dorsal closure. *Developmental Dynamics*, *237*(1), 28–38.

Varshavsky, A. (1997). The n-end rule pathway of protein degradation. *Genes to Cells*, *2*(1), 13–28.

Vaughan, K. T. (2005). Tip maker and tip marker; eb1 as a master controller of microtubule plus ends. *The Journal of cell biology*, *171*(2), 197–200.

Vaughan, K. T., & Vallee, R. B. (1995). Cytoplasmic dynein binds dynactin through a direct interaction between the intermediate chains and p150glued. *The Journal of cell biology*, *131*(6), 1507–1516.

Vincent, S., Perrimon, N., & Axelrod, J. D. (2008). Hedgehog and wingless stabilize but do not induce cell fate during drosophila dorsal embryonic epidermal patterning. *Development*, *135*(16), 2767–2775.

Vogel, S. K., Pavin, N., Maghelli, N., Jülicher, F., & Tolić-Nørrelykke, I. M. (2009). Self-organization of dynein motors generates meiotic nuclear oscillations. *PLoS Biol*, *7*(4), e1000087.

Walker, R. A., Salmon, E. D., & Endow, S. A. (1990). The drosophila claret segregation protein is a minus-end directed motor molecule.

Wang, C., Li, S., Januschke, J., Rossi, F., Izumi, Y., Garcia-Alvarez, G., Gwee, S. S. L., Soon, S. B., Sidhu, H. K., Yu, F., et al. (2011). An ana2/ctp/mud complex regulates spindle orientation in drosophila neuroblasts. *Developmental cell*, *21*(3), 520–533.

Waterman-Storer, C. M., & Holzbaur, E. L. (1996). The product of the drosophila gene, glued, is the functional homologue of the p150glued component of the vertebrate dynactin complex. *Journal of Biological Chemistry*, *271*(2), 1153–1159.

Wenink, A. C., & Zevallos, J.-C. (1988). Developmental aspects of atrioventricular septal defects. *International journal of cardiology*, *18*(1), 65–78.

Wickstead, B., & Gull, K. (2007). Dyneins across eukaryotes: a comparative genomic analysis. *Traffic*, *8*(12), 1708–1721.

Wilkinson, D. G. (2001). Multiple roles of eph receptors and ephrins in neural development. *Nature Reviews Neuroscience*, *2*(3), 155–164.

Wood, W., Jacinto, A., Grose, R., Woolner, S., Gale, J., Wilson, C., & Martin, P. (2002). Wound healing recapitulates morphogenesis in drosophila embryos. *Nature cell biology*, *4*(11), 907–912.

Woodard, G. E., Huang, N.-N., Cho, H., Miki, T., Tall, G. G., & Kehrl, J. H. (2010). Ric-8a and giα recruit lgn, numa, and dynein to the cell cortex to help orient the mitotic spindle. *Molecular and cellular biology*, *30*(14), 3519–3530.

Xiang, X., Han, G., Winkelmann, D. A., Zuo, W., & Morris, N. R. (2000). Dynamics of cytoplasmic dynein in living cells and the effect of a mutation in the dynactin complex actin-related protein arp1. *Current Biology*, *10*(10), 603–606.

Xu, J., Ren, X., Sun, J., Wang, X., Qiao, H.-H., Xu, B.-W., Liu, L.-P., & Ni, J.-Q. (2015). A toolkit of crispr-based genome editing systems in drosophila. *Journal of Genetics and Genomics*, *42*(4), 141–149.

Yamamoto, A., West, R. R., McIntosh, J. R., & Hiraoka, Y. (1999). A cytoplasmic dynein heavy chain is required for oscillatory nuclear movement of meiotic prophase and efficient meiotic recombination in fission yeast. *The Journal of cell biology*, *145*(6), 1233–1250.

Yang, Y., Liu, M., Li, D., Ran, J., Gao, J., Suo, S., Sun, S.-C., & Zhou, J. (2014). Cyld regulates spindle orientation by stabilizing astral microtubules and promoting dishevelled-numa-dynein/dynactin complex formation. *Proceedings of the National Academy of Sciences*, *111*(6), 2158–2163.

Yazdani, U., & Terman, J. R. (2006). The semaphorins. *Genome Biol*, *7*(3), 211.

Yoder, J. H., & Han, M. (2001). Cytoplasmic dynein light intermediate chain is required for discrete aspects of mitosis in caenorhabditis elegans. *Molecular biology of the cell*, *12*(10), 2921–2933.

Young, P. E., Richman, A. M., Ketchum, A. S., & Kiehart, D. P. (1993). Morphogenesis in drosophila requires nonmuscle myosin heavy chain function. *Genes & Development*, *7*(1), 29–41.

Yu, F., Wang, H., Qian, H., Kaushik, R., Bownes, M., Yang, X., & Chia, W. (2005). Locomotion defects, together with pins, regulates heterotrimeric g-protein signaling during drosophila neuroblast asymmetric divisions. *Genes & development*, *19*(11), 1341–1353.

Yu, H.-H., Araj, H. H., Ralls, S. A., & Kolodkin, A. L. (1998). The transmembrane semaphorin sema i is required in drosophila for embryonic motor and cns axon guidance. *Neuron*, *20*(2), 207–220.

A Appendix

Table 7: List of analysed genotypes

Genotype analysed/shown	Figure
w;; *pnrGal4*, UAS-mCherry-Moesin/UAS-GFP-β-tubulin	Fig. 9 Fig. 11B Fig. 12A
w;; *pnrGal4*/UAS-EB1-GFP	Fig. 10A
w;; *pnrGal4*/UAS-GFP-β-tubulin	Fig. 10B, C Fig. 12B, C
w; sGMCA	Fig. 14A, D
w; sGMCA; *Dhc64 4-6*/*Dhc64 4-6*	Fig. 14B, D
w; sGMCA; *Dhc64 4-19*/*Dhc64 4-6*	Fig. 14C, D
w; *enGal4*, UAS-mCherry-Moesin/+; UAS-RNAi-Dhc64/sGMCA	Fig. 15B, C
w;; *pnrGal4*, *arm*GFP/UAS-RNAi-Dhc64	Fig. 15C
w; *enGal4*, UAS-mCherry-moesin/+ ; sGMCA	Fig. 15A, C Fig. 21A Fig. 22
w;; *arm*-GFP	Fig. 15C Fig. 23E Fig. 26 Fig. 27C
Y/w67c23 P{lacW}DlicG0065;; *pnrGal4*, UAS-mCherry-Moesin/+	Fig. 16B, D
Y/w67c23 P{lacW}DlicG0190;; *pnrGal4*, UAS-mCherry-Moesin/+	Fig. 16C, D
w;; *pnrGal4*, UAS-mCherry-Moesin/TM6C	Fig. 16A, D Fig. 23A, D Fig. 25A-D
P(ubi-GFP::Dlic)	Fig. 17A Fig. 19
Y or *w/w67c23 P{lacW}DlicG0190*; *P(ubi-GFP::Dlic)*/UAS-NSlmb-vhhGFP4; *pnrGal4*, UAS-mCherry-Moesin/+	Fig. 18B Fig. 19
Y or *w/w67c23 P{lacW}DlicG0065*; *P(ubi-GFP::Dlic)*/UAS-NSlmb-vhhGFP4; *pnrGal4*, UAS-mCherry-Moesin/+	Fig. 17B Fig. 18C Fig. 19
Y or *w/w67c23 P{lacW}DlicG0065*; *P(ubi-GFP::Dlic)*/*enGal4*, UAS-mCherry-Moesin; UAS-NSlmb-vhhGFP4/+	Fig. 17C Fig. 19
Y or *w/w67c23 P{lacW}DlicG0190*; *P(ubi-GFP::Dlic)*/*enGal4*, UAS-mCherry-Moesin; UAS-NSlmb-vhhGFP4/+	Fig. 18 Fig. 19
Y or w/w67c23 P{lacW}DlicG0190; P(Ubi-GFP::Dlic)/UAS-NSlmb-vhhGFP4; *69BGal4*/+	Fig. 17D Fig. 19
Y or *w/w67c23 P{lacW}DlicG0065*; *P(ubi-GFP::Dlic)*/*actinGal4*; UAS-NSlmb-vhhGFP4/+	Fig. 17E Fig. 19

Continued on next page

Table 7 (*Continued*)

Genotype analysed/shown	Figure
Y or *w/w67c23 P{lacW}DlicG0065*; *P(ubi-GFP::Dlic)/daGal4*; UAS-NSlmb-vhhGFP4/+	Fig. 17F Fig. 19
Y/w67c23 P{lacW}DlicG0190; *P(ubi-GFP::Dlic)*/UAS-NSlmb-vhhGFP4; *pnrGal4*, UAS-mCherry-Moesin/+	Fig. 20
w; UASdnGl84/enGal4, UAS-mCherry-Moesin; sGMCA/+	Fig. 21B Fig. 22A
w; UASdnGl96B/*enGal4*, UAS-mCherry-Moesin; sGMCA/+	Fig. 22B
w; *enGal4*, UAS-mCherry-Moesin/+; *Glued1*/sGMCA	Fig. 22D
w; UASdnGl84/*enGal4*, UAS-mCherry-Moesin/+; *Glued1*/sGMCA	Fig. 21C Fig. 22C
w; UAS DmnD2/+; *pnrGal4*, UAS-mCherry-Moesin/+	Fig. 23B, D
w; UAS DmnD2/+; *Dhc64 4-19/pnrGal4*, UAS-mCherry-Moesin/+	Fig. 23C, D
w; *arm*GFP/+; *Dhc64 4-19*/+	Fig. 23E
w;; Jupiter-GFP	Fig. 24
w; *enGal4*, UAS-mCherry-Moesin	Fig. 33A
w; *enGal4*, UAS-mCherry-Moesin/Cyo; *Ephx652*	Fig. 33B, C
w; *enGal4*, UAS-mCherry-Moesin; *exnEY-δ23*	Fig. 33D, E
w; *sema-2a*; *prdGal4*/UAS-mCherry-Moesin	Fig. 33F

Table 8: List of *Drosophila melanogaster* strains

Strain	Description	Source
w; UAS-mCherry-Moesin/CyO	Moesin tagged with mCherry to label F-actin	P. Martin
w;; *pnrGal4*, UAS-mCherry-Moesin/TM6, Tb	*pnr* enhancer expressing Gal4 in the epidermis	P. Martin
w; *enGal4*, UAS-mCherry-Moesin	*engrailed* enhancer Gal4 in the epidermis stripes; mCherry-Moesin labels F-actin	P. Martin
w; *arm*GFP	Armadillo tagged with GFP to outline cell adherens junctions	BL #8555, BL #8556
w; sGMCA	Moesin-GFP under *sqh* enhancer to label F-actin	D. Kiehart
w;; sGMCA	Moesin-GFP under *sqh* enhancer to label F-actin	D. Kiehart
w1118	white strain with isogensied chromosome 2 and 3	Brunner lab
y w, *nos*::Cas9^{mRFP}	*nanos (nos)* enhancer expressing Cas9. *white*$^{+}$ and mRFP are present	BL #54591
y w, *nos*::Cas9	*nanos (nos)* enhancer expressing Cas9. *white*$^{+}$ and mRFP are removed	Brunner lab
Dhc64 4-6/TM3, Ser	recessive lethal *Dhc64* allele generated by EMS mutagenesis screen	T. Hays
Dhc64 4-19/TM6b, D	recessive lethal *Dhc64* allele generated by EMS mutagenesis screen	T. Hays
Dhc64 4-19/TM6b, Tb+	recessive lethal *Dhc64* allele generated by EMS mutagenesis screen	BL #5274
Dhc64 6-10/TM6b, Tb^{1}	recessive lethal *Dhc64* allele generated by EMS mutagenesis screen	BL #8747
Dhc64 6-8/TM6b, Tb	recessive lethal *Dhc64* allele generated by EMS mutagenesis screen	T. Hays
UASdnGl84/CyGFP; MKRS/TM6B	Glued1 controlled by UAS promoter	D. Graeme
UASdnGl96B/CyGFP; MKRS/TM6B	Glued1 controlled by UAS promoter	D. Graeme
Glued1/TM6B	dominant *Glued* mutation leading to a truncated Glued protein	D. Graeme
w*; *P{UAS-DCTN2-p50.D}2*; TM3, Sb^{1}/TM6B, Tb^{1}	p50 dynamitin under UAS promoter (UASDmn)	BL #8784
p(ubi::GFP::Dlic)	N-terminal GFP-tagged dynein light intermediate (Dlic) chain driven by ubiquitin promoter	C. Lehner
sema-2a/Cyo	*semaphorin-2a* loss of function mutation	BL #11257
Ephx652/*ciD*	proposed loss of function mutation (Boyle et al., 2006)	D. Graeme

Continued on next page

Table 8 (*Continued*)

Strain	Description	Source
w; GluR UAS-YFP-exnFla10a; exnEY-Δ23/TM6B	loss of function mutation generated by imprecise excision of P-element	D. Graeme
w67c23 *P{lacW}DlicG0065*/FM7c	P-element insertion in first intron of *Dlic*	BL #11696
w67c23 *P{lacW}DlicG0190*/FM7c	P-element insertion in splice donor site in 7th intron of *Dlic*	BL #11951
w;; *69BGal4*	*69B enhancer* expressing Gal4 in the ectoderm	BL #1774
pnrGal4, UAS-Eb1-GFP/TM6B	*pannier* enhancer expressing Gal4 in the epidermis; EB1 tagged with GFP labels plus tips of microtubles	Brunner lab
w;; Jupiter-GFP	Jupiter protein tagged with GFP, associates with MTs	BL #6825
w; *actin5cGal4*/CyO	Ubiquitous expression of Gal4 und the control of *actin5C* enhancer	BL #4414
UAS-tubulin-GFP/TM3, Ser	*β*-tubulin tagged with GFP	BL #3039
w;; *pnrGal4*/TM3, Ser	*pannier* enhancer expressing Gal4 in epidermis	BL #3039
UAS-NSlmb-vhhGFP (II and III Chr)	fusion protein for deGradFP	M. Affolter
w; *daGal4*; MKRS/TM6B, Tb[1]	Ubiquitous expression of Gal4 under the control of daughterless	BL #55851

Table 9: List of primers

Primer	Sequence 5' - 3'
OMA31	ttaataccgaaaacctttgtgggacATGTCCAAAGGTGAAGAACTG
OMA32	ggagtcacccatTGGATCTGATATCATCGATGAATTCTCTGTCGGGCCAGCTC CGGCGCCGGCACCCGCTCCGGCGCCAGCACCCTTGTAGAGCTCATCCA TG
OMA33	gccGCGGCCGCaatttaaatttttaaaaactgtatgaatttgtgatgcttgaaaatttttcatacaagttgctag tgacatggtaaggtattccagc
OMA34	GAGAATTCATCGATGATATCAGATCCAatgggtgactccttggagaaccccg
OMA35	ccgaaaacctttgtgggacATGTCTATTACTTCTTTGTACAAGAAG
OMA36	GTAAACAGTTCTTCACCTTTGGACATGGTGGCGGGCTTCTCTAGACAG GCC
OMA37	ATGTCCAAAGGTGAAGAACTG
OMA38	ggtcgtgttcttctcagtgcttgcattataccggtttaattgattgaattgca
OMA39	GGTAAACAGTTCTTCACCTTTGGACATgtcccacaaaggttttcgg
OMA40	GTACAAAGAAGTAATAGACATgtcccacaaaggttttcggtattaaatac
OMA41	cctatttttgtaattgaatttaaattttaaaaactgtatgaatttgtgatgc
OMA67	ccgaaaacctttgtgggacATGAAGATGGACAAAAAGACTATAGTTTGGTTTAGAA GAGACCTAAGGATTGAGG
OMA68	ggttctccaaggagtcacccatAATTAACCCCGCAGGTCCACCGGCTCCACCAGCGC CAGCAGTAGCACCGCCTCCGGAGGGAGCTCCTTTATGACCTAA
OMA91	CCTTTACTTCAGGCGGCCGCGGCTCGAGGGTACCAACTTAAAAAAAAAA AATCAAAATGTCCAAAGGTGAAGAAC
OMA104	gctagTCTAGActtctgattttacgattaattctgaatgcacttttagcaatatcgtaatataaaaaataatcct attttgtaattgaatttaaattttaaaaactgtatg
OMA105	gatttggcccaggtggaaGCCgctgtcattgatg
OMA106	gattcaagagccaatttgaccaccgaGGCGGCattagccatggttcgcacctc
OMA108	gctttagattaaacttttagataccttaggtaaaggctttgaaggaataatttgg
OMA109	cgctgatatgttgaagcgtgtggagGCCcttcgcgaagagctgcgttc
OMA110	gaacgcagctcttcgcgaagGGCctccacacgcttcaac
OMA111	catcaatgacagcGGCttccacctgggccaaatcggcc
OMA112	gaggtgcgaaccatggctaatGCCGCCtcggtggtcaaattgg
OMA115	cgccagatcgtcagcttattgctgaggtgatgttgttctcgcaaggattc
OMA116	CTAATTCTTATCCTTTACTTCAGGCGGCCGCGGCTCGAGGGTACCAACT TAAAAAAAAAAATCAAAatgggtgactccttggagaaccccg
OMA132	tcattgatgcgcaagcagCGgtaagtccatcgg
OMA136	cgttgagcagctcgcagaccgactccaTTgccagcttgaccac
OMA138	ccgcgcggatatcgcTcgcactgaatatctttc
OMA143	ctaatcgacgatgtgcaggtcaagtcaatccgcaag
OMA144	gtcgcccgatggacttactgcttgcgcatcaatg

Continued on next page

Table 9 (*Continued*)

Primer	Sequence 5' - 3'
OMA145	cgtggtcaagctggcAAtggagtcggtctgcgagctgctc
OMA147	CCTATaCtttctagaGAATAGGAACTTCtatatattgtagttatgggtggttc
OMA149	gtactaaagtggattttaataacttcgtataatgtatgctatacgaagttatcgtacgGGATCTAATTCAATTAG
OMA150	cttgcggattgacttgacctgcacatcgtcgattag
OMA151	gaatgtaactaatcctaagcataacttcgtatagcatacattatacgaagttataccggtTAAGATACATTGATG
OMA152	gtatgctatacgaagttatgcttaggattagttacattcggttcg
OMA154	gaaagatattcagtgcgTgcgatatccgcgcgg
OMA155	GAAGTTCCTATTCtctagaaaGtATAGGAACTTCctctatatatacatatacaagcatacaagcaaacaccaaagcatacgcagtgcactggc
OMA156	GAAGTTCCTATaCtttctagaGAATAGGAACTTCactattcacgatcaattcgatataaatcttacctgagcaatggcccatttgacc
OMA157	GTGTCGCCCTTCGCTGAAGCAGGTGggaatccttccaccgatggactcaag
OMA158	CGCCCTTGAACTCGATTGACGGAAGAaaatgtcaagcgatcgatatggatc
OMA159	cttgagtccatcggtggaaggattccCACCTGCTTCAGCGAAGGGCGACACCCCA
OMA160	gatccatatcgatcgcttgacatttTCTTCCGTCAATCGAGTTCAAGGGCG
OMA161	GAAGTTCCTATTCtctagaaaGtATAGGAACTTCtcctaaactgctactttgcc
OMA162	gcatacattatacgaagttattaaaatccactttagtacaatacacatcatattatatcgtagtttatcc
OMA178	ctctttaggtcgctggccatgaccacgccagatcgtcagcttattgctg
OMA179	gtcgcccgatggacttacctgcttgcgcatcaatgacagccggttc
OMA180	gagaaacgcaaatacgttatggccgatttggcccaggtggaaccg
OMA181	ccgcaagcaacagctcgttgaggtgcgaaccatggctaatc
OMA182	gttttttgaatgaaaagagtacgaatatagctttagattaaacttttag
GIB_tagRFP_PacI	GGTTAATTATGTCTGAATTAATTAAAGAAAATATGCATATG
Cry2_PacI	TCTTTAATTAATTCAGACATAATTAACCCCGCAGGTCCACCGGC